SERDP
DoD EPA DOE
Strategic Environmental Research
and Development Program
A Partnership to Improve the
Environment

COMPARISON OF CFC-114 AND HFC-236EA PERFORMANCE IN SHIPBOARD VAPOR COMPRESSION SYSTEMS

by

D. T. Ray
M. B. Pate
H.N. Shapiro
Iowa State University
Ames, IA 50011

Project Officer:

Theodore G. Brna
U.S. Environmental Protection Agency
National Risk Management Research Laboratory
Air Pollution Prevention and Control Division
Research Triangle Park, NC 27711

Prepared for:

U.S. ENVIRONMENTAL PROTECTION AGENCY
OFFICE OF RESEARCH AND DEVELOPMENT
WASHINGTON, DC 20460

NOTICE

This document has been reviewed in accordance with U.S. Environmental Protection Agency policy and approved for publication. Mention of trade names or commercial products does not constitute endorsement or recommendation for use.

FOREWORD

The U.S. Environmental Protection Agency is charged by Congress with protecting the Nation's land, air, and water resources. Under a mandate of national environmental laws, the Agency strives to formulate and implement actions leading to a compatible balance between human activities and the ability of natural systems to support and nurture life. To meet this mandate, EPA's research program is providing data and technical support for solving environmental problems today and building a science knowledge base necessary to manage our ecological resources wisely, understand how pollutants affect our health, and prevent or reduce environmental risks in the future.

The National Risk Management Research Laboratory is the Agency's center for investigation of technological and management approaches for reducing risks from threats to human health and the environment. The focus of the Laboratory's research program is on methods for the prevention and control of pollution to air, land, water, and subsurface resources; protection of water quality in public water systems; remediation of contaminated sites and groundwater; and prevention and control of indoor air pollution. The goal of this research effort is to catalyze development and implementation of innovative, cost-effective environmental technologies; develop scientific and engineering information needed by EPA to support regulatory and policy decisions; and provide technical support and information transfer to ensure effective implementation of environmental regulations and strategies.

This publication has been produced as part of the Laboratory's strategic long-term research plan. It is published and made available by EPA's Office of Research and Development to assist the user community and to link researchers with their clients.

> E. Timothy Oppelt, Director
> National Risk Management Research Laboratory

ABSTRACT

In compliance with the Montreal Protocol and Department of Defense directives, alternatives to refrigerant CFC-114 are being investigated by the U.S. Navy and the U.S. Environmental Protection Agency for use in shipboard chillers. Refrigerant HFC-236ea has emerged as a candidate for drop-in replacement.

A computer model was developed for comparing these two refrigerants in a simulated 440-kilowatt centrifugal chiller system. Equations for modeling each system component were developed and solved using the Newton-Raphson method for multiple equations and unknowns. Correlations were developed for CFC-114 and HFC-236ea boiling and condensing coefficients taken at the Iowa State Heat Transfer Test Facility. The model was tested for a range of inlet condenser water temperatures and evaporator loads. The results are presented and compared with data provided by the Naval Surface Warfare Center in Annapolis, MD.

The experimental data provided by the Naval Surface Warfare Center sufficiently validate the model, and the simulation model predicts that HFC-236ea would perform favorably as a drop-in substitute for CFC-114.

Several recommendations are discussed which may further improve the performance of HFC-236ea in Navy chillers. Recommendations include adjusting the load of the evaporator to achieve positive gage pressure, use of a purge device, use of a variable speed compressor, further testing with azeotropic mixtures, and use of high performance tubes in the heat exchangers.

This report was submitted in fulfillment of Cooperative Agreement No. CR 820755-01-4 by the Engineering Research Institute, College of Engineering, Iowa State University, Ames, IA, under the sponsorship of the United States Environmental Protection Agency with funding from the Strategic Environmental Research and Development Program* (SERDP). This work covers the period from October 1, 1992 to May 3, 1995, and the work was completed as of May 3, 1995.

(*) A joint program of the Department of Defense, the Department of Energy, and the Environmental Protection Agency.

TECHNICAL REPORT DATA
(Please read Instructions on the reverse before completing)

1. REPORT NO. EPA-600/R-97-058	2.		
4. TITLE AND SUBTITLE Comparison of CFC-114 and HFC-236ea Performance in Shipboard Vapor Compression Systems		5. REPORT DATE June 1997	
		6. PERFORMING ORGANIZATION CODE	
7. AUTHOR(S) Daniel T. Ray, M. B. Pate, and H. N. Shapiro		8. PERFORMING ORGANIZATION REPORT NO.	
9. PERFORMING ORGANIZATION NAME AND ADDRESS Iowa State University 2088 H. M. Black Engineering Building Ames, Iowa 50011-2160		10. PROGRAM ELEMENT NO.	
		11. CONTRACT/GRANT NO. CR820755-01-4	
12. SPONSORING AGENCY NAME AND ADDRESS EPA, Office of Research and Development Air Pollution Prevention and Control Division Research Triangle Park, NC 27711		13. TYPE OF REPORT AND PERIOD COVERED Final; 10/92-5/95	
		14. SPONSORING AGENCY CODE EPA/600/13	

15. SUPPLEMENTARY NOTES APPCD project officer is Theodore G. Brna, Mail Drop 04, 919/541-2683.

16. ABSTRACT The report gives results of a comparison of the performance of two refrigerants--1,1,1,2,3,3-hexafluoropropane (HFC-236ea) and 1,2-dichloro-tetrafluoroethane (CFC-114)--in shipboard vapor compression refrigeration systems. (NOTE: In compliance with the Montreal Protocol and Department of Defense directives, alternatives to CFC-114 are being investigated by the U.S. Navy and the U.S. EPA for use in shipboard chillers. HFC-236ea has emerged as a candidate for drop-in replacement.) A computer model was developed for comparing the two refrigerants in a simulated 440-kW centrifugal chiller system. Equations for modeling each system component were developed and solved using the Newton-Raphson method for multiple equations and unknowns. Correlations were developed for CFC-114 and HFC-236ea boiling and condensing coefficients taken at the Iowa State Heat Transfer Test Facility. The model was tested with data provided by the Naval Surface Warfare Center (NSWC) in Annapolis, MD. The experimental data provided by the NSWC sufficiently validate the model, and the simulation model predicts that HFC-236ea would perform favorably as a drop-in substitute for CFC-114. Several recommendations are discussed which may further improve the performance of HFC-236ea in Navy chillers.

17.	KEY WORDS AND DOCUMENT ANALYSIS		
a. DESCRIPTORS		b. IDENTIFIERS/OPEN ENDED TERMS	c. COSATI Field/Group
Pollution Refrigerants Performance Halohydrocarbons Mathematical Models		Pollution Control Stationary Sources Shipboard Chillers Vapor Compression Chlorofluorocarbons Hydrofluorocarbons	13B 13A 14G 07C 12A
18. DISTRIBUTION STATEMENT Release to Public		19. SECURITY CLASS *(This Report)* Unclassified	21. NO. OF PAGES 85
		20. SECURITY CLASS *(This page)* Unclassified	22. PRICE

EPA Form 2220-1 (9-73)

CONTENTS

Contents (continued)

FIGURES

Figures (continued)

TABLES

NOMENCLATURE

$A_{f,c}$	=	total tube flow area of condenser (m^2)
$A_{f,e}$	=	total tube flow area of evaporator (m^2)
$A_{i,c}$	—	total condenser tube inside surface area (m^2)
$A_{i,e}$	=	total evaporator tube inside surface area (m^2)
$A_{o,c}$	=	total outside surface area of condenser (m^2)
$A_{o,e}$	—	total outside surface area of evaporator (m^2)
$\bar{A}_{o,c}$	—	average outside surface area of condenser per length (m^2/m)
$\bar{A}_{o,e}$	=	average outside surface area of evaporator per length (m^2/m)
$\bar{C}_{pchw}$	=	specific heat of chilled water (kJ/kg-°C)
$\bar{C}_{psw}$	=	specific heat of sea water (kJ/kg-°C)
$d_{i,c}$	=	inside diameter of a condenser tube (m)
$d_{i,e}$	=	inside diameter of an evaporator tube (m)
h	—	enthalpy (kJ/kg)
$\dot{h}_{i,c}$	=	condenser water side heat transfer coefficient (kW/m^2-°C)
$\bar{h}_{i,e}$		evaporator water side heat transfer coefficient (kW/m^2-°C)
$h_{o,c}$	=	condenser refrigerant side heat transfer coefficient (kW/m^2-°C)
$\bar{h}_{o,e}$	=	evaporator refrigerant side heat transfer coefficient (kW/m^2-°C)
$\bar{k}_{chw}$	=	thermal conductivity of chilled water (kW/m-°C)
$\bar{k}_{sw}$	=	thermal conductivity of sea water (kW/m-°C)
$L_{eff,c}$	—	effective tube length per pass in condenser (m/tube)
$L_{eff,e}$	=	effective tube length per pass in evaporator (m/tube)
$\dot{m}_{chw}$	=	mass flow rate of chilled water (kg/sec)
$\dot{m}_r$	—	mass flow rate of refrigerant (kg/min)
$\dot{m}_{sw}$	=	mass flow rate of condensing sea water (kg/sec)
n	=	polytropic exponent
N_e	=	number of tubes in evaporator
N_c	=	number of tubes in condenser
P	=	absolute pressure (kPa)
$\bar{Pr}_{chw}$	=	average Prandtl number of chilled water in evaporator
$\bar{Pr}_{sw}$	=	average Prandtl number of sea water in condenser
$\dot{Q}_c$	=	heat transferred in condenser (kW)
$\dot{Q}_e$	=	heat transferred in evaporator (kW)

Nomenclature (continued)

q_c''	=	heat flux in the condenser (kW/m^2)
q_e''	=	heat flux in the evaporator (kW/m^2)
$\overline{Re}_{chw}$	=	average Reynold's number of chilled water in evaporator
$\overline{Re}_{sw}$	=	average Reynolds number of sea water in condenser
T_c	=	refrigerant saturation temperature in condenser (°C)
T_{ce}	=	entering condenser cooling water temperature (°C)
$\overline{T}_{chw}$	=	average chilled water temperature in condenser (°C)
T_{cl}	=	leaving condenser water temperature (°C)
T_e	=	refrigerant saturation temperature in evaporator (°C)
T_{ee}	=	entering evaporator water temperature (°C)
T_{el}	=	leaving evaporator water temperature (°C)
$\overline{T}_{sw}$	=	average sea water temperature (°C)
$\overline{T}_{w,c}$	=	average tube wall temperature in condenser (°C)
$T_{w,e}$	=	average tube wall temperature in evaporator (°C)
$UA_{o,c}$	=	overall heat transfer coefficient times outside surface area (kW/°C)
$UA_{o,e}$	=	overall heat transfer coefficient times outside surface area (kW/°C)
v	=	specific volume (m^3/kg)
$\overline{V}_{chw}$	=	average chilled water velocity in an evaporator tube (m/s)
$\overline{V}_{sw}$	=	average sea water velocity in a condenser tube (m/s)
$\dot{W}_c$	=	compressor power (kW)
$\Delta T_{lm,c}$	=	log mean temperature difference in the condenser (°C)
$\Delta T_{lm,e}$	=	log mean temperature difference in the evaporator (°C)
ρ_{chw}	=	density of chilled water at average chilled water temperature (kg/m^3)
$\overline{\mu}_{chw}$	=	dynamic viscosity of chilled water at average chilled water temperature (kg/m-s)
$\mu_{w,e}$	=	dynamic viscosity of chilled water at average evaporator wall temperature (kg/m-s)
ρ_{sw}	=	density of sea water at average sea water temperature (kg/m^3)
μ_{sw}	=	viscosity of sea water at average sea water temperature (kg/m-s)
$\mu_{w,c}$	=	viscosity of sea water at average condenser tube wall temperature (kg/m-s)

ACKNOWLEDGEMENT

CHAPTER 1. INTRODUCTION

Fully halogenated chlorofluorocarbons (CFCs) are manufactured chemicals with properties that make them useful for such applications as aerosol propellants, foam blowing agents, solvents, and refrigerants for automotive, residential, and commercial applications. Introduced in the U.S. in the 1930's, the use of CFCs grew steadily after World War II and today they play a prominent role in human lifestyle and comfort. CFCs became popular in part because they were chemically stable, non-flammable, and non-toxic. Ironically, the chemical stability of CFCs is the cause for their present perceived threat to the environment. Scientific evidence suggests that the harmful alterations of the earth's atmosphere occurring from the use of CFCs are of regional and global proportions. As early as 1974, concerns about the potential harmful environmental effects associated with the use of CFCs were raised when it was suggested that the chlorine from these compounds could efficiently destroy stratospheric ozone [1]. Additionally, there is a growing consensus among scientists that CFCs may contribute to global warming [2]. In the 1970s, regulatory action banning selected, non-essential CFC compounds used as aerosol propellants temporarily decreased the release of chlorine-containing compounds into the atmosphere. However, the increased use of CFCs, in part by newly industrialized and lesser developed countries, has resulted in the need for stronger control measures. Moreover, hydrogenated chlorofluorocarbons (HCFCs), once thought to be an acceptable replacement for CFCs, have also been implicated as potentially harmful to the environment.

Significant steps have been taken to eliminate CFC and HCFC consumption including restrictive legislation, the development of alternative refrigerants, and the pursuit of new technologies. Policy makers, industry leaders, and researchers worldwide have recognized the need for continued efforts to understand the potential long range impacts that the use of these chemical compounds and their replacements may have on the environment, lifestyle, and economy: on environment, because climate changes and health problems could be significant; on lifestyle, because humans have come to appreciate and demand the comforts of air-conditioning and refrigeration; and on economy because of the potential need to redesign and replace billions of dollars of existing equipment and chemicals (refrigerants).

OZONE DEPLETION

Ozone exists naturally in the upper stratosphere and is a primary absorber of ultraviolet radiation. Ozone concentration determines the amount of ultraviolet radiation reaching the earth's surface. Ozone molecules are broken apart by high energy ultraviolet radiation from the sun and rapidly re-form to maintain a relatively stable level of ozone in the stratosphere. The presence of chlorine in the stratosphere disrupts this natural balance.

Chlorine from natural sources is washed out of the air by rain before it can migrate to the stratosphere. Methyl chloride, given off by ocean plankton, appears to be an exception; however, measurements show it accounts for only one sixth of the chlorine in the stratosphere [3]. Synthetic compounds such as chlorofluorocarbons, on the

other hand, make their way to the stratosphere and disrupt the natural balance of ozone by a series of rapid reactions. Intense ultraviolet light in the stratosphere splits apart the CFC molecule and releases a chlorine atom. The free chlorine radical reacts with ozone, breaking it into an ordinary oxygen molecule and forming a chlorine monoxide molecule. Chlorine monoxide can combine with a single oxygen atom to form a second oxygen molecule. The chlorine atom, freed in this reaction, can then repeat its ozone-destroying cycle a hundred thousand times before being converted to a less reactive form that is eventually removed from the stratosphere by natural processes [3]. Models that simulate this chain suggest that CFCs have long atmospheric lifetimes ranging from decades to centuries [1]. Because of this, it is estimated that concentrations of chlorine in the stratosphere will continue to increase for some period even after CFC emissions cease. The consequences of increased ultraviolet radiation reaching the earth's surface include negative impacts on human health and possible changes in aquatic and terrestrial ecosystems, the total ramifications of which are largely uncertain.

HCFCs retain many of the desirable properties of CFCs; however, as a result of the hydrogen in their molecular structure, they have much shorter lifetimes in the atmosphere. Consequently, their potential effects on ozone and the climate are significantly reduced compared with the compounds they replace. However, with increased use, they could significantly contribute to environmental problems. Hydrogenated fluorocarbons (HFCs), another alternative to CFCs, have no chlorine in their structure and consequently provide no contribution to ozone destruction.

Predicting trends in the ozone depletion rate is very difficult because local ozone concentrations vary with altitude, latitude, temperature, and seasonal changes; they are also affected by natural processes such as air currents. A scale has been developed, based on complex models, to attempt to compare the ozone depletion potential (ODP) of various compounds against CFC-12, which by definition has an ODP of one. For example, CFC-114 has an ODP of 0.7 and HFC-236ea has an ODP of 0. Table 1.1 includes a comparison of ODPs for refrigerants of interest in this study.

Table 1.1: Refrigerant comparisons[a]

	Current CFC Refrigerants		Potential Alternatives			
Refrigerant Designation	CFC-11	CFC-114	HCFC-124	FC-318	E-134	HFC-236ea
Chemical Formula	CCl_3F	$C_2Cl_2F_4$	C_2HClF_4	C_4F_8	$CHF_2\text{-}O\text{-}CHF_2$	$C_3H_2F_6$
Evaporator Pressure (kPa)	48.69	103.38	192.07	152.62	94.97	94.41
Condenser Pressure (kPa)	161.45	311.72	557.45	457.72	322.55	313.93
Flowrate (m^3/min/ton)	0.4517	0.2636	0.1433	0.1960	0.2413	
Power (kW/ton)	0.463	0.518	0.499	0.540	0.488	
Discharge Superheat (°C) or Quality (%)	-10.5 °C	96%	99%	90%	-16.4 °C	
Speed of Sound at Suction (m/sec)	134.7	115.2	128.3	120.1	141.7	122.8
Ozone Depletion Potential	1.0	0.7	0.02	0	0	0
Global Warming Potential	1.0	3.7	0.07	>1	low	low
Atmospheric Lifetime (yr)	75	200	8	>100	short	1.2
Acute Toxicity (1 = high, 6 = low)	5	6	6 ?	6 (est.)	6 (est.)	6 (est.)
Flammable	no	no	no	no	no	no

[a]Properties are from NIST REFPROP computer program version 4.01. Data are based on an evaporating temperature of 4.8°C, a condensing temperature of 38.1°C, and compressor and motor efficiencies of 100%.

GLOBAL WARMING

A natural energy balance exists in the earth and its atmosphere between absorption of solar radiation and emission of infrared radiation to space. Greenhouse gases in the atmosphere are relatively inefficient absorbers of incoming short wavelength energy but strong absorbers of outgoing infrared radiation. Greenhouse gases trap heat that would otherwise radiate from earth leaving the planet with a much colder average surface temperature than the planet's current average surface temperature of 288 K [2]. The concentrations of greenhouse gases in the troposphere determine the net trapping of heat in the atmosphere. To maintain a global energy balance, the likely effect of an increase in greenhouse gas concentrations is a change in atmospheric and surface temperature. Interestingly, in addition to absorbing ultraviolet radiation, ozone is also a greenhouse gas. An observed decrease

in stratospheric ozone over the last decade suggests a global cooling tendency. This cooling tendency, when globally averaged, is comparable in magnitude and opposite in sign to the estimated warming from increased CFC concentrations in the troposphere [2].

Greenhouse gases include water vapor, carbon dioxide, nitrous oxide, CFCs, HCFCs, HFCs, methane, and tropospheric ozone; each is an absorber in specific bands within the infrared spectrum. CFCs, HCFCs and HFCs happen to absorb energy in the wavelength window of 7 to 13 μm where the primary absorbers--carbon dioxide and water vapor--are weak radiation absorbers. Absorption in this region allows gases with much smaller atmospheric concentrations than carbon dioxide and water vapor to exert significant radiative forcing on climate resulting in linear increases in infrared absorption with increasing atmospheric concentration. In contrast, carbon dioxide, having a large atmospheric concentration, already absorbs essentially all of the radiation in the central cores of its absorption lines and will increase infrared absorbtion only slightly with further increased concentration [2]. In other words, comparable increases in the concentration of different greenhouse gases may have vastly different greenhouse effects.

Concern about potential global warming exists because there is a wide range of possible negative effects that include changes in sea level and changes in local climates--the consequences of which are not well understood. There are large uncertainties in predicting greenhouse effects. For example, a major source of uncertainty comes from a poor understanding of cloud dynamics. A scale has been developed to rate the global warming potential (GWP) of various refrigerants relative to the effects of carbon dioxide. Table 1.1 includes a comparison of the GWP for refrigerants of interest in this study.

While refrigerants escaping into the troposphere have a **direct** effect on global warming, fossil fuel energy consumed by refrigerant systems provides an additional **indirect** contribution to global warming by adding carbon dioxide to the atmosphere. Thus, system efficiency is an important consideration in determining the suitability of replacement refrigerants.

MONTREAL PROTOCOL

In September 1987, delegates to the United Nations Environment Program (UNEP) signed the Montreal Protocol for Substances that Deplete the Ozone Layer and, thereby, agreed to limit production of CFCs and halons. Spurred by alarming decreases in stratospheric ozone concentrations in the Antarctic region, UNEP delegates amended the Protocol in 1990 and again in 1992 to broaden the scope of substances covered and to accelerate their phase-out. Similar restrictions were enacted by the United States Congress in the 1990 Clean Air Act Amendments. The Department of Defense (DOD) and the Secretary of the Navy have also issued directives for the Navy's compliance with these policies [4]. Currently, CFCs are scheduled to be phased out of production completely by the end of 1995.

The Environmental Protection Agency has also finalized an accelerated schedule to phase out the production of HCFCs. The latest schedule is as follows:

- By 2003: Ban on production of HCFC-141b
- By 2010: Production frozen at baseline levels for HCFC-22 and HCFC-142b
- By 2010: Ban on use of virgin chemical unless used as a feed stock or refrigerant in appliances manufactured prior to Jan. 1, 2010, for HCFC-22 and HCFC-142b
- By 2015: Production freeze at baseline levels for all other HCFCs
- By 2020: Ban on use of virgin chemical unless used as a feed stock or refrigerant in appliances manufactured prior to Jan. 1, 2020, for all other HCFCs
- By 2020: Ban on production of HCFC-22 and HCFC-142b
- By 2030: Ban on production of all other HCFCs [5]

While these measures were initiated in response to evidence of ozone destruction, a similar movement is underway that may lead to an international protocol regarding the use of substances that contribute to global warming. This could affect the future use of HFCs that currently have no restrictions placed on them.

REFRIGERATION INDUSTRY'S RESPONSE

The refrigeration industry has responded to restrictions on the production of CFCs and HCFCs by developing new environmentally safe refrigerants and refrigerant mixtures with similar thermodynamic and heat transfer characteristics. These alternatives will serve as near term substitutes for existing air-conditioning and refrigeration equipment with remaining useful life. Additionally, new emphasis is being placed on research and development of cooling systems based on emerging new technologies, including alternatives to typical vapor-compression systems. Thus, a two-fold challenge to the refrigeration industry entails replacing CFC refrigerants in existing equipment in the near term, and designing efficient, environmentally safe cooling systems for the future. The urgency of the situation has been emphasized by the series of accelerations to the original phase-out schedule put forth in the Montreal Protocol.

The success of HFC-134a as a replacement for CFC-12 provides an example of the rapid progress that has been made toward replacing refrigerants targeted for elimination, but also illustrates some of the problems encountered along the way. HFC-134a has emerged as a near drop-in replacement for existing CFC-12 systems. Its success has resulted in commercial availability in new products such as new air conditioners for cars. A "drop-in" replacement implies that only minimal and low-cost changes will need to be made in order for the refrigeration system to accept a new refrigerant; this poses several challenges in finding an appropriate alternative refrigerant.

Similar thermodynamic and heat transfer properties are desired which will minimize the changes in efficiency, power consumption, size, volume, and operating pressures of the original system. Similar refrigerant properties will also minimize the need to make costly modifications to the system components such as the heat exchangers and compressors. Material compatibility is a concern because different refrigerants may not be compatible with seals, gaskets, diaphragms, and flexible hoses in the original system. This is also of concern when changing lubricants. Finally, the conversion process itself may be restricted by the nature and importance of the application. For example, a supermarket or a hospital may have to plan carefully so as not to interrupt critical cooling while conversions to a new refrigerant are being made.

While the intense effort to replace CFC-12 has been successful, there is a need to find replacements for other CFCs that are not as widely used, yet are included in the world wide CFC ban. One such refrigerant that needs a suitable replacement is CFC-114, whose characteristics make it favorable for use on Navy ships and submarines.

CFC-114 AND THE U.S. NAVY

CFC-114 has been in use on Naval ships since 1969 and has demonstrated excellent reliability. However, design improvements have often lagged behind commercial advancements in compressor technology, advanced heat transfer surface technology, and intelligent control system technology. It is costly and difficult to keep up with commercial advancements when the Navy uses CFC-114 and the much larger shipping industry uses CFC-11. The Navy, however, has made significant progress in recent years in advanced heat transfer surface technology [6]. CFC-11 was found to be unsatisfactory to the Navy because of problems unique to ship and submarine application. For example, CFC-11 operates at sub-atmospheric pressures and therefore is subject to air and water vapor infiltration leading to corrosion of system components. Additionally, CFC-11 decomposes at high temperatures causing toxicity problems on submarines as the air is recycled in high temperature air purification equipment. In contrast, CFC-114 operates at approximately atmospheric pressure and remains stable at high temperatures.

Some of the Navy's unique requirements include the need for small refrigerant inventory and small components due to space constraints. Efficiency has been a low priority in the past but with shrinking defense budgets it has become more important. Additionally, ships and submarines need to operate silently in tactical situations and recycle air in living spaces. Cooling systems must be able to operate at as low as 10% of maximum capacity during normal peacetime operations yet handle a dramatic increase in load when firing weapons in combat or training situations. Fully halogenated refrigerants, such as CFC-114, generally exhibit the best compatibility and impose the least restriction in choice of materials; a suitable replacement must display similar material compatibility. Other requirements for a suitable replacement include meeting safety and environmental standards for toxicity, flammability, ODP, and GWP.

The Navy will likely design new cooling systems with HFC-134a. However, a need still exists for a suitable near term replacement for existing equipment using CFC-114. Because industry's attention has been focused on CFC-11 and CFC-12 replacements, the Navy must devote substantial resources to address the CFC-114 problem. Current potential alternatives for CFC-114 are not well developed and substantial modifications to system equipment will likely be necessary in order to accommodate them. For example, HCFC-124 operates at much higher condenser pressures than CFC-114 requiring impeller and heat exchanger modifications.

FLUORINATED HYDROCARBONS

At one time, HCFC-123 and HCFC-124 were leading alternatives for CFC-11 and CFC-114, respectively. When it became apparent that these HCFCs would also be phased out as environmentally unsuitable, the EPA began investigating "back up" alternatives [7]. As a result, a series of propanes have emerged as candidate replacements for CFC-114.

The EPA set selection criteria that considered thermodynamic properties, GWP, ODP, ease of manufacture, toxicity, and flammability and then decided to pursue fluorinated ethers and fluorinated propanes. One of the replacement candidates screened, namely HFC-236ea, is the focus of this study. HFC-236ea appears to be less toxic than CFC-114, is miscible with polyolester oils, is not flammable, has a 1.2-year atmospheric lifetime and has a known method of production from hexafluoropropylene. Initial modeling by the EPA predicts performance to be within 1% of CFC-114. However, prior to the present study there were no data available for the performance and heat transfer characteristics of HFC-236ea in a typical shipboard chiller. Design changes to the Navy's existing equipment will likely be required in order to accommodate HFC-236ea or any other alternative refrigerant. A simulation of a typical shipboard chilled water system was therefore deemed useful for future design and optimization of Navy chillers.

SUMMARY

The United States Navy presently uses CFC-114 as the working fluid in water chillers used for electronics and space cooling. With a mandatory phase-out of CFCs in place, it is necessary to replace CFC-114 in these shipboard chillers with an alternative refrigerant that does not contribute to ozone depletion or global warming. Of special importance to the Navy is finding a replacement refrigerant that is non-toxic because of the closed environments aboard ships and submarines. In addition, energy efficiency is important because space-consuming fuel must be carried aboard ships during deployment. Finally, reliability and material compatibility are important for the replacement refrigerant because of the need for combat readiness and the fact that ships are commonly deployed away from repair facilities.

HFC-236ea is a promising candidate for replacing CFC-114 for several reasons. First, unlike other replacements such as E-134, there is currently a commercial production route available for large quantities through the use of hexafluoropropylene. Second, initial modeling conditions appear very favorable as a drop-in substitute, with modeled performance being within 1% of CFC-114 and operating capacities, pressures, and temperatures matching closely [7]. Flammability tests, materials compatibility tests, and oil miscibility tests appear highly favorable. Preliminary results indicate that HFC-236ea is miscible with a commercial polyolester oil and is not flammable. Material compatibility testing confirms HFC-236ea and a polyolester oil in the presence and absence of water to be compatible with aluminum, steel, copper, Mylar, Nomex, Viton and Buna-N. Acute inhalation test results indicate lower acute toxicity than CFC-114, which minimize long term effects on the environment. In addition, estimates predict that HFC-236ea has a short atmospheric lifetime.

CHAPTER 2. CONCLUSIONS

The Montreal Protocol began a worldwide drive to eliminate the production of chloroflourocarbons which are thought to be harmful to the environment. As a result of the restrictive legislation that followed, there is an immediate need to replace CFC-114 which is used extensively on United States Navy's ships and submarines. Preliminary research conducted by the United States Environmental Protection Agency suggested that HFC-236ea might perform suitably as a near term drop-in replacement for CFC-114. However, at the time of this study, heat transfer data for HFC-236ea were not available.

For this reason, a computer model was developed for comparing these two refrigerants in a simulated 125-ton centrifugal chiller system representative of those found in the U.S. fleet. The model is semi-empirical, combining thermodynamic and heat transfer theory, as well as boiling and condensing heat transfer coefficient data measured at the Iowa State University Heat Transfer Test Facility.

The Naval Surface Warfare Center in Annapolis, Maryland also provided data for this study. A 440-kilowatt laboratory centrifugal air conditioning plant and HFC-236ea were used for the data collection. The experimental data provided by the Naval Surface Warfare Center were compared with the modeled predictions.

The model was tested for a range of inlet condenser water temperatures, entering and leaving chilled water temperatures, and evaporator and condenser water flow rates. The simulation model predicts that HFC-236ea would perform favorably as a drop-in substitute for CFC-114.

Additionally, several recommendations were provided for improved performance using HFC-236ea in centrifugal chiller systems. Design recommendations discussed in this study include manipulating the evaporator load to achieve positive gage refrigerant pressure, ensuring the absence of non-condensable gases in the system, using a variable speed compressor with a fixed inlet guide vane angle to the impeller, conducting further research using azeotropic mixtures with HFC-236ea as the major component, and installing high performance enhanced surface tubes in both the evaporator and the condenser.

In conclusion, the simulation developed in this study provides results that are consistent with the expected behavior of a 125-ton refrigeration system. The results provided by the Naval Surface Warfare Center sufficiently validate the model. Finally, the results suggest that HFC-236ea would perform well in existing CFC-114 centrifugal chillers, although design modifications should be considered for optimal performance.

CHAPTER 3. RECOMMENDATIONS

One way to improve the performance of the fleet 125-ton chiller and allow the use of HFC-236ea as an alternative working fluid is to reduce the load on the evaporator by increasing the temperatures of the chilled water entering and leaving the evaporator by a few degrees. This would allow the refrigerant temperature in the evaporator to come up slightly, which in turn would result in an evaporator pressure that is above atmospheric pressure. With a positive gage pressure in the evaporator, there is less possibility of non-condensable gases and contaminants to leak into the system where they can accumulate in the condenser and reduce performance. The low evaporator temperatures and high condenser temperatures reported by the NSWC suggest the possibility of this occurrence. This proposed solution avoids the cost of redesigning system components.

A purge device should also be installed at the highest point of the condenser to allow purging of non-condensable gases that might accumulate there. If non-condensables is a persistent problem, the purge unit may be malfunctioning or the system may have an air leak larger than the purge unit can handle.

A variable speed compressor would eliminate the need for hot gas by-pass or the extensive use of inlet guide vanes in the compressor to control the refrigerant flow. A variable speed chiller would allow the maximum system performance to be realized over a broad range of operating conditions resulting in maximum energy savings.

Another possible improvement might be to mix HFC-236ea with other non-CFC refrigerants to form an azeotropic mixture with properties that allow the saturation point in the evaporator to stay above atmospheric pressure. The mixture could be chosen so as to maintain the positive properties of HFC-236ea.

Additionally, better performance in the Navy's fleet air conditioning units could be realized by investing in commercially available high performance tubes. While not reported in this study, Turbo B tubes were simulated with CFC-114 and HFC-236ea under fleet design conditions and were predicted to perform significantly better than 10.23 fins per centimeter tubes in both the evaporator and in the condenser.

Finally, the model predicts that HFC-236ea used as a drop-in substitute for CFC-114 without any design modifications may result in energy savings. The model predicts that for any set of conditions, the power required for a refrigeration cycle using HFC-236ea as a drop-in will be significantly less than the same cycle using CFC-114 as the working fluid. The predicted savings in power consumption by using HFC-236ea at the design point of operation is 8.6% which is equal to a 550 kW. If HFC-236ea is to be used only as a near term replacement, it may be appropriate to use it without making any significant design changes to the system.

CHAPTER 4. REVIEW OF RELATED LITERATURE

The vapor-compression cycle is the most widely used cycle for refrigeration and air-conditioning. Past investigators have studied the vapor-compression system from both theoretical and experimental points of view. These past studies have been aimed at understanding the behavior of each of the components of a system. Theoretical studies are usually carried out with the aid of modeling techniques that make use of digital computers. As computers have become more powerful, these models have become progressively more detailed.

Many studies of the vapor-compression cycle have focused on modeling reciprocating compressors. Threlkeld provides an example of theory for a simple model of a compressor piston assembly that can readily be written into computer code [8]. This was accomplished in a study by Smith et al. in which several variations of a vapor-compression cycle were modeled in an interactive computer program particularly designed for student use as an investigative tool [9].

Due to the complexity of fluid behavior in a centrifugal compressor, there are few reports of successful computer modeling efforts found in the literature. Some examples are discussed in this chapter. Table 4.1 compares the models mentioned below, highlighting some of the important characteristics of each.

Braun et al. developed a mechanistic model of a centrifugal chiller operating with variable-speed capacity control [10]. The model utilizes mass, momentum, and energy balances on the compressor, evaporator, condenser, and expansion device. Given a chilled water setpoint temperature and entering chilled and condenser water temperatures and flow rates, the model predicts both the required compressor speed and power consumption. The model was compared with performance data for a 5500 ton variable-speed centrifugal chiller at the Dallas/Fort Worth airport. This model requires empirically derived constants to characterize the compressor.

A computer simulation model was developed by Jackson et al. to analyze the performance of a water-cooled, variable-speed centrifugal chiller with hot gas bypass option for capacity control [11]. The model is based on thermodynamic principles and empirical correlations and was calibrated using available capacity test data. The performance of the chiller at various conditions and design modifications was predicted using the calibrated model and results of the parametric performance study were presented. The model requires a compressor map and other empirically derived constants.

Wong and Wang developed a model of a two-stage centrifugal chiller using a water-cooled condenser and CFC-11 as the refrigerant [12]. The heat exchangers were modeled as a shell-and-tube type. The centrifugal chiller was driven by a hermetic motor, and capacity was controlled by the use of inlet guide vanes at the inlet of the first and second-stage impeller. The model was structured such that the load ratio and the entering temperature of condenser water were the two independent variables. The model depends on compressor performance maps and other empirically obtained inputs. The results of the model were compared with actual operating results.

Table 4.1: Comparison of models found in the literature

Author	Type of Model	Compressor Analysis	Type of Compressor	Type of Condenser	Refrigerant
Smith et al.[9]	theoretical	isentropic	reciprocating	no restriction	12, 22, 502
Braun et al.[10]	semi-empirical	polytropic	centrifugal	water cooled	12, 22, 500,
Jackson et al.[11]	semi-empirical	isentropic	centrifugal	water cooled	114
Wong and Wang [12]	semi-empirical	isentropic	centrifugal	water cooled	11
Domanski and McLinden [13]	theoretical	isentropic	reciprocating	air cooled	mixtures -
Barc [7]	theoretical	isentropic	n/a	no restriction	propanes and ethers

A simulation program, "CYCLE11" was developed by Domanski and McLinden [13]. This model simulates vapor-compression cycles in a heat pump and in a refrigerator. The model requires the input of an average effective temperature difference representing a generalized temperature difference between the heat transfer fluids in the heat exchangers. The model utilizes the Carnahan-Starling-DeSantis equation of state which provides the thermodynamic properties for several refrigerants and refrigerant mixtures.

Chlorine-free fluorinated ethers and fluorinated hydrocarbons were studied by Barc as potential long-term replacements for CFC-11 and CFC-114 [7]. A model was used to predict the performance of these chlorine-free compounds in a variety of refrigeration applications. The model utilizes the Carnahan-Starling-DeSantis equation of state and allows analysis of a simple theoretical vapor compression cycle. The model predicts that HFC-236ea will perform within 1% of CFC-114 based on a thermodynamic analysis only. All simulations were based solely on thermodynamic properties and analyses; transport properties were not included in the model and heat transfer effects were not taken into account.

CHAPTER 5. VAPOR-COMPRESSION CYCLE

There are many types of refrigeration cycles that perform the function of removing heat from a region of low temperature and discharging this heat to a region of higher temperature. Examples of these cycles include air, steam-jet, absorption, thermoelectric, and vapor-compression refrigeration cycles. All of the above cycles have been described and compared in detail by Gauger et al., 1995 [14]. Of these cycles, the vapor-compression refrigeration cycle is the most commonly used system in commercial and residential applications.

The vapor-compression cycle is characterized by a working fluid that is vaporized, compressed, condensed, and expanded in a complete cycle. The basic components of this closed system are shown in Figure 5.1 and include two heat exchangers, a compressor, and an expansion device. Also shown in the figure are the work and heat transfers, which are positive in the direction of the arrows.
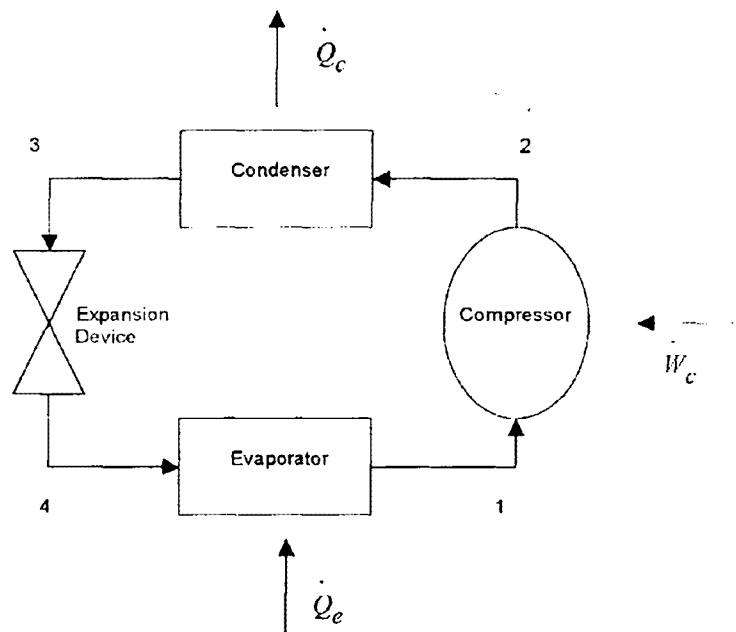
Figure 5.1: Components of a vapor-compression refrigeration system

The refrigerant vapor is moved by the compressor to the condenser where it is de-superheated, condensed and possibly subcooled by heat transfer to a circulating coolant. The liquefied refrigerant then moves through an expansion device where the pressure is reduced and the liquid partially flashes into vapor, thereby lowering its temperature. The two-phase mixture then flows through the evaporator, where it is fully evaporated and slightly superheated, while absorbing heat from the fluid to be cooled by the cycle. The low-pressure refrigerant vapor leaving the evaporator is then drawn to the compressor and the cycle is repeated.

13

The simple vapor-compression cycle is better understood with the aid of a temperature-entropy diagram. In Figure 5.2, a typical simple vapor-compression cycle is represented by the path 1-2-3-4-1. The compressor receives low-pressure refrigerant vapor and compresses it adiabatically and reversibly. The high-pressure, superheated vapor enters the condenser and condenses at constant pressure to a liquid. Irreversible and adiabatic expansion takes place in the expansion device, and the resulting low pressure refrigerant absorbs heat in the evaporator at constant pressure to complete the cycle.
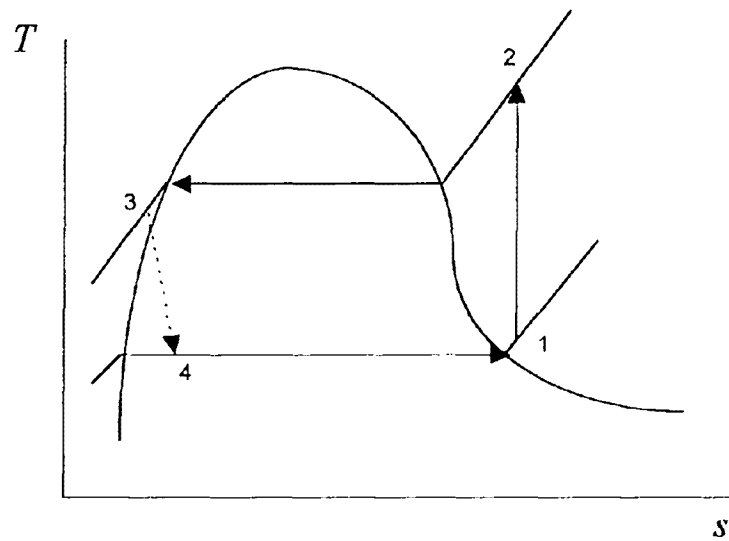
Figure 5.2: T-s diagram of a typical vapor-compression refrigeration cycle

Some differences between ideal and actual refrigeration systems are briefly discussed below.

- In an ideal cycle, the refrigerant vapor leaving the evaporator is often assumed to be saturated vapor. In an actual cycle, refrigerant vapor leaving the evaporator is superheated a few degrees to add a safety margin in avoiding the undesirable effects of wet compression.

- Similarly, the refrigerant liquid leaving the condenser is often assumed to be saturated liquid. However, the refrigerant liquid leaving the condenser is preferably subcooled.

- Ideal cycle heat transfer processes in the evaporator and condenser are internally reversible. In an actual cycle, however, friction causes pressure drops in the heat exchangers as well as local temperature differences. External irreversibilities require that a finite temperature difference between heat transfer fluids and the refrigerant exist to allow heat transfer. This is illustrated in Figure 5.2 where the warm region (heat sink) may

be a heat transfer fluid flowing through the condenser to which heat is rejected. Likewise, the cool region (heat source) may be another heat transfer fluid circulating through the evaporator which absorbs heat from the refrigerant.

- The ideal compressor operates reversibly and adiabatically, whereas the real compressor experiences friction, heating, and irreversibility.

- No state changes in the working fluid occur except in the components in an ideal cycle. In reality, pressure drops occur in the long suction and discharge line piping resulting in increased compression work.

- In an ideal cycle, components including the compressor and the suction and discharge lines are assumed to be isentropic (reversible adiabatic). However, in a real cycle, heat transfer occurs between system components and their surroundings.

- In an idealized model and in this study, changes in kinetic or potential energies throughout the system are assumed to be negligible.

- Finally, ideal cycle components operate at steady state while actual systems experience transient effects.

The following is a brief discussion of the major components of a vapor-compression system including the condenser, evaporator, compressor, and expansion device. The discussion includes an explanation of the assumptions made in modeling these components in this study.

CONDENSER

The condenser receives superheated vapor from the compressor, removes the superheat, and then liquefies the refrigerant. Different types of condensers include air-cooled, water-cooled, and evaporative condensers. A water cooled, shell-and-tube condenser is modeled in this study. When adequate low-cost condensing water is available, water-cooled condensers are often desirable because lower condensing pressure and better control of the discharge pressure is possible. Water, especially when obtained from underground sources or a big heat sink, such as the ocean, is usually much colder than daytime ambient air temperatures. Because of the excellent heat transfer characteristics of water, water-cooled condensers are usually quite compact. A shell-and-tube condenser acts as both a condenser and a liquid receiver. It is constructed of a vessel having a refrigerant inlet and outlet. An example of a typical shell-and-tube condenser is shown in Figure 5.3.

The condenser modeled in this study is assumed to be internally reversible. The specifications provided by the NSWC include the following: The shell consists of 246 copper finned tubes at 10.23 fins per centimeter (26 fins per inch). The water on the tube-side makes two passes through the shell. The shell is 55.88 centimeters outside diameter (OD) and 237.49 centimeters in length. The effective tube length is 220.31 centimeters and the average tube outside surface area-to-length ratio is 0.64. Based on this information, the calculated outside surface area is 105.81 square meters.

Figure 5.3: Diagram of a typical shell-and-tube condenser

EVAPORATOR

The evaporator in a refrigeration system is a heat exchanger that removes heat from the space or heat transfer fluid being cooled. A flooded shell-and-tube evaporator is modeled in this study. Flooded systems operate with a definite liquid refrigerant level in the evaporator. This liquid refrigerant level is maintained in the evaporator through the action of a refrigerant flow control device. There are several advantages of the flooded system over other systems. A few of these advantages are: higher efficiency, lower operating costs, less cycling, higher rate of heat transfer, and closer control of temperature. More liquid on the low-pressure side of the system, as in the flooded system, provides a greater area of wetted surface and allows a higher rate of heat transfer through the evaporator walls and tubing. An example of a typical shell-and-tube flooded evaporator is shown in Figure 5.4.

The specifications provided by the NSWC for the evaporator of interest in this study are similar to those for the condenser mentioned above. The evaporator is assumed to be internally reversible. The shell holds 246 copper, 10.23 fins per centimeter tubes. The water flowing through the tubes makes two passes through the shell. The shell's outside diameter (OD) is 81.28 centimeters and its length is 237.49 centimeters. The effective tube length is 220.31 centimeters and the average tube outside surface area-to-length ratio is 0.64. Based on this information, the calculated outside surface area is 105.81 square meters.
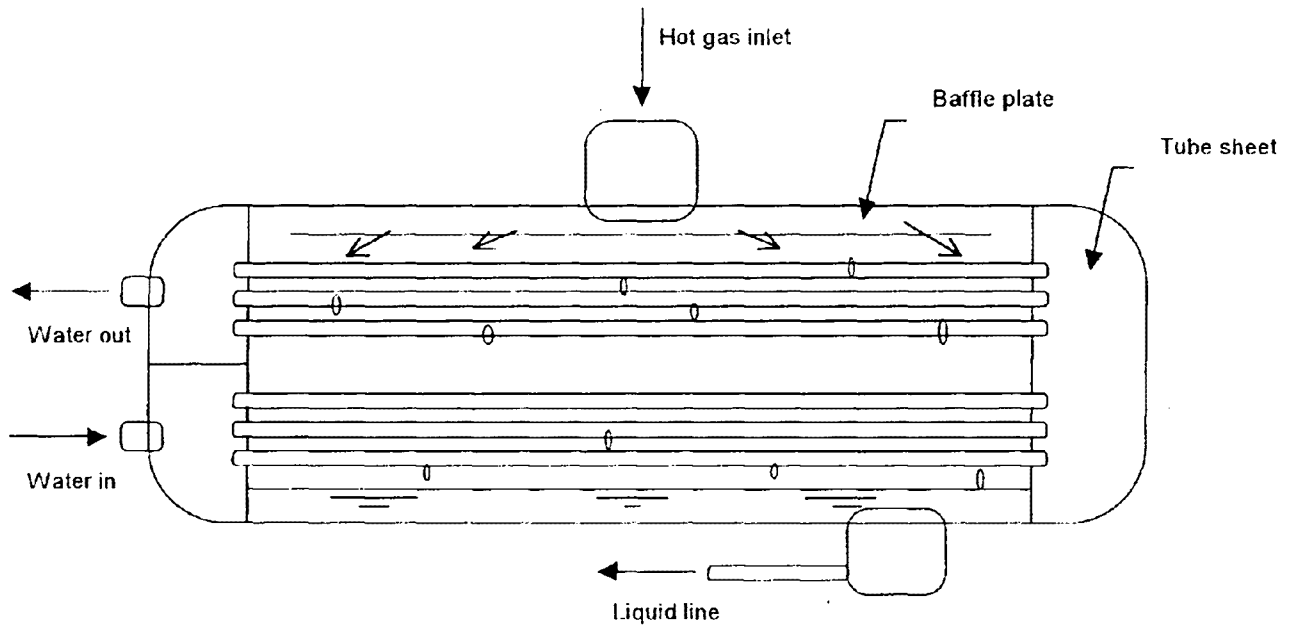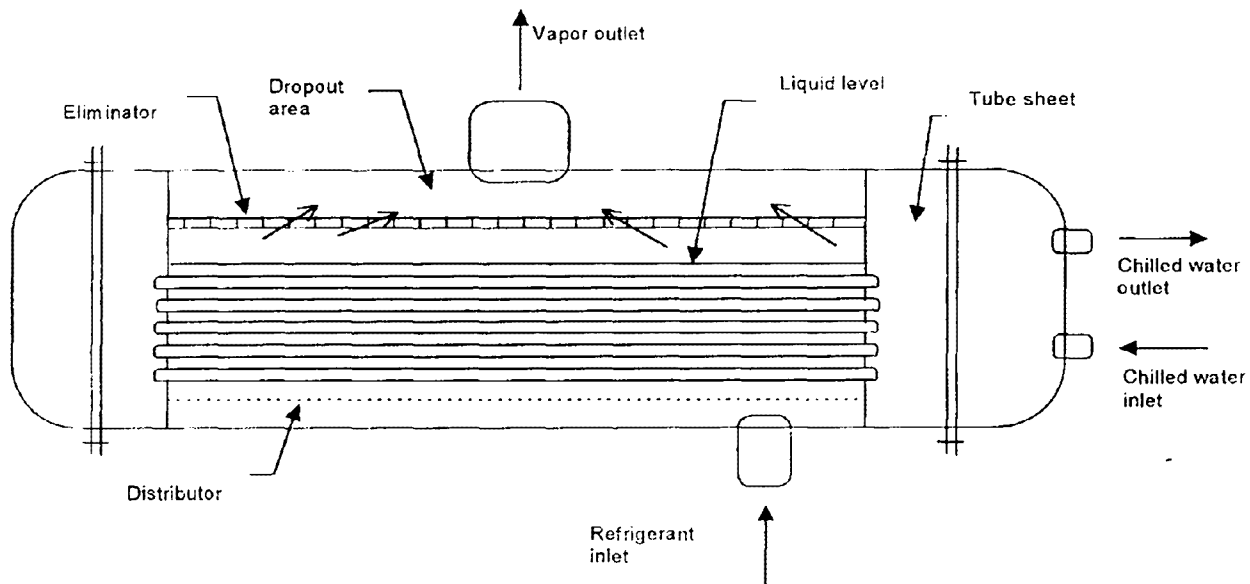
Figure 5.4: Diagram of a typical shell-and-tube flooded evaporator

COMPRESSOR

The compressor draws vapor from the suction line or accumulator, compresses it to a higher temperature and pressure, and then discharges the superheated vapor into the condenser. Types of compressors include reciprocating, rotary, helical rotary (screw), and centrifugal. In reciprocating and rotary compressors, the refrigerant molecules are squeezed together inside the cylinder by the positive action of the piston or rotor. Compression is produced and maintained by the action of the suction and discharge valves. In contrast, centrifugal compressors are characterized by a continuous exchange of momentum between an impeller and a steadily flowing fluid. Pressure is produced when gaseous refrigerant, whirled at a high rate of speed, is thrown outward by centrifugal force and caught in a channel. The centrifugal compressor is the dominant type of compressor used in large installations and is the type modeled in this study.

Centrifugal compressors are in the family of turbomachines, which also include fans, propellers, and turbines. Because their flows are continuous, they have large volumetric capacities. Multiple stages can be installed to increase the pressure lift of the compressor. Centrifugal compressors are efficient and well suited for large capacity refrigerating plants ranging from 175 to 10,500 kilowatts [15]. They are efficient at a wide range of operating temperatures. Because they are not positive-displacement type compressors, they are flexible under varying load conditions and operate at good efficiencies even when the demand is less than 40% of their designed capacity [16].

17

Although centrifugal compressors require high rotative speeds, there is minimal wear and vibration due to the lack of contact between moving parts. Lubrication is not needed at any place on the centrifugal compressor except at the end bearings of the shaft. Since these end bearings are the only internal friction surfaces, the refrigerant vapor compressed by a centrifugal compressor is free from oil, giving it the advantage of preventing an accumulation of oil on the heat transfer surfaces of the condenser and evaporator.

The compressor modeled in this study is assumed to follow a reversible polytropic process. A constant polytropic exponent, $n = 1.04$, is assumed based on an average value calculated from a representative sample of performance data provided by the NSWC. The compressor specifications provided by the NSWC include the following: the compressor is an open, single-stage, centrifugal compressor-motor driven unit in a refrigeration system having 125 tons of cooling. The compressor is direct-driven through a torque meter station and operates at an impeller speed of 11,918 revolutions per minute through an internal compressor gear arrangement.

EXPANSION DEVICE

The expansion device regulates the flow of refrigerant from the high-pressure to the low-pressure side of the system. Some common types of flow control devices include orifices, capillary tubes, high pressure float valves, and thermostatic expansion valves. Capillary tubes are passive devices, common for small applications such as domestic refrigerators. A thermostatic expansion valve controls the degrees of superheat at the evaporator outlet. An adjustable orifice is modeled in this study as a throttling process.

An orifice is a refrigerant flow control device used to control the refrigerant level in the flooded evaporator. Orifices and capillary tubes perform basically the same function, and they are practical only for systems which operate at nearly constant capacity. They are sized to pass refrigerant liquid at a slightly greater rate than desired for the pressure difference available. This results in exhausting the liquid supply in the condenser. The disadvantage of this type of control is that it allows some gas to leave the condenser and carries additional enthalpy to the evaporator. This loss is not large in a reasonably constant capacity system. The low-cost, simplicity, and dependability of this type of liquid feed control more than compensates for its slight inefficiency in centrifugal chilled water systems. For the purpose of this study, it is assumed that the oriface is ideal and that the liquid leaving the condenser is slightly subcooled.

CHAPTER 6. MODEL DESCRIPTION

A computer program has been developed that simulates the performance of a 440-kilowatt capacity, single-stage, centrifugal, chilled water air-conditioning plant. The design conditions shown in Table 6.1 are based on the design of a typical air-conditioning plant in use on Navy ships and submarines.

Table 6.1: Simulated design conditions

Component	Design Condition	Value
Evaporator	chilled water flow rate	28.4 l/s
Evaporator	entering chilled water temperature	10.7 °C
Evaporator	leaving chilled water temperature	7.0 °C
Condenser	water flow rate	31.5 l/s
Condenser	entering water temperature	31.4 °C

Given the entering and leaving temperatures of the chilled water, the entering temperature of the condenser water, and the flow rates of the chilled water and condenser water, the model predicts the required compressor power and the saturation temperatures in the heat exchangers. With knowledge of fluid properties and tube geometries, the performance of the system with different refrigerants and enhanced surface tubes can be compared under similar operating conditions. For the purpose of this study, the model is used to compare refrigerants CFC-114 and HFC-236ea using 10.23 fins per centimeter tubes in the condenser and evaporator. The results are presented in the next chapter.

The model allows imposed evaporator superheat and imposed condenser subcooling. If wet compression is encountered during the iteration procedure, the model adjusts the degrees of superheat just enough to stay in the dry region. The compressor is modeled using a polytropic analysis [17]. The polytropic exponent is estimated from data provided by the Naval Surface Warfare Center and is assumed constant at $n = 1.04$. The externally adiabatic heat exchangers are assumed to be internally reversible. Heat transfer coefficients are provided from heat flux data taken on a single tube testing facility at Iowa State University. The throttling process is assumed to be adiabatic and irreversible. An iteration procedure is used to solve for the evaporator and condenser saturation temperatures.

PROPERTIES

Properties for this simulation are estimated using subroutines from a computer program, "REFPROP" version 4.01, developed by the National Institute of Standards and Technology [18]. The utility of REFPROP includes the ability to estimate thermodynamic and transport properties for refrigerant mixtures of up to five components using the Carnahan-Starling-DeSantis equation of state. For pure refrigerants, such as CFC-114 and HFC-236ea, the REFPROP subroutines calculate properties using an extended corresponding states model. In this model, the properties of a range of related fluids are scaled to a well characterized reference fluid, HFC-134a. The transport properties of thermal conductivity and viscosity, which are important in calculating heat transfer coefficients in the heat exchangers, are also calculated using an extended corresponding states model [18, 19].

This study is limited to a comparison of two pure refrigerants, namely CFC-114 and HFC-236ea. However, by using REFPROP subroutines, other pure refrigerants or refrigerant mixtures supported by REFPROP may be simulated as the working fluid in the refrigeration system of this study within the constraints of the laws of thermodynamics. Thus, it is a useful tool in evaluating alternative non-CFC refrigerants in existing systems and would also be a useful tool in future simulations of innovative vapor-compression cycles.

PROGRAM DESCRIPTION

A complete listing of the Fortran code for the main program is included as Appendix A. A description of the main program structure is described in the paragraphs that follow. Throughout the description, both the numerical procedure and the modeling theory are discussed in detail. Figure 6.1 is a flow diagram of the computer program. Common blocks and dimension statements are set up for use with REFPROP subroutines and Newton-Raphson subroutines. A series of data statements and input prompts are used to identify the design conditions, initial temperature estimates, and tube geometries. REFPROP subroutines are then initialized by identifying the number of components, mixture composition, component names, and the choice of computational model. Additionally, the reference values for enthalpy and entropy are selected. Subroutine BCONST is then called to set up equation-of-state parameters from stored property data. All units for REFPROP subroutines are specified using the International System of Units (SI). After the program is initialized, simulation conditions are selected and varied over an appropriate range of operating conditions. Default values for the model are equivalent to fleet design conditions and are listed in Table 6.1.
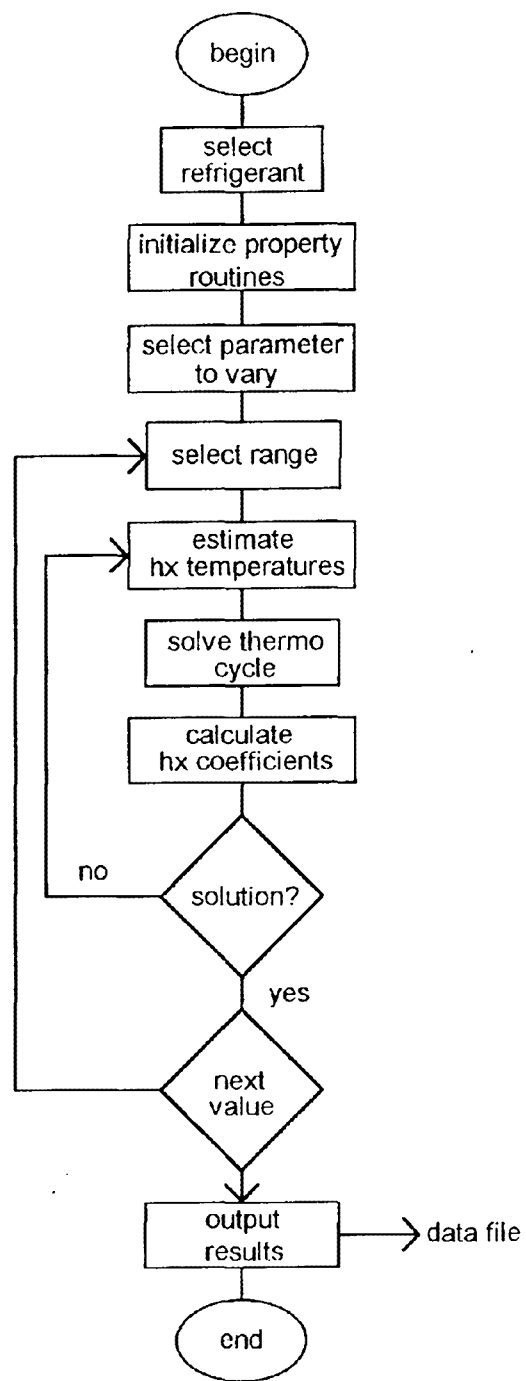
Figure 6.1: Program flow diagram

THERMODYNAMIC ANALYSIS

Each of the four basic components of a vapor-compression system--namely the compressor, the condenser, the expansion device, and the evaporator--has its own peculiar behavior. At the same time, each component is influenced by conditions imposed by the others. For example, a change in the condenser water temperature may change the rate of refrigerant flow, which in turn may cause the heat exchanger temperatures and pressures to change as well as change the power required to the compressor. This study models the individual components of the vapor-compression cycle and also observes how they interact with each other as a system.

Pressure (P) and enthalpy (h) are two properties that may conveniently represent a vapor-compression system. A P-h diagram for refrigerants CFC-114 and HFC-236ea is shown in Figure 6.2. Simple vapor-compression cycles for CFC-114 and HFC-236ea at fleet design conditions are also shown in Figure 6.2. Four state points for each cycle are identified respectively as: (1) evaporator outlet and also compressor inlet, (2) compressor outlet and also condenser inlet, (3) condenser outlet and also expansion device inlet, and (4) expansion device outlet and also evaporator inlet. Often, when modeling a simple vapor-compression cycle, superheat at the evaporator outlet (state 1) and subcooling at the condenser outlet (state 3) are either imposed or assumed to be zero. Superheat at the compressor inlet is normally desired to avoid the occurrence of "wet compression" which degrades system performance and may cause damage to the compressor impeller over time. Subcooling at the condenser outlet is beneficial to the performance of the system because it allows a greater enthalpy difference across the evaporator resulting in greater cooling capacity. Constant pressure is often assumed in both heat exchangers and in the suction and discharge lines to the compressor, although in reality the irreversible nature of the processes in these components will result in slight pressure differences.

With initial estimates of saturation temperatures for the evaporator and condenser, all remaining thermodynamic and transport properties of interest can be calculated for the cycle modeled in this study. Much of the theory for the thermodynamic analysis that follows is discussed in more detail in Moran and Shapiro [20].

State point (1) is defined as saturated vapor at the estimated refrigerant temperature in the evaporator. The state of the pure refrigerant is thereby fixed, and the remaining thermodynamic properties of interest including pressure, enthalpy, and specific volume are calculated using property subroutines.

$$P_1 = f1 \, (T_e) \qquad\qquad (6.1a)$$

$$h_1 = f2 \, (T_e) \qquad\qquad (6.1b)$$

$$v_1 = f3 \, (T_e) \qquad\qquad (6.1c)$$

Similarly, the outlet of the condenser is defined as state point (3) and is fixed by the estimated temperature of the condenser at the saturated liquid point. The pressure and enthalpy are then determined with equation of state calculations.

$$P_3 = f4\,(\,T_c\,) \qquad\qquad (6.2a)$$

$$h_3 = f5\,(\,T_c\,) \qquad\qquad (6.2b)$$
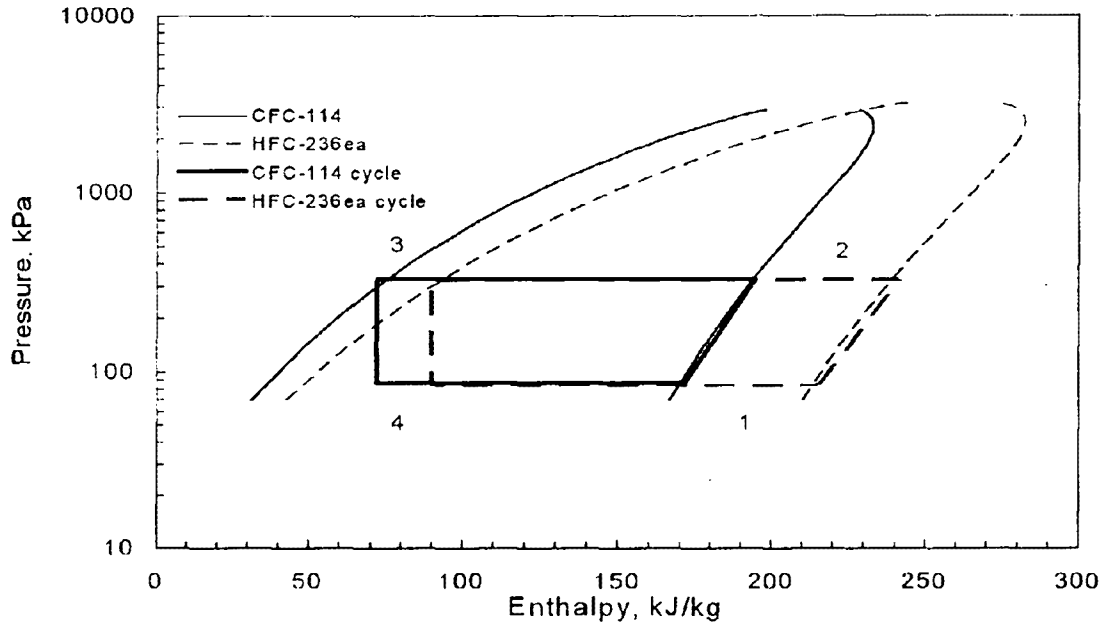
Figure 6.2: *P-h* diagram for CFC-114 and HFC-236ea

The outlet to the compressor, state point (2), is next determined by the polytropic relationship.

$$v_2 = v_1 \left(\frac{P_1}{P_2}\right)^{(\,1/n\,)} \qquad\qquad (6.3)$$

The polytropic exponent, n, is assumed constant at $n = 1.04$ based on data from an operational 125-ton air-conditioning plant. The condenser pressure, $P_2 = P_3$, corresponds to the estimated refrigerant saturation temperature in the condenser. The two independent properties v_2 and P_2 fix the state point at (2) and the remaining thermodynamic properties of interest, temperature and enthalpy, are calculated using REFPROP.

$$T_2 = f6\,(\,P_2, v_2\,) \qquad\qquad (6.4a)$$

$$h_2 = f7\,(\,P_2, v_2\,) \qquad\qquad (6.4b)$$

The inlet to the evaporator, state point (4), is determined by assuming adiabatic expansion through an adjustable orifice resulting in a constant enthalpy process.

$$h_4 = h_3 \qquad\qquad (6.5)$$

The pressure at state point (4) corresponds to the estimated saturation temperature of refrigerant in the evaporator, and the state is fixed in the two-phase region. The basic thermodynamic properties of each state point of the refrigeration system are known based on estimated saturated temperatures of the evaporator and condenser, and on a constant polytropic exponent obtained from performance data. Energy balances are used along with minimum input design conditions to iteratively solve for the evaporator and condenser saturation temperatures.

Energy Balance

The evaporator load is determined by the first law relationship:

$$\dot{Q}_e = (\dot{m}_{chw})(\overline{C_{p_{chw}}})(T_{ee} - T_{el})$$ (6.6)

where the flow rate of the chilled water, $\dot{m}_{chw}$, along with the entering and leaving temperatures of the chilled water, T_{ee} and T_{el}, are known. The specific heat, $\overline{C_{p_{chw}}}$ is calculated as a function of the average chilled water temperature, $\overline{T}_{chw}$.

$$\overline{T}_{chw} = \frac{T_{ee} + T_{el}}{2}$$ (6.7)

Fresh water and sea water properties are calculated using property subroutines so that temperature effects are taken into account in calculating specific heats.

$$\overline{C_{p_{chw}}} = f(\overline{T}_{chw})$$ (6.8)

Next, the mass flow rate of the refrigerant is calculated as:

$$\dot{m}_r = \frac{\dot{Q}_e}{h_1 - h_4}$$ (6.9)

and the heat removal rate in the condenser as:

$$\dot{Q}_c = \dot{m}_r(h_2 - h_3)$$ (6.10)

Finally, making use of knowledge of the flow rate of sea water in the condenser and the temperature of the entering sea water:

$$T_{cl} = T_{ce} + \frac{\dot{Q}_c}{(\dot{m}_{sw})(\overline{C_{p_{sw}}})}$$ (6.11)

$$\overline{T}_{sw} = \frac{T_{ce} + T_{cl}}{2}$$ (6.12)

$$\overline{C_{p_{sw}}} = f(\overline{T}_{sw})$$ (6.13)

24

Since estimates of T_c and T_e have been used up to this point, they represent two unknowns in the set of equations for which two additional equations are needed to make the set complete. These equations are:

$$\dot{Q}_e = UA_{o,e} \, \Delta T_{lm,e} \qquad (6.14)$$

$$\dot{Q}_c = UA_{o,c} \, \Delta T_{lm,c} \qquad (6.15)$$

where the log mean temperature for the evaporator is defined as:

$$\Delta T_{lm,e} = \frac{T_{ee} - T_{el}}{\ln(T_{ee} - T_e) - \ln(T_{el} - T_e)} \qquad (6.16)$$

and the log mean temperature for the condenser is:

$$\Delta T_{lm,c} = \frac{T_{cl} - T_{ce}}{\ln(T_c - T_{ce}) - \ln(T_c - T_{cl})} \qquad (6.17)$$

and all the temperatures are either known or estimated.

HEAT TRANSFER ANALYSIS

The overall heat transfer coefficient for the heat exchanger, U, is multiplied by the total outside surface area, A_o, of the heat exchanger. The overall heat transfer coefficient is a function of temperature and other fluid properties, and it can be predicted using a variety of published correlations.

Evaporator

The evaporator modeled is a shell-and-tube type with 246 tubes. The tube-side water makes two passes through the heat exchanger. The actual cooling surface (outside tube) area varies with the tube type, but it is known to be 105.81 square meters for 10.23 fins per centimeter tubes. The shell is 81.28 centimeters OD and 237.49 centimeters in length. The design conditions for the evaporator, as stated previously, are chilled water flow rate equal to 28.4 liters per second and inlet and outlet chilled water temperatures of 10.7 °C and 7 °C, respectively. The heat transfer analysis begins by examining the heat exchanger geometry. The total outside tube surface area, $A_{o,e}$, of the evaporator is equal to the number of tubes times the average outside surface area per length of the tube times the effective tube length-per-pass, in the heat exchanger. Note that the average outside surface area of the tube, $\overline{A}_{o,e}$, is expressed as surface area per unit length (m²/m) which includes the actual surface area of the fins. The value used was provided by the NSWC.

$$A_{o,e} = N_e \, (\overline{A}_{o,e})(L_{eff,e}) \qquad (6.18)$$

25

The inside surface area of the evaporator tube (smooth) is calculated as the total number of tubes times the inside perimeter times the effective tube length-per-pass through the heat exchanger:

$$A_{i,e} = N_e \, \pi (d_{i,e})(L_{eff,e})$$

(6.19)

The total flow area of the evaporator tubes is equal to half the total number of tubes (two pass) times the cross-sectional area of the tube:

$$A_{f,e} = \frac{N_e}{2} \left(\frac{\pi (d_{i,e})^2}{4} \right)$$

(6.20)

The average water velocity in an evaporator tube is then calculated as:

$$\overline{V}_{chw} = \frac{\dot{m}_{chw}}{(\overline{\rho}_{chw})(A_{f,e})}$$

(6.21)

where the average water density is based on the average chilled water temperature in the evaporator. The average Reynolds number follows as:

$$\overline{Re}_{chw} = \frac{(\overline{\rho}_{chw})(\overline{V}_{chw})(d_{i,e})}{\overline{\mu}_{chw}}$$

(6.22)

and average Prandtl number as:

$$\overline{Pr}_{chw} = \frac{(\overline{C}_{p_{chw}})(\overline{\mu}_{chw})}{\overline{k}_{chw}}$$

(6.23)

The inside heat transfer coefficient and the tube wall temperature are then calculated by iteration. The average wall temperature is initially assumed to be equal to the saturated refrigerant temperature in the evaporator:

$$T_{w,e} \cong T_e$$

(6.24)

The average viscosity of water is then calculated at the estimated temperature:

$$\overline{\mu}_{w,e} = f(\overline{T}_{w,e})$$

(6.25)

The inside or water-side heat transfer coefficient for the evaporator is calculated using the Dittus-Boelter correlation [21]:

$$\overline{h}_{i,e} = 0.023 \, (\overline{Re}_{chw})^{0.8} \, (\overline{Pr}_{chw})^{0.3} \left(\frac{\overline{\mu}_{chw}}{\mu_{w,e}} \right)^{0.14} \left(\frac{\overline{k}_{chw}}{d_{i,e}} \right)$$

(6.26)

All water properties are calculated at the average chilled water temperature unless otherwise subscripted. The wall temperature of the tube is then recalculated as:

$$\overline{T}_{w,e} = \overline{T}_{chw} - \frac{\dot{Q}_e}{(\overline{h}_{i,e})(A_{i,e})}$$

(6.27)

26

The outside boiling coefficient of the evaporator, $h_{o,e}$, is calculated from measured heat flux data provided from a separate study conducted at the Iowa State University Heat Transfer Test Facility [22]. Boiling coefficients for CFC-114 and HFC-236ea using a single tube 10.23 fins per centimeter test rig were calculated as a function of heat flux and constant saturation temperature. For HFC-236ea and 10.23 fins per centimeter the correlation is given as:

$$\bar{h}_{o,e} = 2.22792 + 0.1742529\,(q_e'') - 1.766886\text{E}^{-3}\,(q_e'')^2 \tag{6.28}$$

and for CFC-114 and 10.23 fins per centimeter the correlation is given as:

$$\bar{h}_{o,e} = 0.8431786 + 0.1359888\,(q_e'') - 8.738483\text{E}^{-4}\,(q_e'')^2 \tag{6.29}$$

Finally, the overall heat transfer coefficient neglecting thermal resistance of tube wall is calculated as:

$$UA_{o,e} = \left[\frac{1}{(\bar{h}_{i,e})(A_{i,e})} + \frac{1}{(\bar{h}_{o,e})(A_{o,e})} \right]^{-1}. \tag{6.30}$$

Condenser

The condenser is modeled as a shell-and-tube falling film condenser. The shell is 55.88 centimeters OD and 237.49 centimeters in length. The heat exchanger is designed for sea water at a flow rate of 31.5 liters per second with an entering temperature of 31.4°C, making two passes through the shell. There is a total of 246 tubes in the shell and a heat exchanger outside surface area of 105.81 square meters for 10.23 fins per centimeter tubes. The area varies with tube type.

The total outside tube surface area, $A_{o,c}$, of the condenser is equal to the number of tubes, N_c, times the average outside surface area per length of the tube, $\bar{A}_{o,c}$, times the effective tube length per pass, $L_{eff,c}$, in the heat exchanger:

$$A_{o,c} = N_c\,(\bar{A}_{o,c})(L_{eff,c}) \tag{6.31}$$

The inside surface area of the condenser tubes is calculated as the total number of tubes times the inside perimeter times the effective tube length per pass through the heat exchanger:

$$A_{i,c} = N_c\,\pi(d_{i,c})(L_{eff,c}) \tag{6.32}$$

The total flow area of the condenser tubes is equal to half the total number of tubes (two-pass) times the cross-sectional area of a tube:

$$A_{f,c} = \frac{N_c}{2}\left[\frac{\pi(d_{i,c})^2}{4} \right] \tag{6.33}$$

The average water velocity in the condenser tubes is then calculated as:

$$\overline{V}_{sw} = \frac{\dot{m}_{sw}}{(\overline{\rho}_{sw})(A_{f,c})} \tag{6.34}$$

where the average water density is based on the average sea water temperature in the condenser. The average Reynolds number follows as:

$$\overline{Re}_{sw} = \frac{(\overline{\rho}_{sw})(\overline{V}_{sw})(d_{i,c})}{\overline{\mu}_{sw}} \tag{6.35}$$

and average Prandtl number as:

$$\overline{Pr}_{sw} = \frac{(\overline{C}_{p_{sw}})(\overline{\mu}_{sw})}{\overline{k}_{sw}} \tag{6.36}$$

The inside heat transfer coefficient and the tube wall temperature are then calculated by iteration. First, the wall temperature is assumed to be equal to the saturated refrigerant temperature in the condenser:

$$\overline{T}_{w,c} \cong T_c \tag{6.37}$$

The average viscosity of water is then calculated at the estimated temperature:

$$\overline{\mu}_{w,c} = f(\overline{T}_{w,c}) \tag{6.38}$$

The inside or water-side heat transfer coefficient for the condenser is calculated using the Dittus-Boelter correlation [21]:

$$h_{i,c} = 0.023 \, (\overline{Re}_{sw})^{0.8} \, (\overline{Pr}_{sw})^{0.3} \left(\frac{\mu_{sw}}{\mu_{w,c}}\right)^{0.14} \left(\frac{\overline{k}_{sw}}{d_{i,c}}\right) \tag{6.39}$$

All water properties are calculated at the average sea water temperature unless otherwise subscripted. The tube wall temperature is then:

$$\overline{T}_{w,c} = \overline{T}_{sw} + \frac{\dot{Q}_c}{(h_{i,c})(A_{i,c})} \tag{6.40}$$

The outside heat transfer coefficient in the condenser is calculated from measured heat flux data provided from a separate study conducted at the Iowa State University Heat Transfer Test Facility [22]. Condensing coefficients for CFC-114 and HFC-236ea using a single tube 10.23 fins per centimeter test rig were calculated as a function of heat flux and constant saturation temperature. For HFC-236ea and 10.23 fins per centimeter the correlation is given as:

$$\overline{h}_{o,c} = 4.09314 + 0.1415326 \, (q_c'') - 1.62029E^{-3} \, (q_c'')^2 \tag{6.41}$$

and for CFC-114 and 10.23 fins per centimeter the correlation is given as:

$$\bar{h}_{o,c} = 3.620498 + 0.1494268 \, (q_c'') - 2.087891E^{-3} \, (q_c'')^2 \tag{6.42}$$

The overall heat transfer coefficient is calculated as:

$$UA_{o,c} = \left[\frac{1}{(\bar{h}_{i,c})(A_{i,c})} + \frac{1}{(\bar{h}_{o,c})(A_{o,c})} \right]^{-1} \tag{6.43}$$

NUMERICAL PROCEDURE

The equations above may be solved simultaneously with the use of a computer. The method chosen for this simulation is the Newton-Raphson procedure for multiple equations and unknowns based on a Taylor-series expansion. This method is explained in more detail by Stoecker [23]. The unknown values in the above set of equations are essentially T_c and T_e, which are present in both the log mean temperature and the UA calculations. The basic steps to the Newton-Raphson procedure are as follows:

1) Solve as many of the equations outside of the iteration scheme as possible.

2) Identify the remaining equations to solve using the Newton-Raphson method.

3) Rewrite the equations so that all of the unknown terms are on one side of the equality sign.

4) Assume initial values for the variables.

5) Calculate values of f1 through f# at the temporary values (this becomes the B matrix). The functions are stored in a separate function routine allowing the main program to remain flexible for use in solving future problems.

6) Compute partial derivatives of all functions with respect to all variables (this becomes the A matrix). This procedure is accomplished by repeated calls to a function routine that numerically calculates the derivatives of the input functions with respect to the input variables.

7) Using LINPACK routines, the set of equations AX = B can now be solved where "A" is the matrix of partial derivatives and "B" is the matrix with values of functions using temporary values of unknown variables. "X" is equal to the difference between the temporary values and the correct values of the variables.

8) Update the values of the variables.

9) Test for convergence (within 0.001 for all variables).

10) When the routine has met the established convergence criteria for all of the variables, return to the main program where final calculations of interest may be performed and the results printed to a file.

CHAPTER 7. RESULTS AND DISCUSSION

To evaluate HFC-236ea as a potential drop-in replacement for CFC-114 in existing shipboard chillers, it is useful to examine predicted performance of both refrigerants under the same operating conditions. It is also both interesting and necessary to compare the modeled performance of both refrigerants with actual performance data. Finally, comparisons of individual component performance may provide additional insight into the suitability of an alternative refrigerant.

The model developed in this study allows comparisons to be made using different refrigerants as well as several different fin tube types. Refrigerant property routines developed by the National Institute of Standards and Technology support both pure refrigerants HFC-236ea and CFC-114. Single tube heat transfer data for plain, 10.23 fins per centimeter, 15.75 fins per centimeter, and Turbo B tubes were provided by the Iowa State University Heat Transfer Test Facility [22]. The data include boiling and condensation heat transfer coefficients as functions of heat flux for a given saturation temperature for both CFC-114 and HFC-236ea. Both property data and fin tube data were incorporated into the model. Thus, by specifying the refrigerant and tube geometry at an initial prompt in the computer routine, the model could be exercised repeatedly to simulate different refrigerants operating under the same conditions.

COMPARISON OF MODEL AND EXPERIMENTAL RESULTS

The Naval Surface Warfare Center (NSWC), in cooperation with the United States Environmental Protection Agency (EPA), has tested CFC-114 and HFC-236ea in a 440-kilowatt laboratory centrifugal chiller representative of those used in the United States Navy's fleet of ships and submarines. The laboratory chiller is fully-instrumented, and sample data are included in Appendix B.

Figure 7.1 is a comparison of modeled and measured compressor power. The measured compressor power provided by the NSWC was calculated from measurements of torque and speed of the compressor shaft. Therefore, the measured value of compressor power is the shaft power. The modeled value of compressor power is the rate of work performed directly on the fluid and does not include the mechanical or heat losses as the power is transferred from the compressor shaft to the impeller and ultimately to the working fluid. A linear relationship was found to exist between the shaft power and the power transferred to the fluid for the data provided by the NSWC. This correlation, Equation (7.1), was applied to the results of the model as an assumed mechanical efficiency factor where X is the energy transfer rate to the refrigerant, and Y is the measured compressor shaft power.

$$Y = 391.46 + 1.0637 * X \qquad (7.1)$$

Even with an efficiency factor applied, the model consistently underpredicts the amount of compressor power required to meet the specified load. This could be related to the use of inlet guide vanes to the compressor which are not modeled in this study.
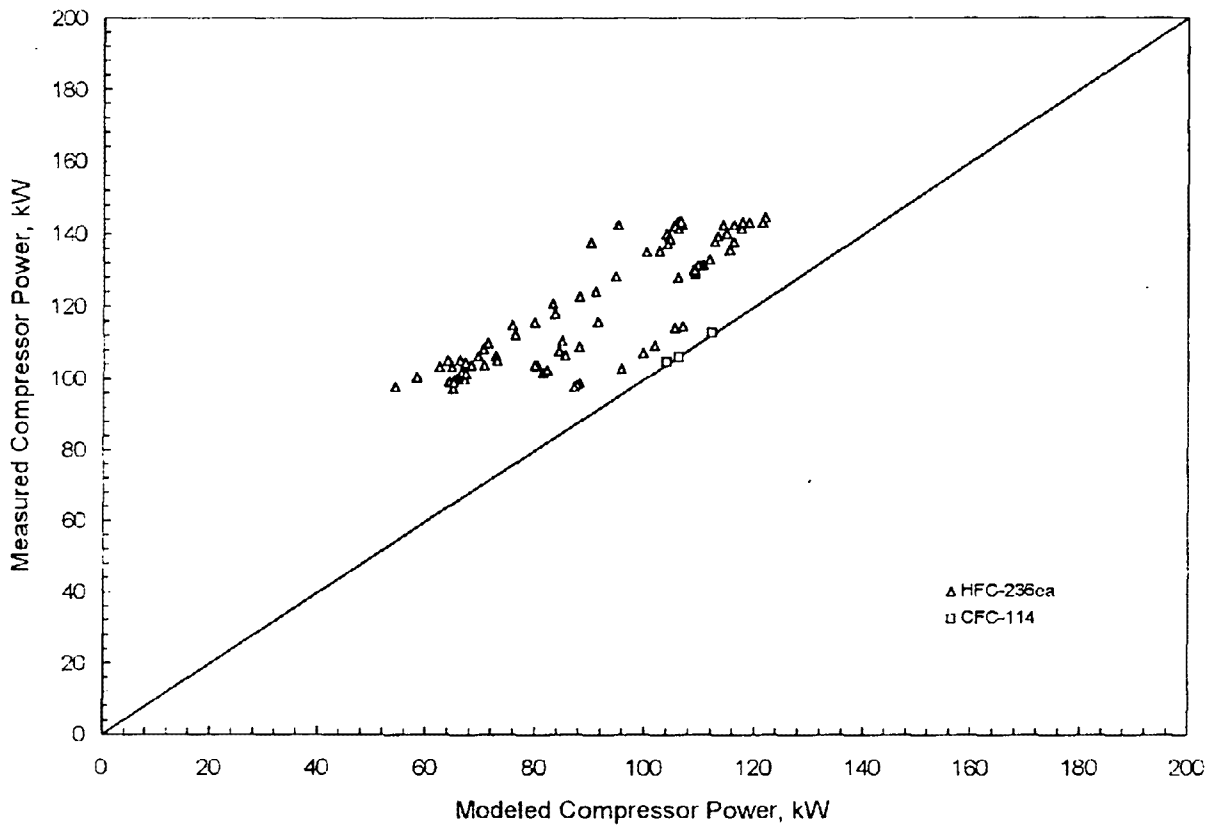
Figure 7.1: Comparison of modeled and measured compressor power

Figure 7.2 is a comparison of the system coefficient of performance, COP, calculated using NSWC measurements and predicted using the model developed in this study. The model overpredicts the coefficient of performance for both CFC-114 and for HFC-236ea. The trend is consistent and is what one would expect when comparing modeled with measured results. Since models often make use of simplifying assumptions, the results tend to be idealized. One would expect to see the test results to be less favorable than modeled results.
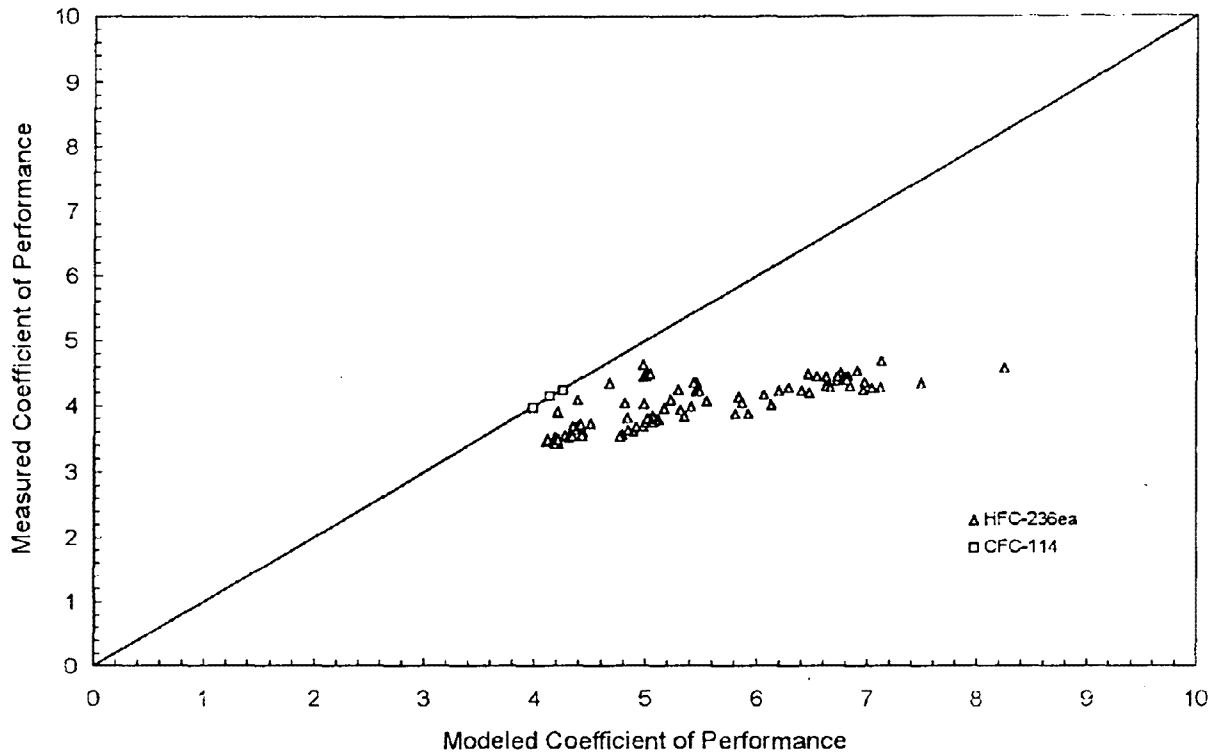
Figure 7.2: Comparison of modeled and measured coefficient of performance

The measured performance data appear to be fairly constant with COP values of approximately four. It appears from the data that as the temperature of water entering the condenser decreases, the difference between the predicted and measured values of the coefficient of performance increases. The trend can be seen with HFC-236ea as shown in Table 7.1. Measured data for an entering condenser water temperature of approximately 31.4 °C are closer to the predicted values. However, as the temperature of the water entering the condenser decreases, the measured coefficient of performance values increase at a slower rate than predicted values.

As the temperature of the cooling water entering the condenser decreases, the heat transfer in the condenser is enhanced due to the increased temperature difference, and the cooling capacity increases. It should follow that overall system performance improves. However, inlet guide vanes in the compressor are used to control the flow of refrigerant and balance the system without reducing the speed of the compressor shaft. This causes the compressor to be less efficient and counters the effects of improved condenser performance on the overall coefficient of performance. The model developed in this study does not account for the effects of inlet guide vanes. Thus, when inlet guide vanes are in use--for example, when the entering condenser water temperature is below the design point--one would expect to see greater differences between measured and modeled results as shown in Figure 7.2.

Table 7.1: Effect of entering condenser water temperature on measured and modeled COP for HFC-236ea

Entering Condenser Water Temp, °C	COP modeled	COP measured	modeled/ measured
88.9	4.05	3.89	1.04
86.1	4.22	3.69	1.14
80.2	4.91	3.96	1.24
79.9	5.23	3.83	1.35
67.1	6.55	4.28	1.53
60.4	7.66	4.57	1.68

Figure 7.3 is a comparison of modeled and measured refrigerant temperatures in the condenser. The measured temperature is the saturation temperature corresponding to the measured liquid pressure of the refrigerant. The model predictions compare well with the CFC-114 data; however, the model underpredicts the condenser temperature for most HFC-236ea data. This difference could be caused, in part, by poor heat transfer in the condenser. If this were the case, then the temperature in the condenser would have to increase in order to overcome whatever resistance is present. More compressor power would be required to provide this additional temperature lift resulting in lower system performance. Because the refrigerant temperature in the condenser is closely tied to the condensing heat transfer coefficient by use of the log mean temperature difference equation for heat transfer in the condenser, one would also expect to see an offset in a comparison of measured and modeled condensing coefficients. As the condensing temperature increases while entering and leaving water temperatures remain constant, the log mean temperature difference increases. This would result in a modeled decrease in the condensing coefficient.
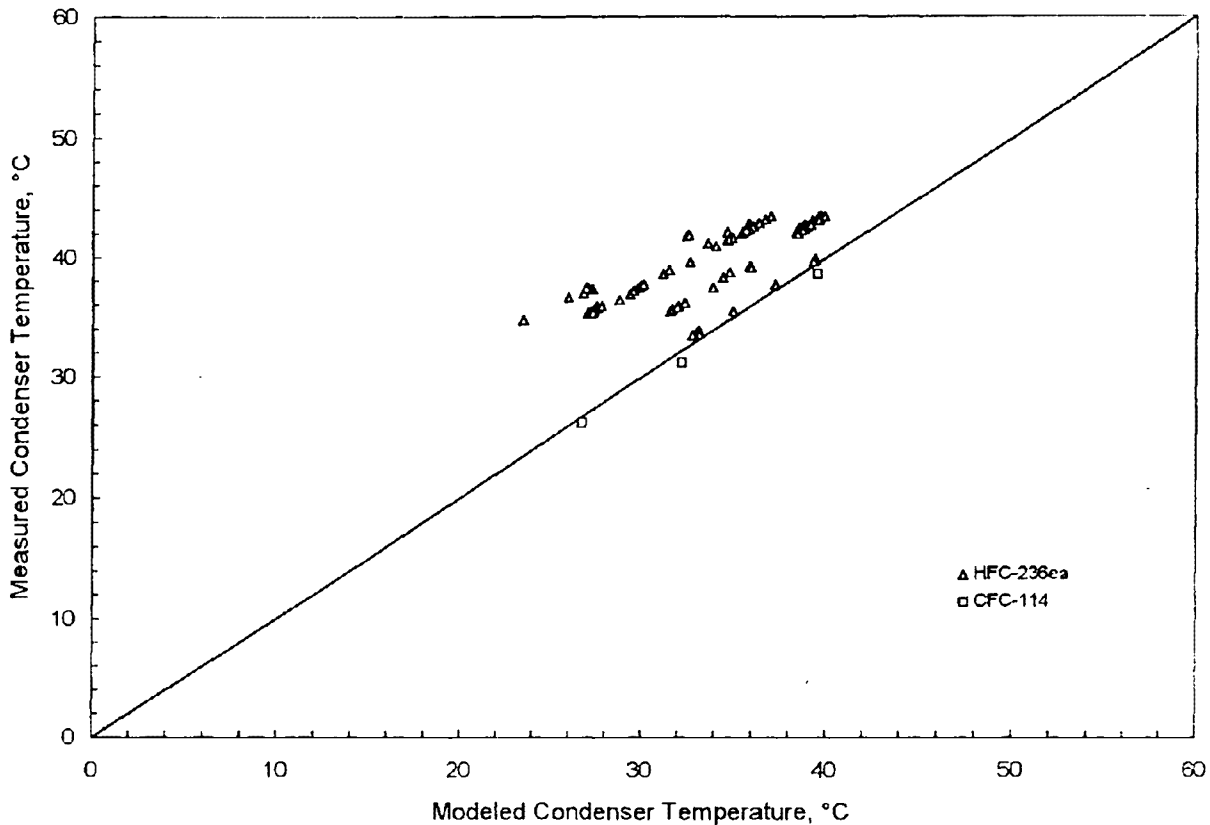
Figure 7.3: Comparison of modeled and measured condenser temperature

An example of when conditions may exist in the condenser that hamper heat transfer is when non-condensable gases, left unpurged, accumulate in the upper vapor space of the condenser. This is a plausible explanation for the difference in the condenser saturation temperatures observed in Figure 7.3. As previously mentioned, by fixing the inlet and outlet chilled water conditions as well as the chilled water flow rate, the saturation temperature of the refrigerant in the evaporator is determined by the overall heat transfer equation (Equation 6.14). For HFC-236ea, both the measured and modeled evaporator temperatures are near 2 °C. The corresponding saturation pressures for these saturation temperatures are less than the atmospheric pressure. This could cause non-condensable gases to leak into the evaporator due to the negative gage pressure. These gases would migrate and collect in the condenser and could significantly degrade the performance of the condenser and the entire system. If air, in fact, was present in the condenser, it would drive the outside heat transfer coefficient down resulting in a high condenser saturation temperature.

To avoid or minimize this problem, the system should be thoroughly leak-checked and a purge installed in the condenser. An alternate solution is to avoid negative gage pressure in the evaporator by manipulating the chilled water mass flow rate and the chilled water temperature difference so that the saturated temperature of the

refrigerant in the evaporator is raised to a minimum temperature corresponding to a saturation pressure of at least normal atmospheric pressure. This could be accomplished with minimal effect on the evaporator capacity but would depend on the flexibility of the shipboard heat exchangers utilizing the chilled water.

Figure 7.4 is a comparison of modeled and measured condenser capacity. The model slightly underpredicts condenser capacity for both refrigerants. The trends are consistent with Figure 7.5.
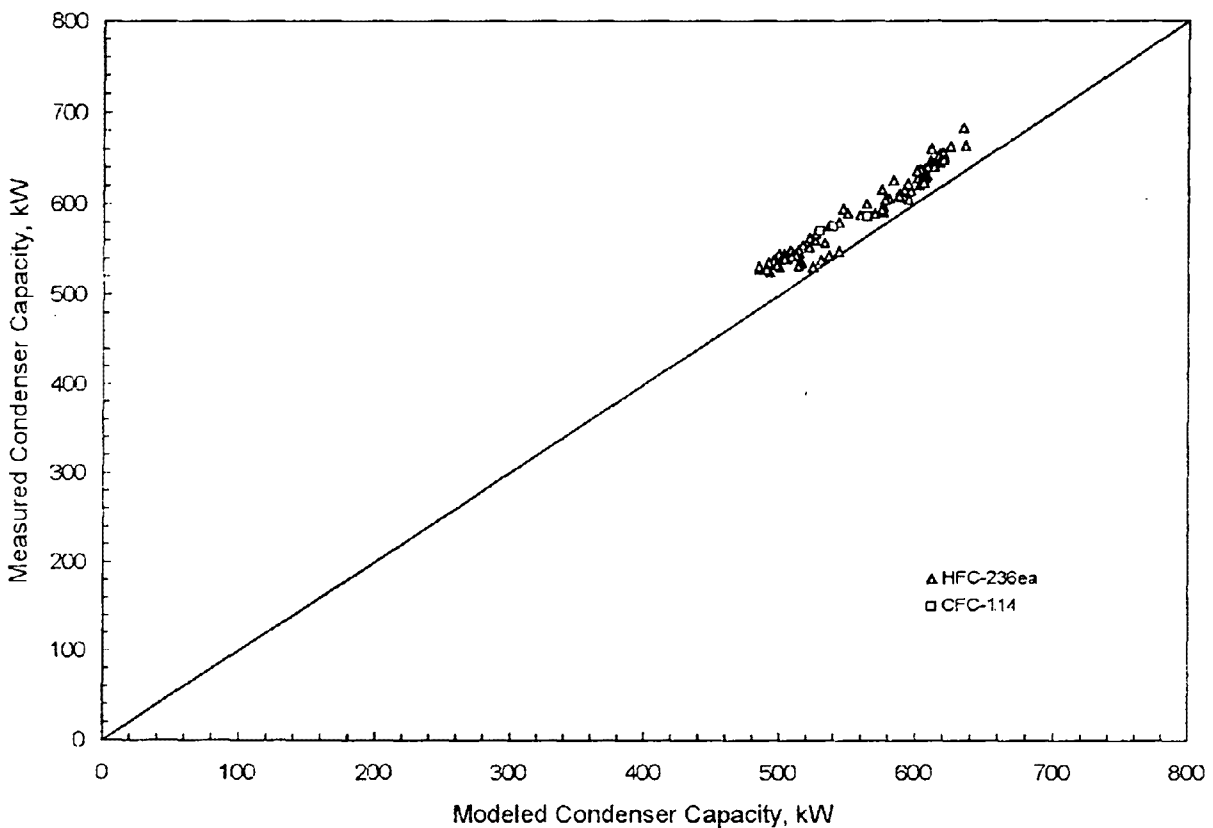
Figure 7.4: Comparison of modeled and measured condenser capacity

Figure 7.5 is a comparison of modeled and measured cooling water temperatures leaving the condenser. Modeled values are within 0.5°C of measured values. This is consistent with Figure 7.4 which shows the same trend for condenser capacity. This is expected, since the rate of heat transfer and the temperature of the water leaving the condenser are the two variables in the water-side heat transfer equation for the condenser.

Figure 7.6 is a comparison of modeled and measured evaporator saturation temperatures. The figure shows that modeled and measured boiling coefficients compare well with some variance. One would therefore expect to see a variance of the measured and modeled boiling coefficients since these variables must balance in the log mean temperature difference equation for the heat transfer in the evaporator.

35
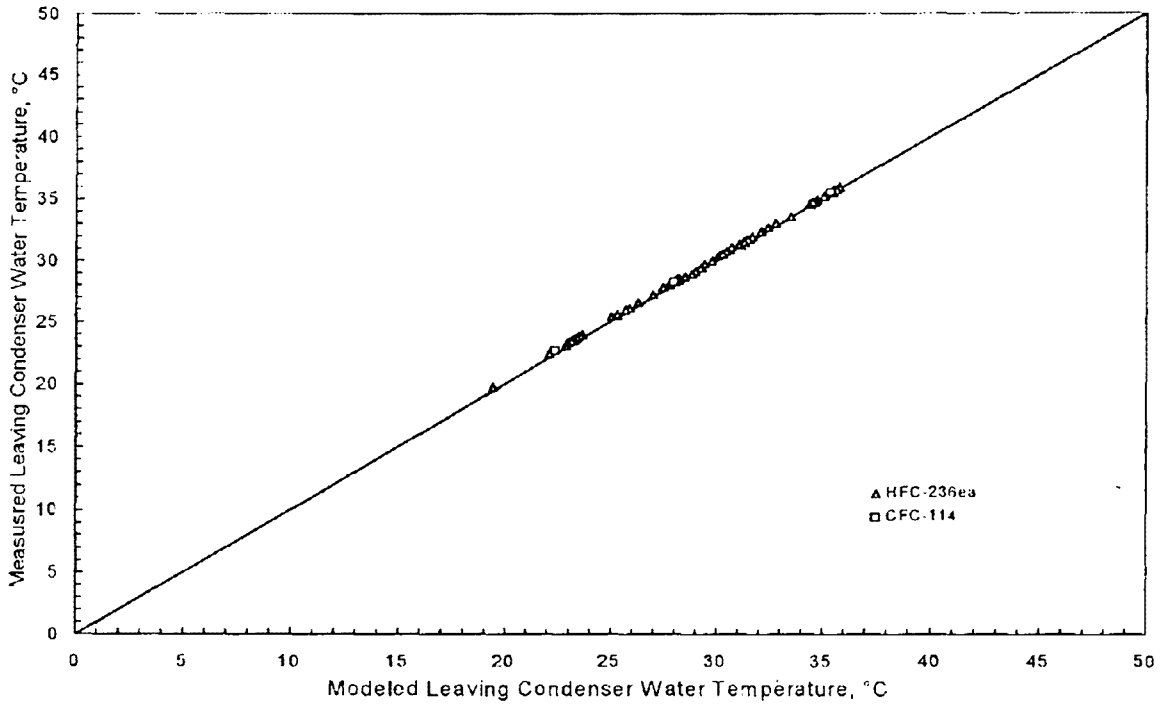
Figure 7.5: Comparison of modeled and measured leaving condenser water temperature
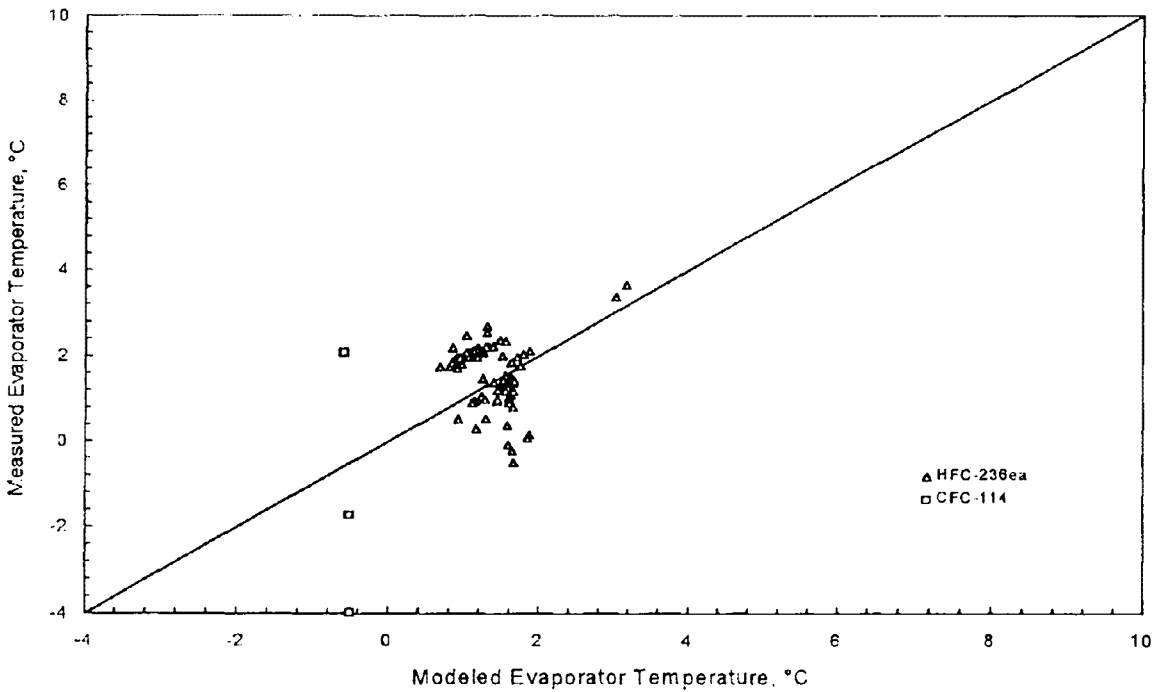
Figure 7.6: Comparison of modeled and measured refrigerant saturation temperatures in the evaporator

Figure 7.7 is a comparison of modeled and measured refrigerant flow rate. The model consistently predicts the flow rate for both refrigerants within ±5 percent. This suggests that the enthalpy differences also compare favorably since the rate of heat transfer in the evaporator is constant and is equal to the refrigerant mass flow rate times the enthalpy difference across the evaporator.
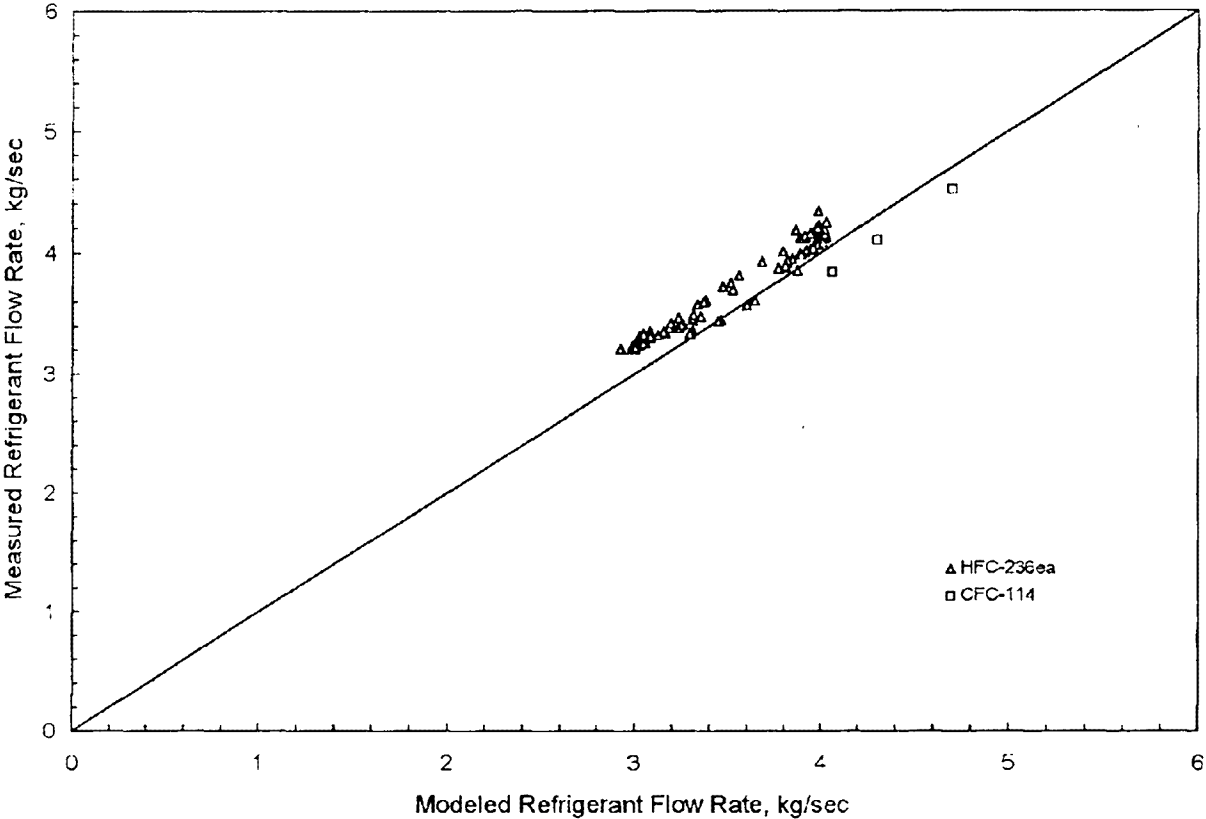
Figure 7.7: Comparison of modeled and measured refrigerant flow rate

COMPARISON OF CFC-114 AND HFC-236ea PERFORMANCE

The previous figures and discussion have served to validate the model developed in this study, and it is appropriate to further exercise the model to predict the performance of both refrigerants through a range of operating conditions. This is done by using the fleet design point as the default and varying one parameter at a time over an appropriate range to see the effects on the system. The results yield additional insight as to the possible suitability of HFC-236ea as a drop-in substitute for CFC-114.

Entering Condenser Water Temperature

As the Navy operates its fleet around the world, ships encounter a wide range of condenser water temperatures because sea water is used directly in the condenser to remove heat from the working fluid. Chillers for Navy ships are designed for a condenser water temperature of 31.4 °C; however, temperatures encountered may range from -1.3 °C to 35.3 °C depending on where the ship is operating. Since heat transfer in the condenser is driven by the temperature difference between the sea water (coolant) and refrigerant, a condenser water temperature that is too high would lower the performance of the condenser and subsequently the entire refrigeration cycle. Thus, the entering condenser water temperature is important to the performance of the overall system.

In this simulation, the evaporator load is kept constant, simulating the design conditions of chilled water entering and leaving the evaporator at 10.7 °C and 7 °C, respectively, and a constant chilled water flow rate of 28.4 liters per second. Additionally, the condenser water flow rate is held constant at the design condition of 31.5 liters per second. As the temperature of the water entering the condenser is varied, a solution is obtained and may be expressed in terms of performance parameters such as the compressor power required or the coefficient of performance.

For example, Figure 7.8 illustrates that the predicted power required to drive the compressor more than doubles for both refrigerants as the water temperature entering the condenser increases from 16 °C to 38 °C. The increasing power input trend is expected since better heat transfer and increasing heat rejection in the condenser occurs as the temperature of the cooling water entering the condenser decreases. The efficiency of the refrigeration cycle should thereby improve resulting in less power input required to the compressor. Figure 7.8 shows a trend for both refrigerants of increased power required with increased temperature of the entering cooling water to the condenser. Additionally, the model predicts that HFC-236ea used as a drop-in substitute for CFC-114 may result in energy savings. Figure 7.8 shows that at the design point of operation the predicted power required to drive the compressor using HFC-236ea is 91.4 percent of the power required using CFC-114. The model predicts that for any cooling water temperature the power required for a refrigeration cycle using HFC-236ea as a drop-in will be significantly less than the same cycle using CFC-114 as the working fluid. The predicted savings in power consumption by using HFC-236ea at the design point of operation is 10 kW.

Data from the NSWC are also shown on Figure 7.8. The data for CFC-114 show nearly constant compressor power input over the range of entering condenser water temperatures. The data for HFC-236ea show significant scatter. Both the CFC-114 and HFC-236ea measured values of required compressor power are above the predicted values for the range of entering condenser water temperatures. When a centrifugal chiller is using more energy than it should as suggested by Figure 7.8, a common culprit is excess air in the condenser. This condition increases the pressure in the condenser and forces the compressor to work harder to maintain the required cooling.
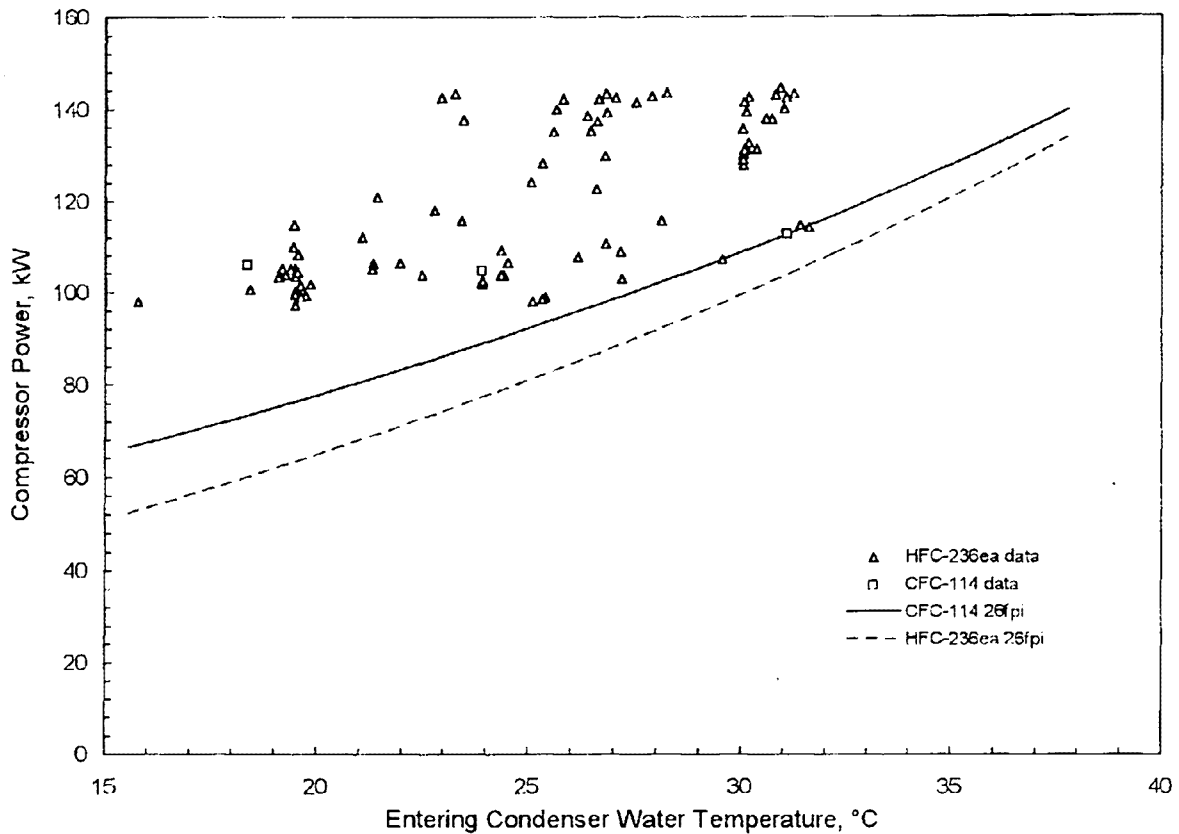
Figure 7.8: Dependence of compressor power requirement on entering condenser water temperature

The coefficient of performance, COP, is a ratio of the cooling capacity of the evaporator over the net power input to the compressor and is a standard measure of the performance of a refrigeration cycle. Figure 7.9 shows the refrigerating coefficient of performance as a function of the temperature of the cooling water entering the condenser. As expected, the coefficient of performance is shown to decrease as the inlet condenser water temperature increases. Additionally, at the design point of 31.4 °C, the predicted coefficient of performance for HFC-236ea is 4.25 compared to 3.91 for CFC-114. The model predicts better performance using HFC-236ea over the range of condenser water temperatures simulated.

The measured values of coefficient of performance for both CFC-114 and HFC-236ea are less than the predicted values. As the entering condenser water temperature increases, the measured and predicted values of the coefficient of performance move toward better agreement.
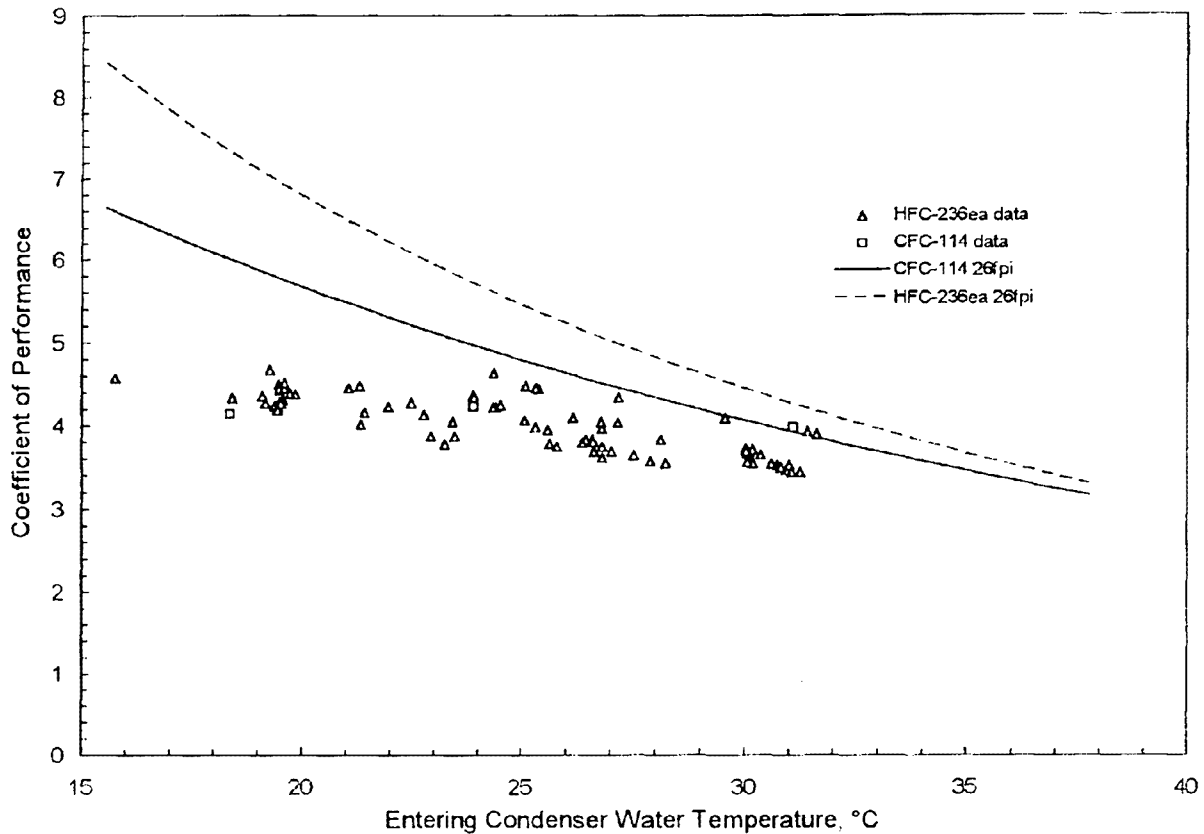
Figure 7.9: Dependence of refrigerating performance on entering condenser water temperature

Another parameter that gives insight into the performance of a refrigeration cycle is the refrigerating efficiency which is defined as the ratio of the coefficient of performance of the modeled refrigeration cycle to the coefficient of performance of a reversed Carnot cycle operating between the same source and sink temperatures. In a sense, this parameter gives a clearer picture of the cycle's true performance because it is referenced to the cycle's best possible performance as limited by the Second Law of Thermodynamics.

The curves in Figure 7.10 show an increase in refrigeration efficiency that approach an asymptotic limit as the temperature of the cooling water entering the condenser increases. The performance of the system at temperatures lower than the design point is less than the possible performance which could be achieved under those conditions. This is reasonable considering that the system being modeled was originally designed for optimum performance at an entering condenser water temperature of 31.4 °C. The possibility that lower temperatures result in lower refrigerating efficiencies is not of great concern for Navy applications since the cooling fluid--in this case ocean sea water--is essentially free. The system may be designed for optimal performance about an average cooling water temperature of 31.4 °C and any temperature encountered which is less than that will provide extra cooling potential at no extra cost. For this reason, it doesn't have to perform optimally.

In any case, the efficiency doesn't decrease by much and, more importantly, it remains stable at higher temperatures. Additionally, for all temperatures modeled, HFC-236ea outperforms CFC-114. At the design point of 31.4 °C, the refrigerating efficiency of HFC-236ea is 0.332 and for CFC-114 is 0.294.

Trends in Figures 7.9 through 7.10 show that the performance indicators--compressor power requirement and coefficient of performance--both improve as the inlet condenser water temperature decreases from 38°C to 16° C. The required power consumption decreases and the coefficient of performance increases. These are expected trends since lower condenser water temperatures provide a higher temperature difference between heat transfer fluids resulting in increased cooling potential in the condenser. The refrigerating efficiency in Figure 7.10 decreases with decreasing condenser water temperature; however, this is expected since the system is designed for optimal performance at an entering condenser water temperature of 31.4 °C. As observed in these figures, HFC-236ea is predicted to outperform CFC-114 over a range of inlet condenser water temperatures. This is partly due to the fact that measured heat transfer coefficients for HFC-236ea were found to be greater than those of CFC-114 [22].
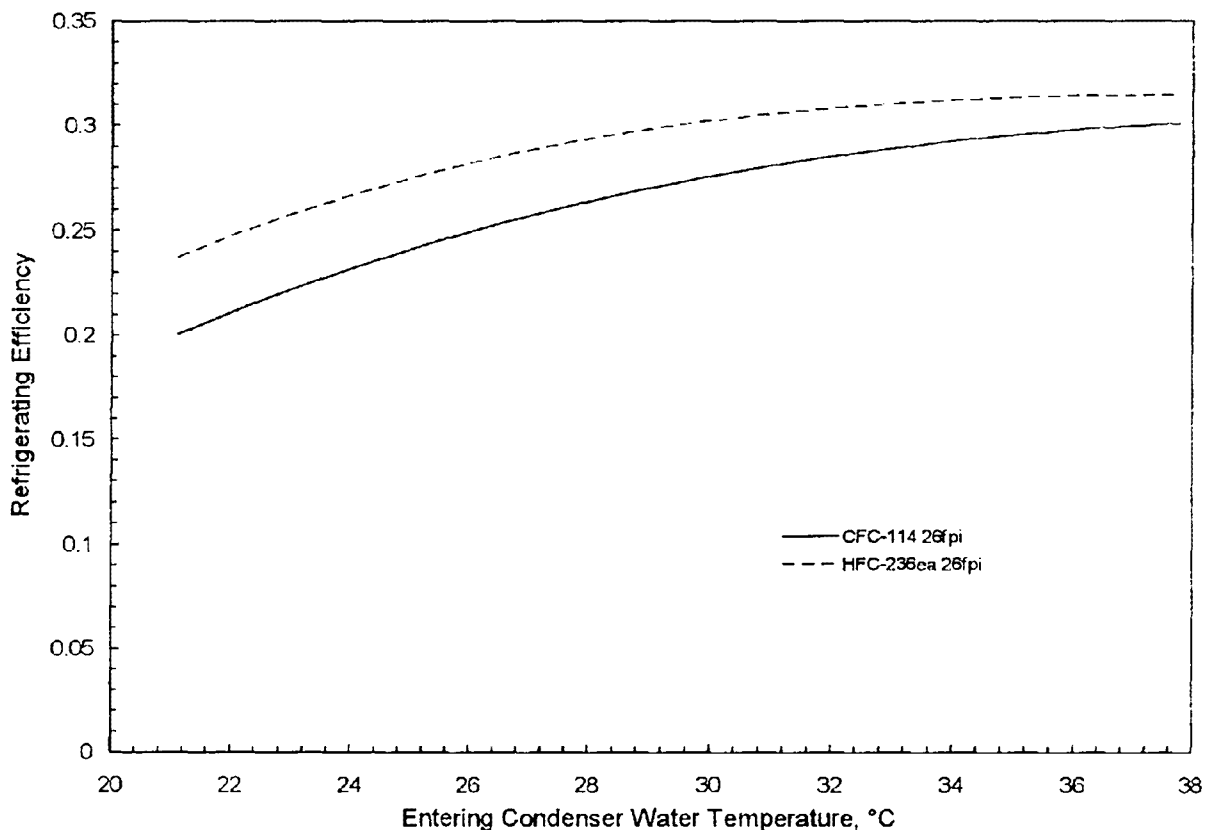
Figure 7.10: Dependence of refrigerating efficiency on entering condensing water temperature

41

Figure 7.11 shows the refrigerant's saturation temperature in the condenser relative to the temperature of the cooling water entering the condenser. The predicted saturation temperatures for CFC-114 and HFC-236ea are nearly identical. The measured values of the condenser saturation temperature for CFC-114 agree with the predicted values while the HFC-236ea data show the same trend but are generally higher than predicted values.
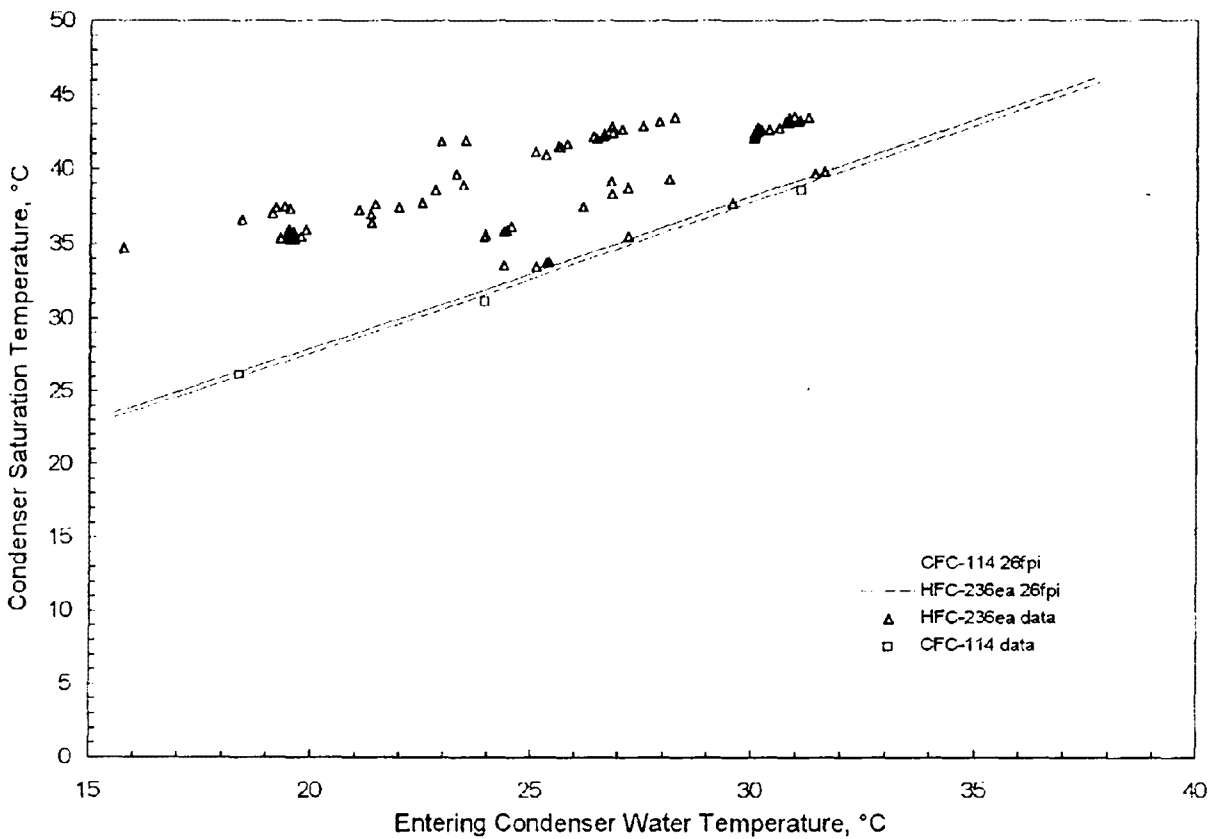
Figure 7.11: Dependence of condenser temperature on entering condenser water temperature

Figure 7.12 shows the saturation temperature of the refrigerant in the evaporator as a function of the entering condenser water temperature. The predicted saturation temperature for HFC-236ea is higher than the predicted value for CFC-114 over the range of entering condenser water temperatures. The HFC-236ea data compare well with predicted values while there appears to be less agreement between measured and modeled values for CFC-114.
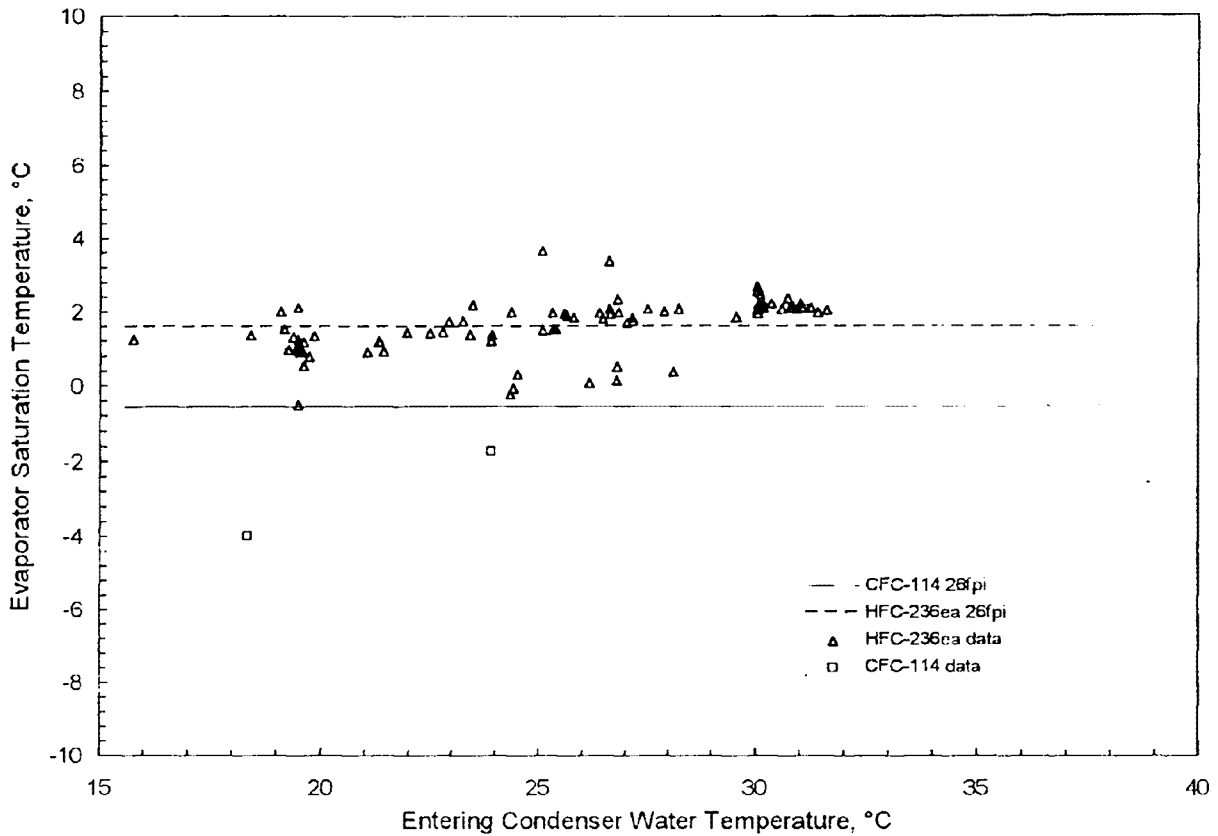
Figure 7.12: Dependence of evaporator temperature on entering condenser water temperature

Figure 7.13 shows the relationship between the evaporator capacity and the temperature of the water entering the condenser. Since the evaporator capacity is fixed by holding the water-side conditions constant, the predicted values for HFC-236ea and CFC-114 are identical. Scatter is shown for measured values of HFC-236ea while measured values of CFC-114 agree with predicted values. In the model, the capacity is fixed for both CFC-114 and HFC-236ea by the chilled water conditions.

Figure 7.14 shows the condenser capacity as a function of the entering condenser water temperature. Predicted values for CFC-114 and HFC-236ea are nearly equal. Both the CFC-114 and HFC-236ea measured values are higher than predicted values with significant scatter observed in the HFC-236ea data. This result is consistent with previous results and discussion.
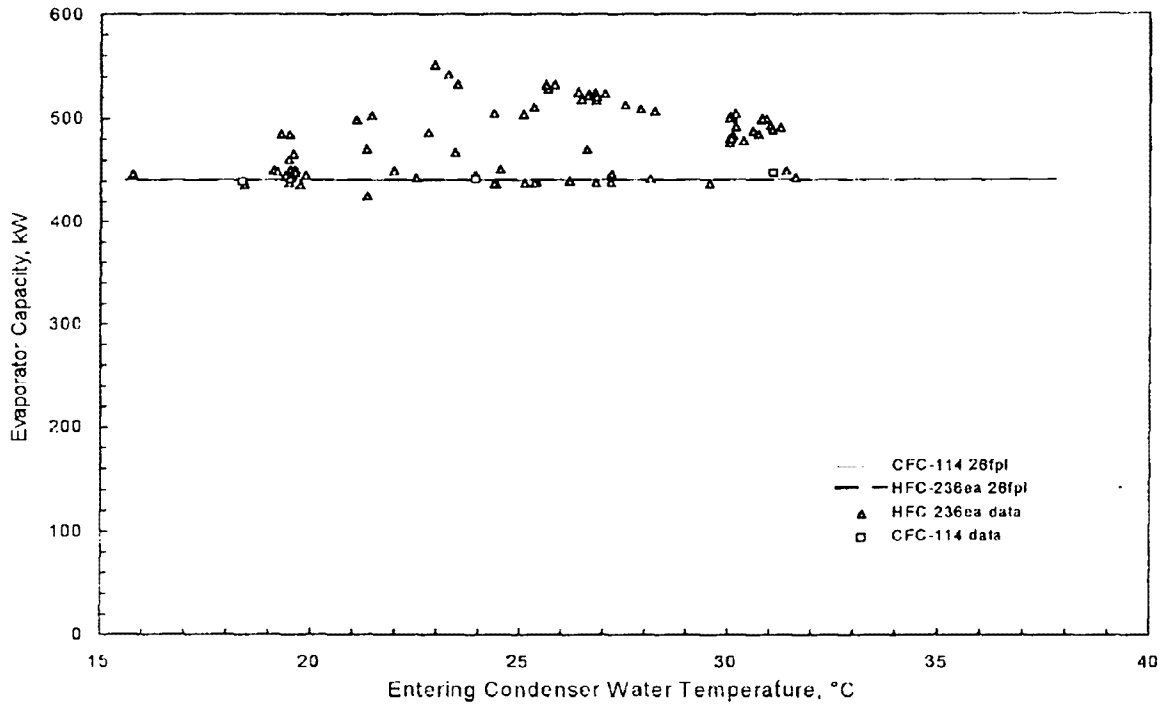
Figure 7.13: Dependence of evaporator capacity on entering condenser water temperature
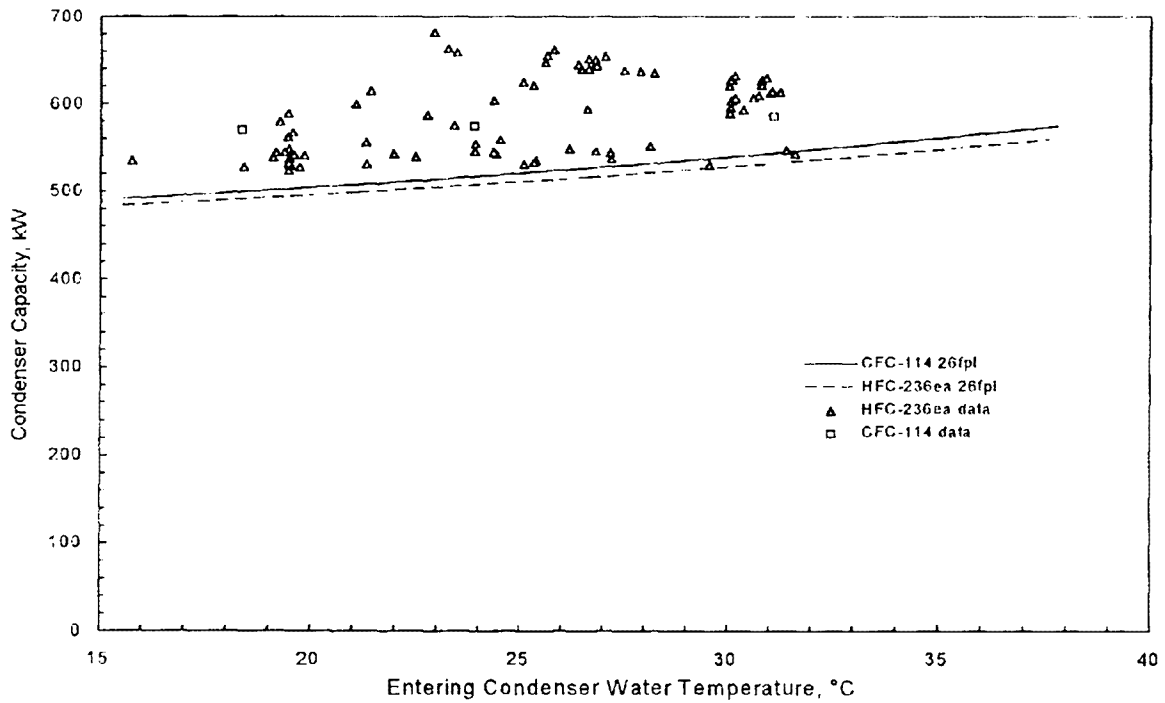
Figure 7.14: Dependence of condenser capacity on entering condenser water temperature

44

Figure 7.15 shows the relationship between the refrigerant mass flow rate and the temperature of the water entering the condenser. The measured and predicted values for CFC-114 are in close agreement while there is significant scatter in the data for HFC-236ea. As condensing water temperature increases, this figure shows an increasing trend in the refrigerant mass flow rate. This is an expected trend since Figure 7.12 shows the evaporator saturation temperature (and thus pressure) to be constant, and Figure 7.11 shows the condenser pressure and temperature of the refrigerant to increase with increasing condenser water temperature. It follows that the enthalpy difference across the evaporator will decrease which requires an increase in refrigerant mass flow rate to meet the given (or fixed) evaporator load.
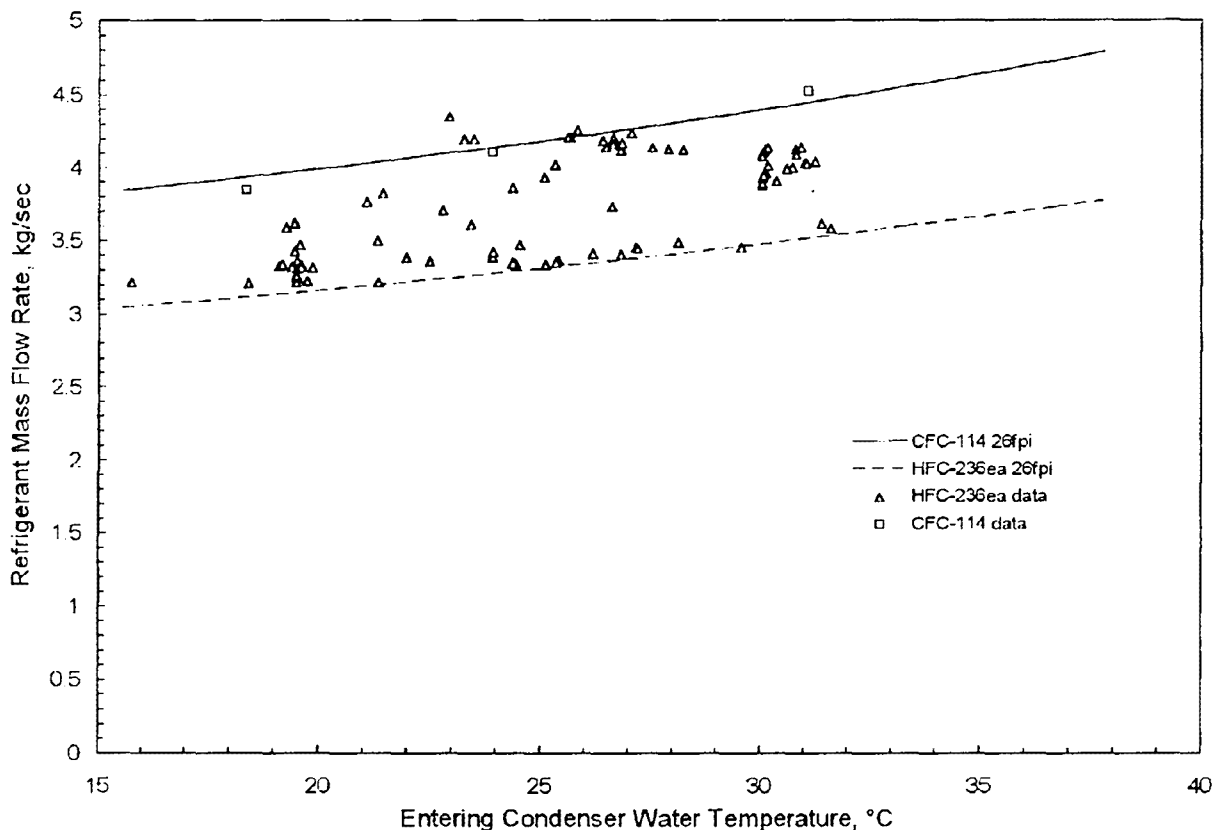
Figure 7.15: Dependence of refrigerant mass flow rate on entering condenser water temperature

Entering Evaporator Water Temperature

In this situation, the evaporator load is defined by a constant chilled water flow rate of 28.4 liters per second, a chilled water inlet temperature of 7 °C, and a chilled water exit temperature ranging from 9.2 to 12.6 °C. Additionally, the temperature of the water entering the condenser is held constant at 31.4 °C and the flow rate of

the condenser water is held constant at 31.5 liters per second. As the cooling load is systematically varied, its effect on various performance indicators may be observed.

As the temperature of the chilled water leaving the load and entering the evaporator increases while other design operating conditions remain constant, there is an increasing trend in the power required to drive the compressor as shown by Figure 7.16. This is an expected trend because as the water temperature entering the evaporator increases, the demand is increased on the evaporator. In order to accommodate this increased demand, either the refrigerant mass flow rate or the enthalpy difference in the evaporator must increase in order to provide enough heat transfer to maintain a constant chilled water exit temperature. The result is the need for more power required to drive the compressor. The comparison of HFC-236ea and CFC-114 in Figure 7.16 shows that for the range of chilled water temperatures entering the evaporator, HFC-236ea always requires less compressor power when modeled as the working fluid.
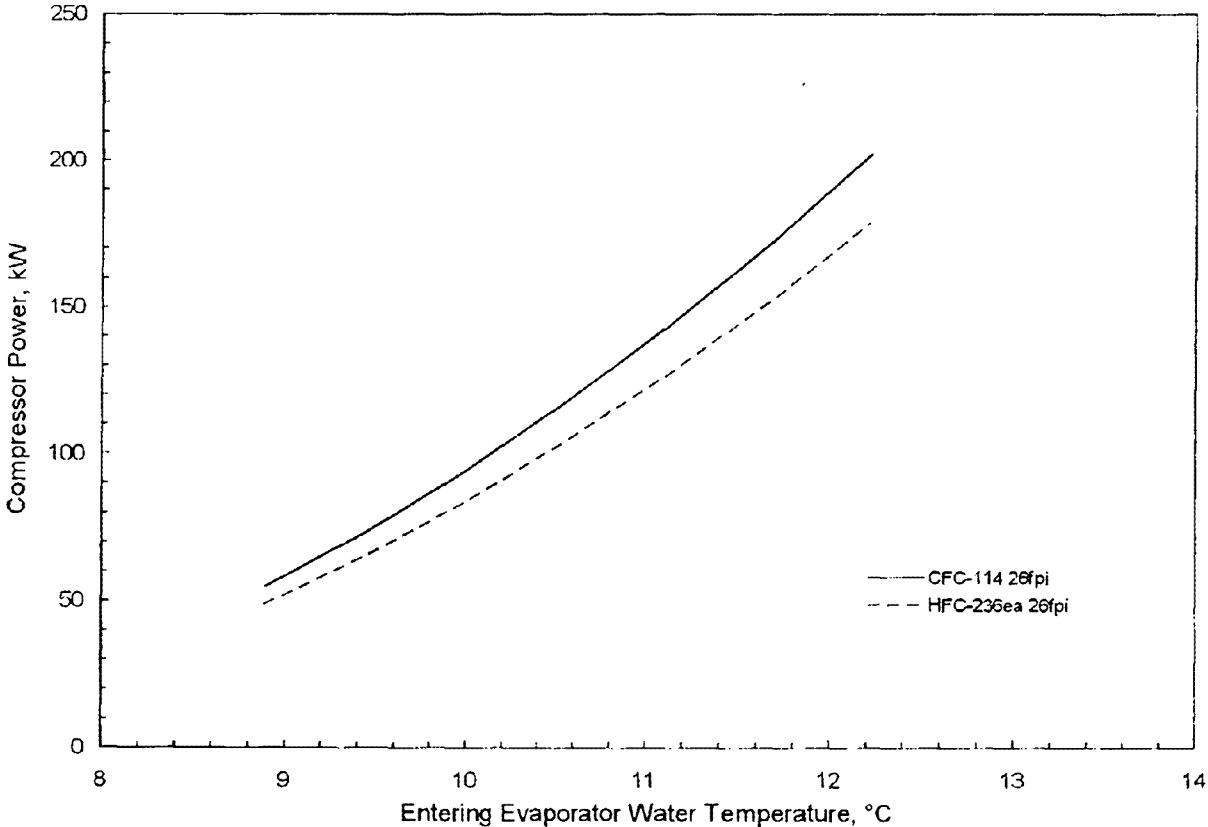
Figure 7.16: Dependence of compressor power for CFC-114 and HFC 236ea on entering evaporator water temperature

A comparison of the coefficient of performance as a function of chilled water temperature entering the evaporator shows that as the temperature increases the coefficient of performance decreases. This means that as the temperature increases, the increase of power required by the compressor is greater than the increase in cooling capacity. Additionally, as shown in Figure 7.17, the coefficient of performance for HFC-236ea is higher than the coefficient of performance for CFC-114 for the range of temperatures modeled.

Finally, Figure 7.18 shows that as the temperature of the chilled water entering the evaporator increases, the refrigerating efficiency decreases. This figure also shows that only a narrow range of temperatures are both realistic and optimum. By definition, the refrigerating efficiency lies between the values of zero and one. There is a general drop-in efficiency of 10 percent for a 2°C temperature increase. Thus, while the refrigerating efficiency remained relatively stable for a wide range of condenser water temperatures, it is more sensitive to a change in chilled water temperatures which essentially represent a change in capacity. HFC-236ea maintains a 3 to 5 percent higher efficiency than CFC-114 for the range of temperatures modeled.
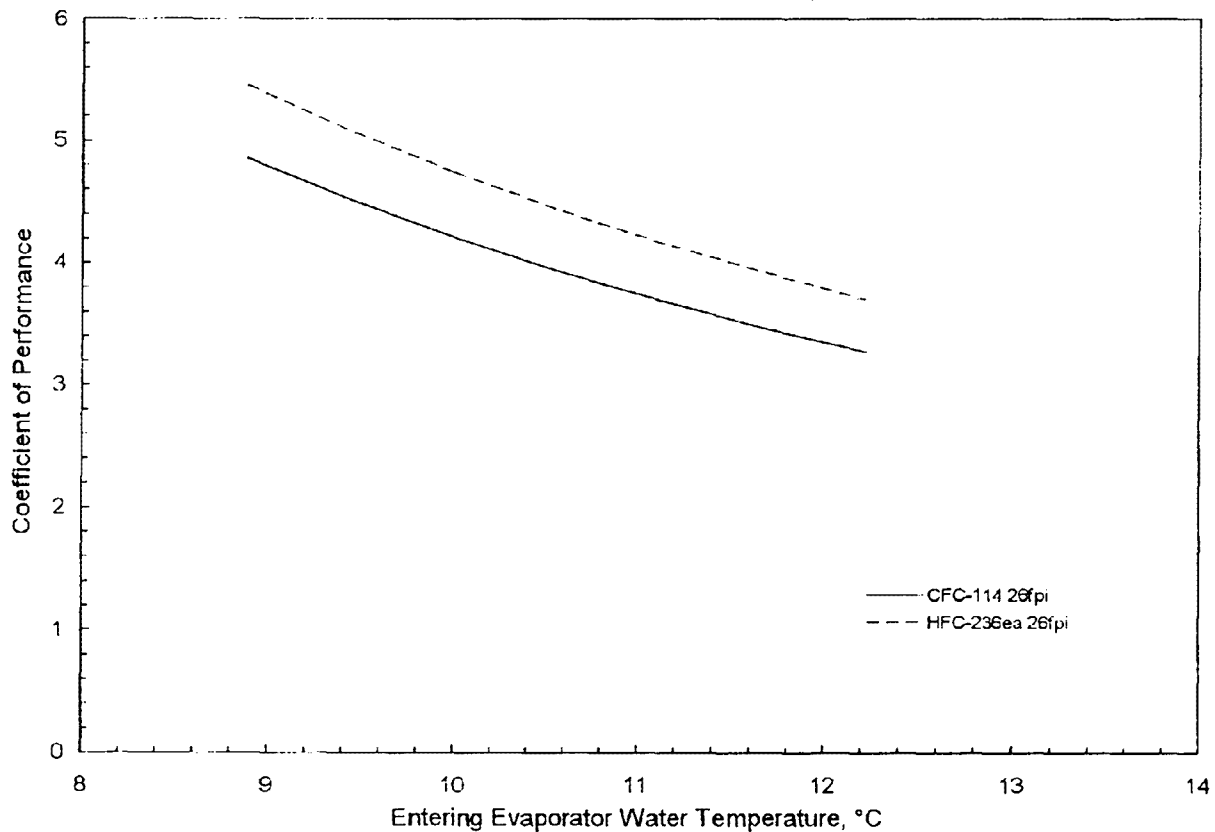
Figure 7.17: Dependence of refrigerating performance on entering evaporator water temperature

Figure 7.18: Dependence of refrigerating efficiency on entering evaporator water temperature

The trends associated with varying the chilled water temperature entering the evaporator are summarized in Figures 7.17 through 7.19. In the simulated refrigeration cycle, the temperature is varied over a range of 9.2 °C to 12.6 °C. The designed chilled water operating point for CFC-114 is 10.7 °C. As the temperature increases, the shaft power to the compressor increases, and the coefficient of performance and refrigeration efficiency both decrease.

Leaving Evaporator Water Temperature

The temperature of the chilled water leaving the evaporator is also a parameter that can be studied to provide insight into the sensitivity of system performance under varying conditions. The design operating point of the Navy's 440-kilowatt CFC-114 refrigeration system is a chilled water set point of 7 °C. When this temperature is varied, trends may be observed and comparisons made with HFC-236ea. The effects of varying the outlet chilled water temperature are similar to those of varying the inlet chilled water temperature. However, differences occur due to the log-mean-temperature-difference equations used in the model as well as the calculated specific heats

48

which are a function of average water temperature. Since the results are similar to the previous figures, the following discussion will be brief.

Figure 7.19 is a plot of the chilled water temperature leaving the evaporator and the resulting effect on the power consumption of the compressor. As the temperature increases, the cooling load decreases and the subsequent power required of the compressor diminishes. This plot also shows that for the range of temperatures simulated HFC-236ea requires less predicted compressor power than CFC-114.
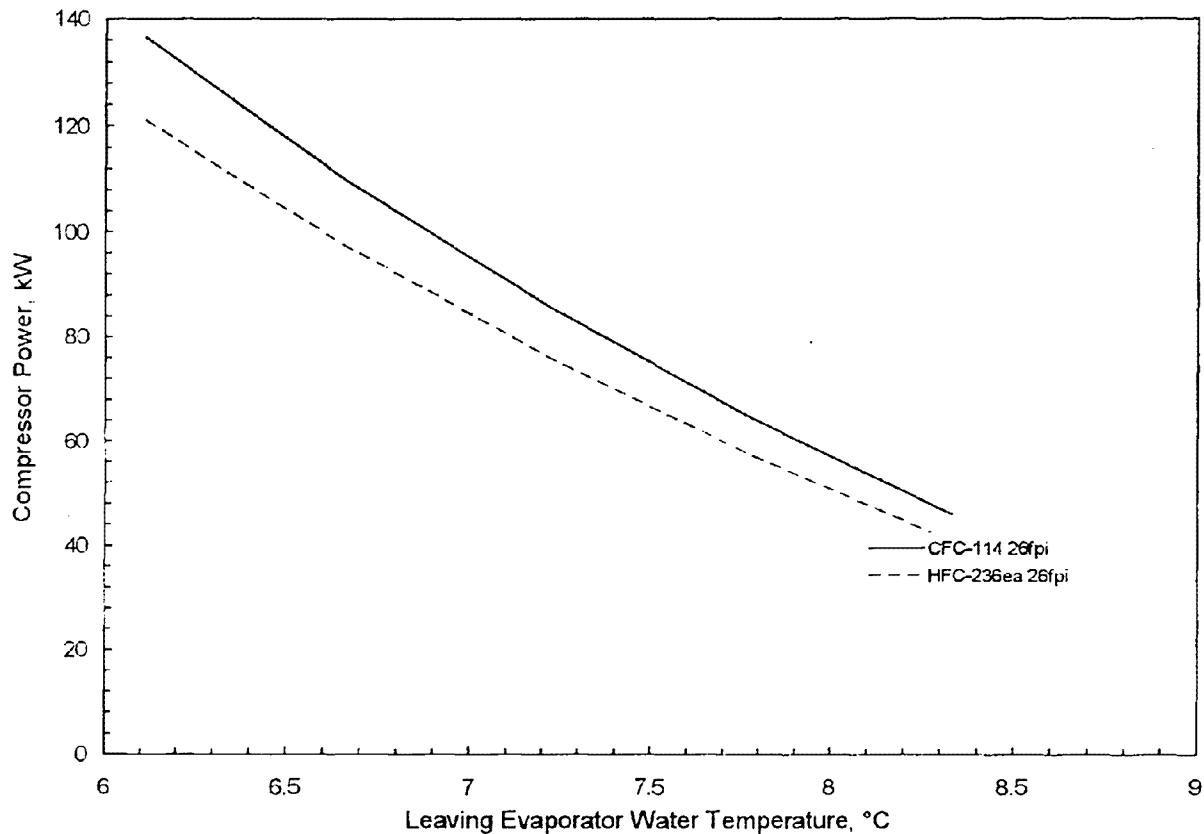
Figure 7.19: Dependence of compressor power input on leaving evaporator water temperature

As the chilled water temperature leaving the evaporator increases, the coefficient of performance tends to increase as shown in Figure 7.20. This observed trend shows that as the load is relaxed, the reduction in required compressor power is even greater causing the overall performance coefficient to increase. Again, HFC-236ea is predicted to perform better than CFC-114 for the range of temperatures simulated.

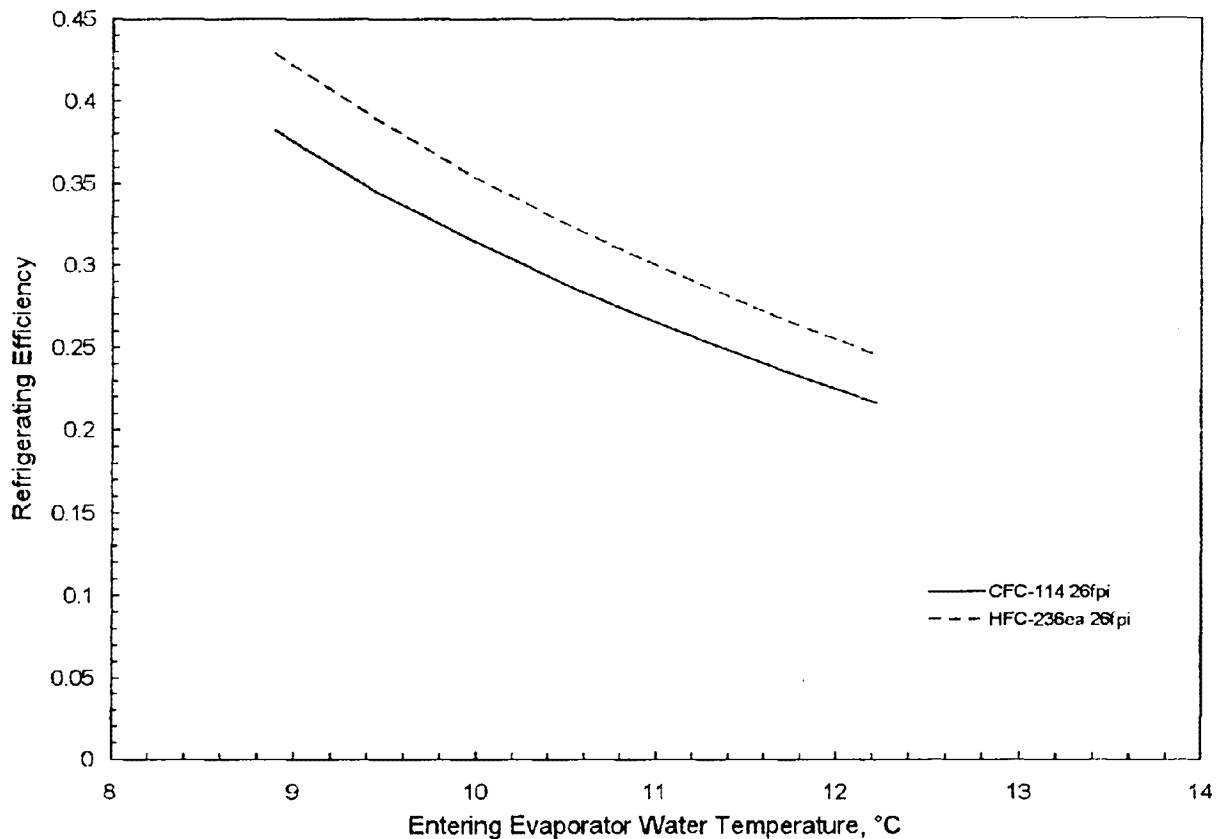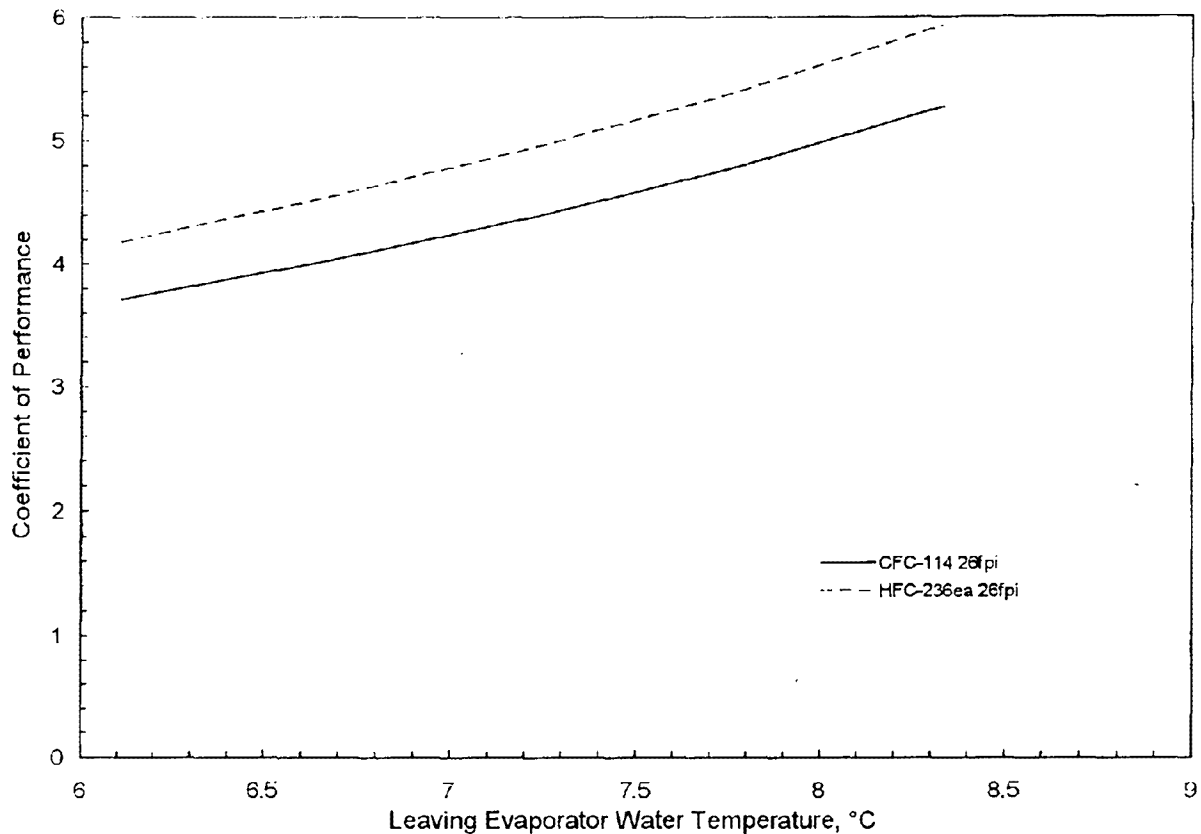Figure 7.20: Dependence of refrigerating performance on leaving evaporator water temperature

The refrigerating efficiency varies as a function of the chilled water temperature exiting the evaporator as illustrated by Figure 7.21. As the temperature increases, the refrigerating efficiency increases. Raising the temperature of the set point reduces the water temperature difference across the evaporator and thereby reduces the evaporator cooling capacity. Apparently, as the load is reduced, the corresponding compressor work is even less, thereby causing the coefficient of performance to improve in relation to the maximum possible coefficient of performance.

The trends of compressor power, coefficient of performance, and refrigerating efficiency as leaving evaporator water temperature is varied over a range of 6.4 °C to 8.7 °C are shown in Figures 7.19 through 7.21. The design point for the leaving chilled water evaporator temperature is 7 °C. As this value increases, the shaft power requirement decreases, and the coefficient of performance and refrigerating efficiency increase.
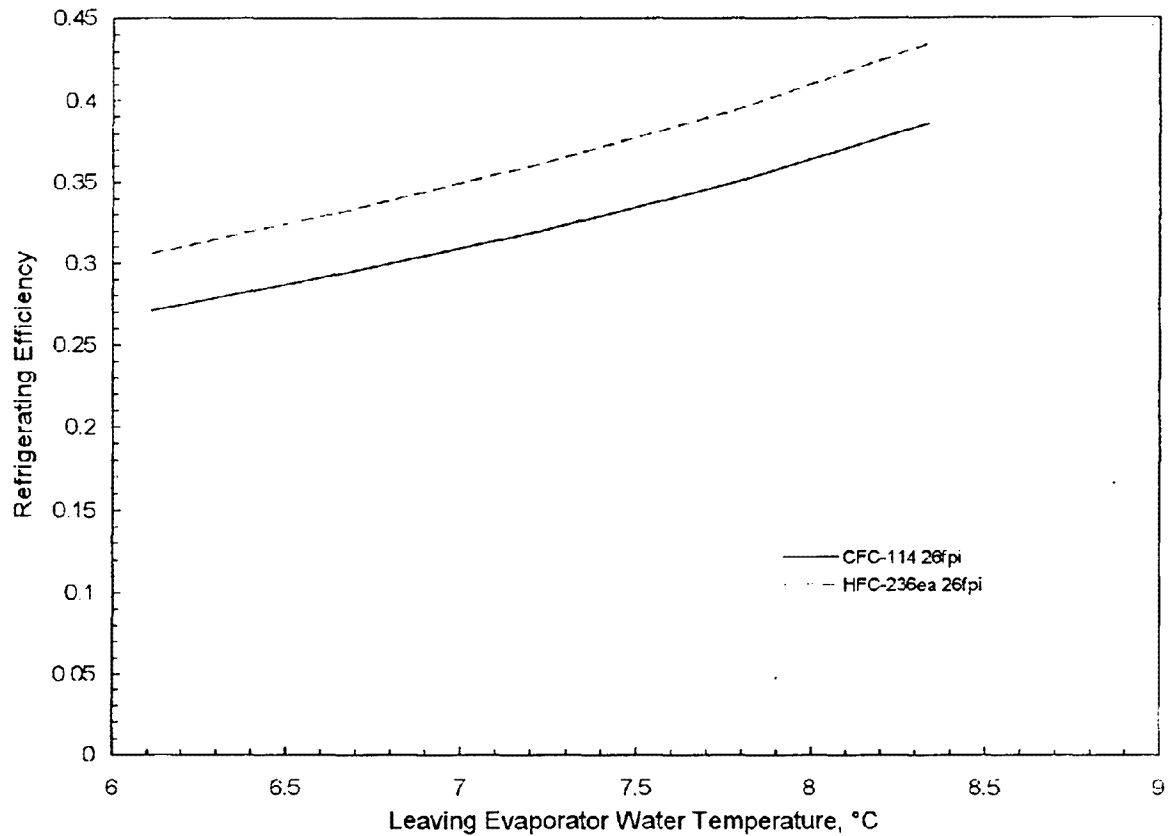
Figure 7.21: Dependence of refrigerating efficiency on leaving evaporator water temperature

Evaporator Water Flow rate

Evaporator chilled water flow rate is a parameter that can be used to evaluate the performance of HFC-236ea and CFC-114. Figure 7.22 demonstrates that as the flow rate is increased, the power required to drive the compressor shaft also increases. Over the range of flow rates simulated, HFC-236ea requires less power than CFC-114 to drive the compressor as predicted by the model.

As the simulated evaporator water flow rate is increased, the coefficient of performance decreases slightly. The designed operating flow for the 125-ton chiller is 28.4 l/s. HFC-236ea has a consistently higher coefficient of performance than CFC-114.
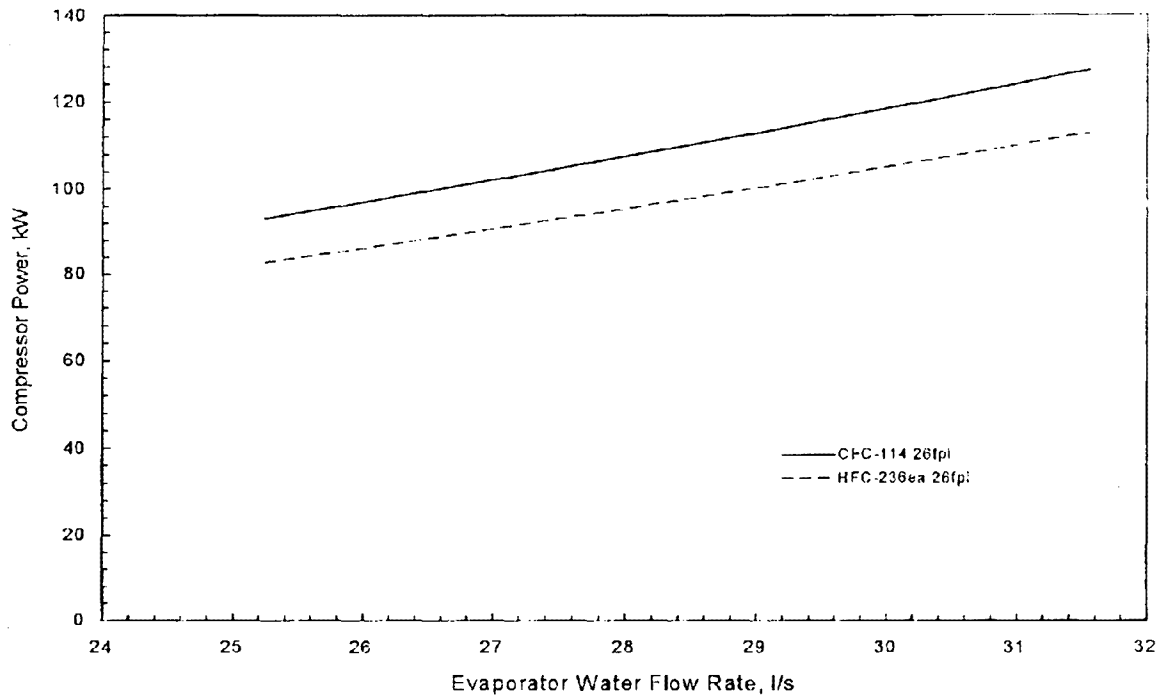
Figure 7.22: Dependence of power on evaporator water flow rate
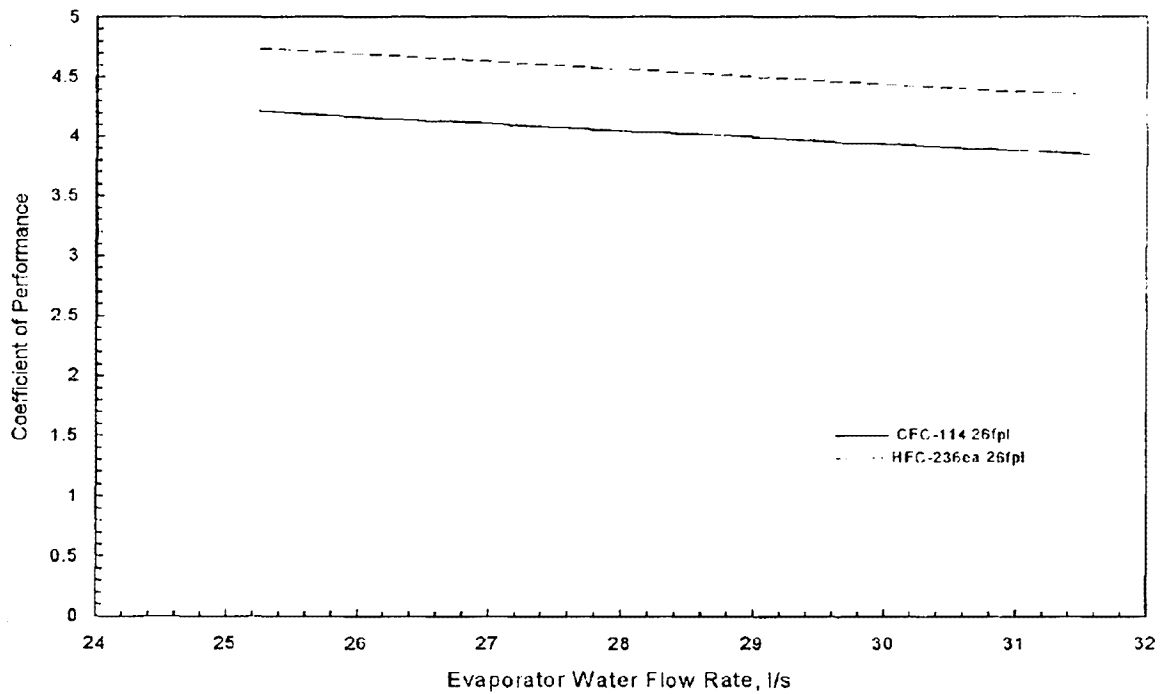
Figure 7.23: Dependence of refrigerating performance on evaporator water flow rate
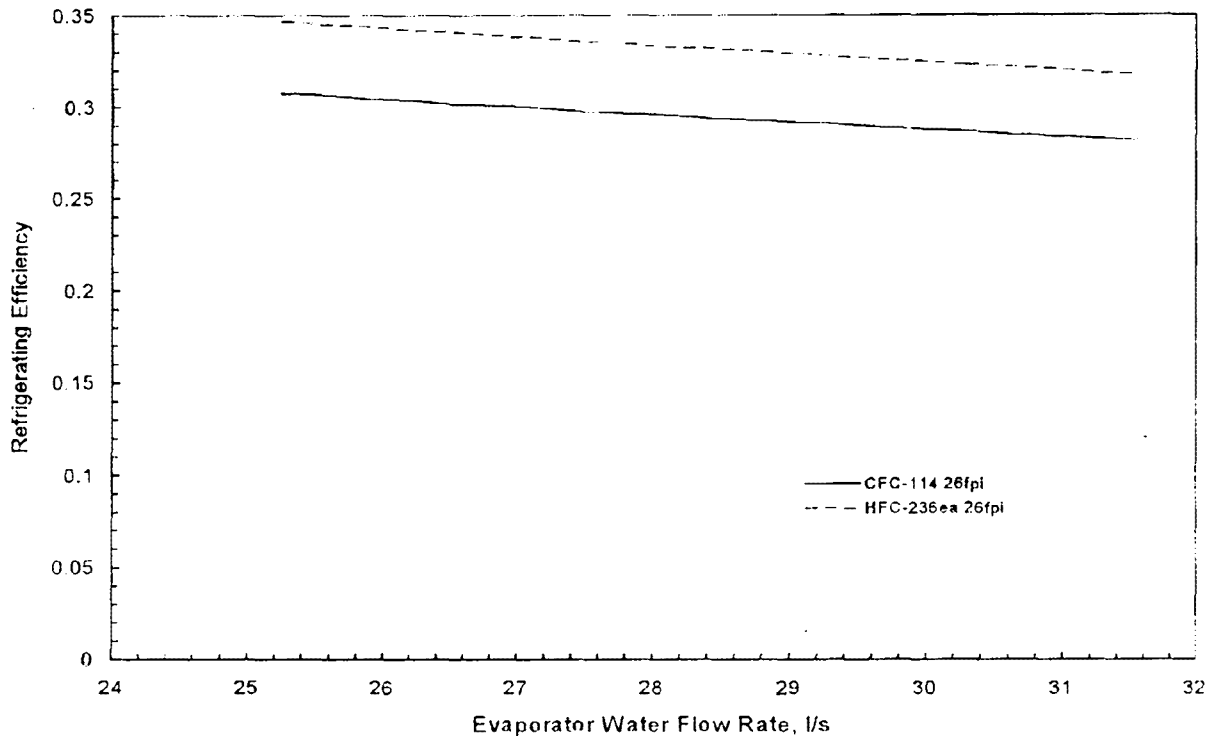
Figure 7.24: Dependence of refrigerating efficiency on evaporator water flow rate

Finally, as the evaporator water flow rate increases, Figure 7.24 illustrates that the refrigerating efficiency steadily decreases, and again, HFC-236 is predicted to outperform CFC-114 for the range simulated.

The flow rate of the evaporator chilled water is varied to see its effect on system performance. Figures 7.22 through 7.24 show the significance of varying these parameters. As with the previous results, HFC-236ea is predicted to outperform CFC-114 in every test case. The evaporator flow rate has a more significant effect for each liter per second than does the condenser water flow rate as will be shown next. As the evaporator chilled water flow rate increases, the load on the evaporator also increases. It follows that the corresponding shaft power required increases while the other performance indicators decrease.

Condenser Water Flow rate

As the condenser sea water flow rate is increased, the rate of heat transfer from the condenser increases and the result is a decrease in power requirement and increases in coefficient of performance and refrigerating efficiency. These observations are illustrated by Figures 7.26 through 7.28, respectively. In each case the change is small over the range of condenser water flow rates simulated. Additionally, in each case, the model predicts that HFC-236ea will perform significantly better than CFC-114 under the same operating conditions.

53
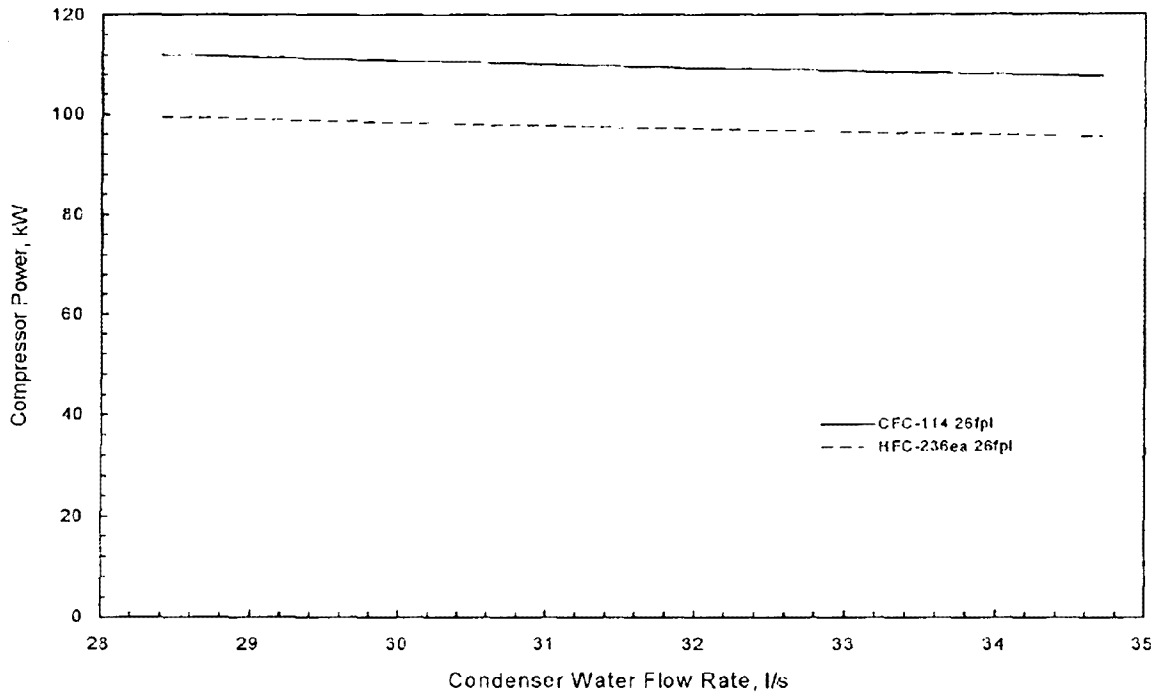
Figure 7.25: Dependence of power on condenser water flow rate
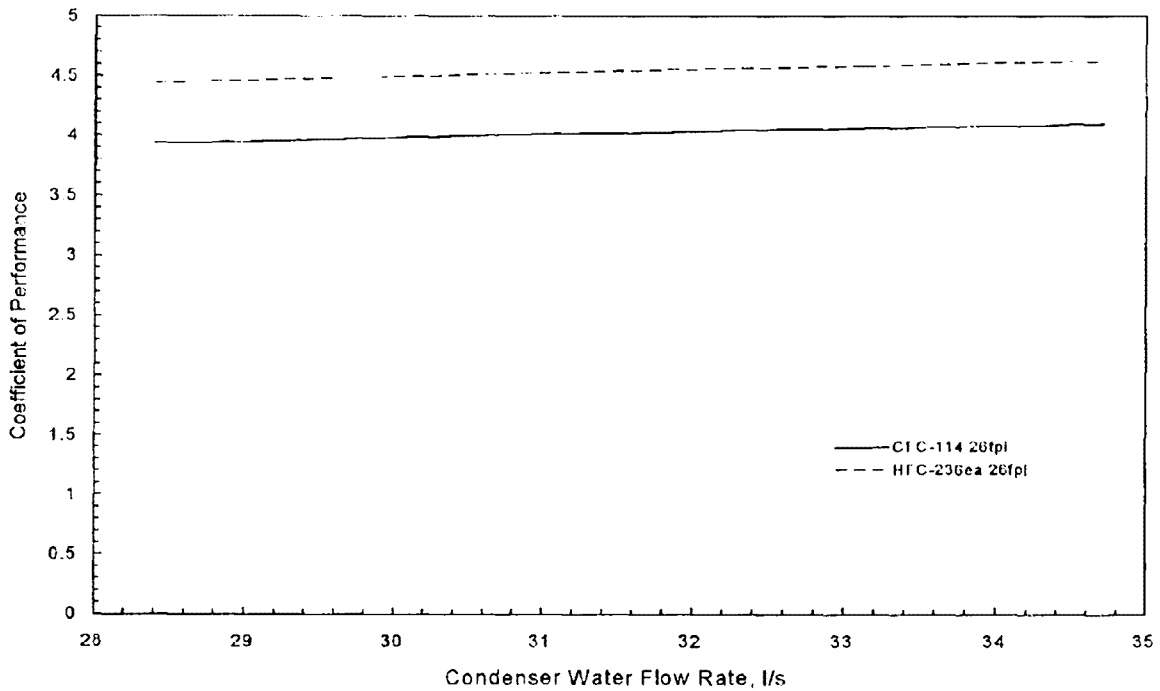
Figure 7.26: Dependence of refrigerating performance on condenser water flow rate

54
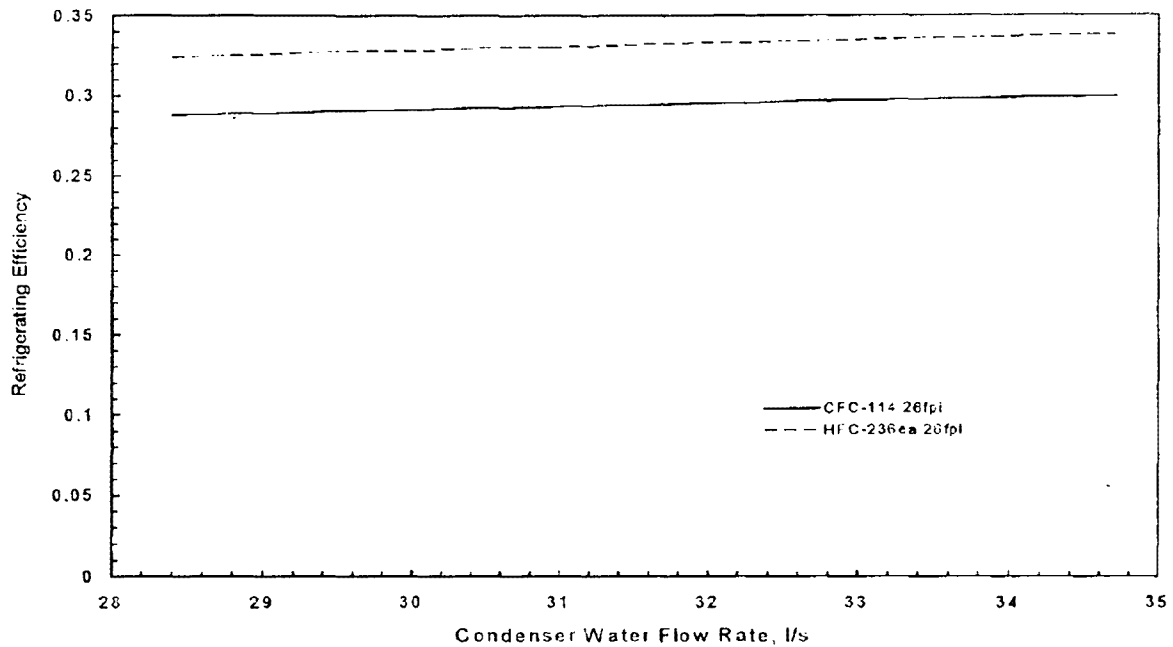
Figure 7.27: Dependence of refrigerating efficiency on condenser water flow rate.

SUMMARY

A parametric study was conducted using the computer program developed. Five parameters, including entering condenser water temperature, entering and leaving evaporator water temperatures, and condenser and evaporator water flow rates, were tested over an appropriate range and comparison plots were generated. The results of the model at design conditions suggest that HFC-236ea would outperform CFC-114 in a 440-kilowatt centrifugal chiller. At design conditions, identified in Table 6.1, the coefficient of performance was modeled to be 12.9 percent greater for HFC-236ea than for CFC-114. The predicted shaft power required is 11.3 percent less for HFC-236ea, and the refrigerating efficiency is predicted to be 12.9 percent higher for HFC-236ea.

The results of this study differ from those presented by Bare [7]. The difference can be attributed in part to the effects of heat transfer which were taken into account in this study by incorporating correlations for measured heat transfer coefficients for the evaporator and condenser. The measurements were taken in a separate study using a single-tube heat transfer test facility at Iowa State University [22]. The reported results present pool boiling and condensation heat transfer coefficients as functions of heat flux at constant saturation temperature for 10.23 fins per centimeter tubes and two refrigerants. The results showed that for a given heat flux and constant saturation temperature for a single 10.23 fins per centimeter tube, HFC-236ea performed with slightly higher heat transfer coefficients than CFC-114. This helps to explain some of the trends seen in the previous figures and is responsible, in part, for the predicted higher performance of HFC-236ea as a drop-in substitute for CFC-114.

55

CHAPTER 8. REFERENCES

[1]   Molina, M.J. and F.S. Rowland. "Stratospheric sink for chlorofluoromethanes: chlorine atom-catalysed destruction of ozone." *Nature* 249 (1974): 810-814.

[2]   Wuebbles, D.J. "The role of refrigerants in climate change." *International Journal of Refrigeration* 17 (1994): 7-17.

[3]   Budiansky, S. "The doomsday myths." *U.S. News & World Report* (December 1993): 81-91.

[4]   Doyle, T.J., W.K. Raymond, and A.L. Smookler. "Surface ship machinery - a survey of propulsion, electrical and auxiliary system development." *Marine Technology* 29(3) (1992): 115-143.

[5]   Miro, C.R., and J.E. Cox. "Global environment policies enter critical phase in the near-future." *ASHRAE Journal* (March 1994): 14-15.

[6]   Helmick, Richard L., Bruce G. Unkel, Robert A. Cromis, and A. Lynn Hershey. "Development of an advanced air conditioning plant for DDG-51 class ships." *Naval Engineers Journal* (May 1987): 112-123.

[7]   Bare, J.C. "Simulation of performance of chlorine-free fluorinated ethers and fluorinated hydrocarbons to replace CFC-11 and CFC-114 in chillers." *ASHRAE Transactions* 99 (1993): 397-407.

[8]   Threlkeld, J.L. *Thermal Environmental Engineering*, 2nd Ed., Englewood Cliffs, NJ: Prentice-Hall, 1970.

[9]   Smith, T.E., R.M. Nelson, and M.B. Pate. "An interactive computer program for analyzing refrigeration cycles in hvac courses." *ASHRAE Transactions* 93 (1987): 870-882.

[10]   Braun, J.E., J.W. Mitchell, S.A. Clein, and W.A. Bechman. "Models for variable-speed centrifugal chillers." *ASHRAE Transactions* 93 (1987): 1794-1813.

[11]   Jackson, W.L., F.C. Chen, and B.C. Hwang. "The simulation and performance of a centrifugal chiller." *ASHRAE Transactions* 93 (1987): 1751-1767.

[12]   Wong, S.P.W., and S.K. Wang. "System simulation of the performance of a centrifugal chiller using a shell-and-tube-type water-cooled condenser and R-11 as refrigerant." *ASHRAE Transactions* 95 (1989): 445-454.

[13]   Domanski, P.A., and M.O. McLinden. "A simplified cycle simulation model for the performance rating of refrigerants and refrigerant mixtures." *International Journal of Refrigeration* 15 (1992): 81-88.

[14]   Gauger, D.C., H.N. Shapiro, and M.B. Pate. "Alternative Technologies for Refrigeration and Air-Conditioning Applications. EPA-600/R-95-066 (NTIS PB95-224531), (May 1995), U.S. Environmental Protection Agency, Research Triangle Park, NC.

[15]   Stoecker, W.F. *Refrigeration and Air Conditioning*, 2nd Ed, New York: McGraw-Hill, 1982.

[16]   Langley, B.C. *Refrigeration and Air Conditioning*, 3rd Ed, Englewood Cliffs, NJ: Prentice-Hall, 1986.

[17]   Schultz, J.M. "The polytropic analysis of centrifugal compressors." *Journal of Engineering for Power: Transactions of the ASME* (1962): 69-82.

[18] National Institute of Standards and Technology, Thermodynamic Properties of Refrigerants and Refrigerant Mixtures Database (REFPROP version 4.01). Gaithersburg, MD, 1990.

[19] Morrison, G., and M. O. McLinden. "Application of a hard sphere equation of state to refrigerants and refrigerant mixtures." *National Bureau of Standards Technical Note 1226*, National Bureau of Standards, Department of Commerce, Washington, DC, 1986.

[20] Moran, M.J., and H.S. Shapiro. *Fundamentals of Engineering Thermodynamics*, 2nd Ed., New York: John Wiley and Sons, 1992.

[21] Incropera, F.P., and D.P. DeWitt. *Fundamentals of Heat and Mass Transfer*, 3rd Ed., New York: John Wiley and Sons, 1990.

[22] Huebsch, W. *Heat transfer evaluation of R-236ea and R-114 in condensation and evaporation*. Master's thesis, Iowa State University, Ames, IA, 1994.

[23] Stoecker, W.F. *Design of Thermal Systems*, 3rd Ed. New York: McGraw-Hill, 1989.

APPENDIX A. COMPUTER PROGRAM

```
      PROGRAM CHILLER
      IMPLICIT DOUBLE PRECISION (A-H,O-Z)
      LOGICAL LBUB, LCRIT, LLIQI, LVCON
C "PREFS" IS USED TO PASS THE VALUE OF IEQN
      COMMON /PREFS/ NUNITS,NREFST,INTACT,ICLMN,JCLMN(7),IEQN
C "ESDATA" CONTAINS THE VALUES OF THE MOLECULAR WEIGHTS IN CRIT(1,N)
      COMMON /ESDATA/ COEFF(10,40),CRIT(5,40)
C "MOLX" IS USED TO PASS THE VALUES OF THE MOLAR COMPOSITION IN X
      COMMON /MOLX/ WMI(5),WMR,WMX,X(5)
C COMMON BLOCKS "CMNOM" AND "HREF1" GIVE ACCESS TO THE NAMES OF THE
C COMPONENTS: LNAME IS THE CHEMICAL NAME AND HREF IS THE REFRIGERANT #
      CHARACTER*30 LNAME
      CHARACTER*10 SYNM
      CHARACTER*6 HREF
      COMMON /CMNOM/ SYNM(5),LNAME(5)
      COMMON /HREF1/ HREF(0:40)
      DIMENSION XL(5),XV(5)
C     dimension F(5,5), FT(5,5),XW(5) ! needed with mixtures
      common/group1/Tee,Tel,Tce,Qe,Tcl,Qc,V2,p2,uae,uac
      common/evap/hiev,atevsi,atevso,ttwev,ebc
      common/cond/hicd,atcdsi,atcdso,ttwcd,dtcdi,dtcdo,cdc
      common/misc/eLMTD,cLMTD,itube,ir(5)
      double precision ntev,ntcd

C These statements are for use with LINPACK subroutines
      real a(50,50),b(50),z(50)
      dimension y(3),yold(3)
      integer ipvt(50),lda
      data lda,n/50,3/

      data y/40,100,110/    ! initial estimates: y(1)=Te, y(2)=Tc, y(3)=T2
      data tol/.001/        ! convergence criteria for N-R iteration

C Design conditions:
      data Tce,Tee,Tel,gpme,gpmc/88.,50.67,44.,450.,500./
      data pexp,dsh,dsc/1.05,5.,5./

      data PI/3.1415927/

C Heat Exchanger data for Laboratory 125-ton AC plant
      data XLTEV/7.228/,NTEV/246./,XLTCD/7.228/,NTCD/246./
C
C FOR PURE FLUID CALCULATIONS, IT IS RECOMMENDED TO USE
C IEQN = 2 UNLESS THE FLUID IS NH3 (FOR NH3 USE IEQN = 3)
C    THIS APPLIES THE MODIFIED BENEDICT WEBB RUBIN EOS IF AVAILABLE,
C    OTHERWISE THE EXTENDED CORRESPONDING STATES MODEL
C
C INITIALIZE REFPROP VARIABLES
```

```
C
      NC = 1                       ! number of components
      print*,'input refrigerant  11 = R114,  29 = R236ea'
      read*,ir(1)                  ! component name
      X(1) = 1.D0                  ! mole fraction of component
      IEQN = 2                     ! ECS model

C CHOOSE REFERENCE STATE FOR ENTHALPY AND ENTROPY:  NREFST
C  1:  H,S = 0 FOR LIQUID AT NBPT
C  2:  H,S = 0 FOR LIQUID AT -40C (ASHRAE)
C  3:  H = 200KJ/KG, S=1 KJ/KG K FOR SATURATED LIQUID AT 0C (IIR)
C
      NREFST = 2
C
      CALL BCONST(NC,IR)           ! To obtain EOS parameters from BLOCK DATA

C WRITE NAME OF CHOSEN FLUID
      WRITE(*,*) IR(1),' ',HREF(IR(1)),' ',LNAME(1)
C
C set up an output file
      open(unit=13, file='results')

    2 print*,'input tube 1)Plain 2)26fins per inch 3)40fins per inch 4)TurboB'
      read*,itube
      if(itube.gt.4)goto 2
      if(itube.eq.1)then           ! Plain tube geometry
        DTEVI=.017312*39.3696      ! (root diameter - 2*wall thickness)  inches
        DTEVO=.019446*39.3696      ! (root diameter + 2*fin height)  inches
        DTCDI=.017312*39.3696
        DTCDO=.019446*39.3696
      elseif(itube.eq.2)then       ! 26fins per inch tube geometry
        DTEVI=.0143002*39.3696
        DTEVO=.01905*39.3696
        DTCDI=.0143002*39.3696
        DTCDO=.01905*39.3696
      elseif(itube.eq.3)then       ! 40fins per inch tube geometry
        DTEVI=.0155702*39.3696
        DTEVO=.0188722*39.3696
        DTCDI=.0155702*39.3696
        DTCDO=.0188722*39.3696
      elseif(itube.eq.4)then       ! Turbo-B tube geometry (40fins per inch for condenser)
        DTEVI=.0160528*39.3696
        DTEVO=.0184912*39.3696
        DTCDI=.0155702*39.3696
        DTCDO=.0188722*39.3696
      endif

    1 print*,'input variable 1)tce 2)tee 3)tcl 4)we 5)wc'
      read*,ivar
      if(ivar.gt.5)goto 1
      print*,'input range (from,to,step)'
```

```fortran
      read* j1,j2,j3
      do 100 var=j1,j2,j3    ! parameter to vary

      if(ivar.eq.1)then
        tce=var
      elseif(ivar.eq.2)then
        tee=var
      elseif(ivar.eq.3)then
        tel=var
      elseif(ivar.eq.4)then
        we=var
      elseif(ivar.eq.5)then
        wc=var
      endif


      iter=1


C-----------------------------------------------------------------
C               THERMODYNAMIC ANALYSIS
C-----------------------------------------------------------------


C note: Be extremely careful with units!
C       property subroutines (REFPROP) have units in molar SI:
C       T(K), P(kPa), v(L/mol), h(J/mol), etc...


C properties at the compressor inlet (statepoint 1)
   20 T=(y(1)-459.67)/1.8                    ! (K)


C Use the BUBLT Routine to find saturation boundary
      LBUB = .TRUE.
      XL(1) = X(1)
      CALL BUBLT(T,XL,XV,P,VL,VI,LBUB,LCRIT)
      if(lcrit)print*,'input above critical point'
      p1=p/6.8948                            ! evaporator pressure (psia)
C GET OTHER SATURATED VAPOR PROPERTIES
      if(dsh.eq.0.d0)then
        CALL HCVCPS(1,T,VI,XV,HV,d,d,d)
      elseif(dsh.gt.0.d0)then
        T=(y(1)+dsh+459.67)/1.8               ! (K)
        lliqi=.false.
        call vit(T,P,d,d,VI,LLIQI,LVCON)
        if(lvcon)print*,'vit did not converge'
        call hcvcps(1,T,VI,XV,HV,d,d,d)
      endif
      h1=hv/crit(1,IR(1))/2.326                ! (Btu/lbm)


C properties at the condenser outlet (state point 3)

      T=(y(2)+459.67)/1.8                      ! (K)


C Use the BUBLT Routine to find saturation boundary
```

```
      CALL BUBLT(T,XL,XV,P,VL,VV,LBUB,LCRIT)
      if(lcrit)print*,'input above critical point'

      p2=p/6.8948                      ! condenser pressure (psia)

C calculate enthalpy at the saturated vapor point
      call hcvcps(1,T,VV,XV,HV,d,d,d)
      h2s=hv/crit(1,IR(1))/2.326       ! (Btu/lbm)

C GET OTHER SATURATED LIQUID PROPERTIES
      if(dsc.eq.0.)then
        CALL HCVCPS(1,T,VL,XL,HL,d,d,d)
      elseif(dsc.gt.0.)then
        T=(y(2)-dsc+459.67)/1.8        ! (K)
        lliqi=.true.
        call vit(T,P,d,d,VL,LLIQI,LVCON)
        if(lvcon)print*,'vit did not converge'
        call hcvcps(1,T,VL,XL,HL,d,d,d)
      endif
      h3=hl/crit(1,IR(1))/2.326        ! (Btu/lbm)
C properties at the compressor outlet (state point 2)

C calculate v2 using compressor polytropic analysis
      v2=(p1/p2)**(1./pexp)*v1         ! (l/mol)
      if(vv.gt.v2)then
        print*,'wet compression'
        goto 100
      endif


C isenthalpic expansion
      h4=h3                            ! (Btu/lbm)
C estimate value of T2 (F)
      T=(y(3)+459.67)/1.8              ! (K)
C calculate h2 = f(T2,v2)
      CALL HCVCPS(1,T,V2,XV,H,d,d,d)
      h2=h/crit(1,IR(1))/2.326         ! (Btu/lbm)


C Convert gpm to lbm/min
      CALL WATER(tee,1,d,d,d,dens,d)
      We=gpme*35.314/264.17*dens
      CALL WATER(tce,2,d,d,d,dens,d)
      Wc=gpmc*35.314/264.17*dens


C
C --- Average Evaporator Water Temp (Deg F)---
C
      TWEVA=(tee+tel)/2.
C
C --- Evaporator Water Properties ---
```

```fortran
C
      CALL WATER(TWEVA,1,VSWEV,CNWEV,CPWEV,DNWEV,FFEV) ! fresh water
C
      Qe=we*cpwev*(tee-tel)  ! (kW)
      Wr=Qe/(h1-h4)          ! (lbm/min)
      Qc1=Wr*(h2-h2s)
      Qc2=Wr*(h2s-h3)
      Qc=Qc1+Qc2             ! (kW)


C iterate to find condenser leaving water temperature, tcl
      tcl=tce+5  ! estimate
      do 210 i=1,100
      t=tcl
C --- Average Condenser Water Temp ---
C
      TWCDA=(tce+tcl)/2
C
C --- Condenser Water Properties ---
C
      CALL WATER(twcda,2,vswcd,cnwcd,cpwcd,dnwcd,d)   ! seawater
C
      tcl=tce+qc/wc/cpwcd
C
C --- Check for Convergence ---
C
      IF(ABS(tcl-t).LT..001) GO TO 200
      IF(I.EQ.100) THEN
        print*,' No convergence on tcl'
        STOP
      END IF
  210 continue


C----------------------------------------------------------------
C              HEAT TRANSFER ANALYSIS
C----------------------------------------------------------------


C --- ALL COEFFICIENTS BASED ON GIVEN TUBE DIAMETERS ---
C
C ************* EVAPORATOR **************
C
C --- Total Evap Tube Outside Surface Area ---

  200 ATEVSO=NTEV*PI*DTEVO*XLTEV/12.
C
C --- Evap Tube Inside Surface Area ---
C
      ATEVSI=NTEV*PI*DTEVI*XLTEV/12.
C
C --- Evap Total Tube Flow Area ---
C
      ATEVF=NTEV*PI*(DTEVI/12.)**2/8.    ! (2 pass hx)
```

```
C
C --- Evap Tube Water Velocity ---
C
      CALL WATER(tee,1,VISC,COND,CP,DWEVS,FOULF) ! fresh water

      vwevt=we/dwevs/atevf/60.
C
C --- Evap Tube Reynolds Number ---
C
      REEVT=DNWEV*VWEVT*DTEVI*3600./12./VSWEV
C
C --- Evap Tube Prandtl Number ---
C
      PREVT=CPWEV*VSWEV/CNWEV
C
C --- Iteration for Tube Wall Temp and Water Heat Transfer Coeff ---
C
C --- Initial guess for Tube Wall Temperature ---
C
      TTWEV=y(1)
C
C --- Iteration Loop ---
C
      DO 70 I=1,100
      T=TTWEV
      CALL WATER(TTWEV,1,VSEVTW,COND,CP,DENS,FOULF) ! fresh water
C
C --- Water Side Coeff --- (Btu/hr/sqft/F)
C
      HIEV=.027*REEVT**.8*PREVT**.333*(VSWEV/VSEVTW)**.14
     &     *CNWEV/DTEVI*12.
C
C --- Tube Wall Temp ---
C
      TTWEV=(tee+tel)/2.-Qe*60./HIEV/ATEVSI
C
C --- Check for Convergence ---
C
      IF(ABS(TTWEV-T).LT..001) GO TO 80
      IF(I.EQ.100) THEN
        print*,' No convergence on evap tube wall temp'
        STOP
      END IF
  70 CONTINUE


C
C ************* CONDENSER **************
C


C
C --- Condenser Total Tube Flow Area (sqft) ---   ! (2 pass hx)
```

```fortran
C
   80 ATCDF=NTCD*PI*(DTCDI/12.)**2/8.
C
C --- Total Condenser Tube Outside Surface Area (sqft) ---
C
      ATCDSO=NTCD*PI*DTCDO*XLTCD/12.
C
C --- Total Condenser Tube Inside Surface Area (sqft) ---
C
      ATCDSI = NTCD*PI*DTCDI/12.*XLTCD
C
C --- Tube Water Velocity ---
C
      CALL WATER(tce,2,VISC,COND,CP,DWCDS,FOULF) ! seawater
      vwcdt=wc/dwcds/atcdf/60.
C
C --- Condenser Tube Reynolds Number ---
C
      RECDT = dnwcd*VWCDT*DTCDI*3600./12./vswcd
C
C --- Condenser Tube Prandl Number ---
C
      PRCDT = cpwcd*vswcd/cnwcd
C
C --- Initialize Tube Wall Temperature ---
C
      TTWCD = y(2)
C
C --- Iteration Loop for Tube Wall Temp. and Water Heat Transfer Coeff.
C
      DO 110 J=1,100
      T = TTWCD
      CALL WATER(TTWCD,2,VSCDTW,COND,CP,DENS,FOULF) ! seawater
C
C --- Water Side Coefficient ---
C
      HICD = .027*RECDT**.8*PRCDT**.333*(VSWCD/VSCDTW)**.14
     &    *CNWCD*12./DTCDI
C
C --- Tube Wall Temperature ---
C
      TTWCD = (tce+Tcl)/2.+Qc*60./HICD/ATCDSI
C
C --- Check for Convergence ---
C
      IF(ABS(TTWCD-T).LT..001) GO TO 120
      IF (J .EQ. 100) THEN
      print*,' No convergence on cond tube wall temperature'
      STOP
      END IF
  110 CONTINUE
```

```fortran
C--------------------------------------------------------------------
C          Newton-Raphson Iteration Scheme      Ref: Stoecker
C--------------------------------------------------------------------

C Keep old values of variables to later test for convergence
      120 do 25 i=1,n
       25 yold(i)=y(i)

C Calculate magnitudes of the functions at the temporary values
C of the variables   (B matrix)
          do 30 i=1,n
       30 b(i)=ff(i,y)

C Calc magnitudes of partial derivatives of all functions with respect
C to all variables  (A matrix)
          do 40 i=1,n
          do 40 j=1,n
       40 a(i,j)=df(i,j,y)

C Call LINPACK subroutines to solve simultaneous equations
          call sgeco(a,lda,n,ipvt,rcond,z)
          call sgesl(a,lda,n,ipvt,b,0)

C Corrected values of the variables (y new - y old - (yt - yc))
          do 35 i=1,n
       35 y(i)=y(i)-b(i)

C Check for convergence
          iflag=0
          do 50 i=1,n
       50 if(abs(y(i)-yold(i)).gt.tol)iflag=1
          if(iflag.ne.1)goto 90
          iter=iter+1
          goto 20


C--------------------------------------------------------------------
C              Final Calculations
C--------------------------------------------------------------------

       90 call water(tee,1,d,d,d,dens,d)
          gpme=we/35.314/dens*264.17
          call water(tce,2,d,d,d,dens,d)
          gpmc=wc/35.314/dens*264.17
          copr=(h1-h4)/(h2-h1)      ! COP refrigeration side
          coph=(h2-h3)/(h2-h1)      ! COP heating side
          copc=(tee+459.67)/(tce-tee)   ! COP carnot
          wp=(pexp/(pexp-1))*P1*v1*((p2/p1)**((pexp-1)/pexp)-1)*144./778.17
         +*.0353/crit(1,ir(1))*1000./2.2    ! polytropic work (Btu/lbm)
          effr=copr/copc            ! refrigerating efficiency
          pact=Wr*(h2-h1)              ! compressor power (actual)
```

65

```
      ue=uae/atevso*60.
      uc=uac/atcdso*60.
      write(13,1030)var,hicd,cdc,uac,hiev,ebc,uae
      print*,'wr = ',wr
      print*,'h1,h4 = ',h1,h4
      print*,'te = ',y(1)
      write(*,1030)var,hicd,cdc,uac,hiev,ebc,uae
1030  format(1x,f9.2,6f10.0)

C     write(13,1010)var,y(2),y(1),y(3),clmtd,elmtd
C    +,wr,qe,qc,pact,ppol,copr,coph,wp,effp,effr
C 1010 format(1x,f9.2,5f7.2,5f10.2,3f6.2,2f6.3)
C     write(*,1020)var,hiev,ebc,hicd,cdc,ue,uc
C 1020 format(1x,5f10.0,2x,2f10.0)
C     write(*,1020)var,y(2),y(1),y(3),clmtd,elmtd,copr,uae,uac
C 1020 format(1x,f9.2,5f7.2,f6.2,2f9.2)
   100 continue

      end




C These are the functions to be set equal to zero.
      function ff(i,y)
      implicit double precision(a-h,o-z)
      logical lliqi,lvcon
      COMMON /MOLX/ WMI(5),WMR,WMX,X(5)
      common/group1/Tee,Tel,Tce,Qe,Tcl,Qc,V2,p2,uae,uac
      common/evap/hiev,atevsi,atevso,ttwev,ebc
      common/cond/hicd,atcdsi,atcdso,ttwcd,dtcdi,dtcdo,cdc
      common/misc/cLMTD,cLMTD,itube,ir(5)
      dimension y(50)
      COMMON /ESDATA/ COEFF(10,40),CRIT(5,40)
      goto(1,2,3)i
    1 eLMTD=((tee-y(1))-(tel-y(1)))/log((tee-y(1))/(tel-y(1)))

C convert Qe to Heat Flux (qef) in SI units
      qef=qc/atevso*60.   ! Btu/hr/ft^2
      qef=qef/0.3171/1000.  ! kW/m^2

C choose correlation based on tube type
C correlations based on data taken at the ISU H.T. Test Facility

      if(itube.eq.2 .and. ir(1).eq.11)then
C File   E11426P.TXT
C Standard Deviation =  3.265132E-02
C Error Sum of Squares = 3.198326E-03
C Coefficients          Significant Figures   F test (1/3)   Pr > F
C  C 0 = .8431786            X              28.69      0.012
C  C 1 = .1359888            X +0.81        125.41     0.001
```

C C 2 = -8.738483E-04   X +0.22   16.04   0.025
    ebc= .8431786 + .1359888 * qef -8.738483E-04 * qef**2

    elseif(itube.eq.3 .and. ir(1).eq.11)then
C File = E11440P.TXT
C Standard Deviation = 2.006233E-02
C Error Sum of Squares = 1.207491E-03
C Coefficients   Significant Figures   F test (1/3)   Pr > F
C C 0 = .5452108   X   34.17   0.009
C C 1 = .1244462   X +0.96   298.86   0.000
C C 2 = -7.701729E-04   X +0.36   35.52   0.009
    ebc= .5452108 + .1244462 * qef -7.701729E-04 * qef**2

    elseif(itube.eq.1 .and. ir(1).eq.11)then
C File = E114PLP.TXT
C Standard Deviation = 1.865557E-02
C Error Sum of Squares = 1.044091E-03
C Coefficients   Significant Figures   F test (1/3)   Pr > F
C C 0 = .5603604   X   39.64   0.007
C C 1 = 9.845413E-02   X -0.85   205.56   0.001
C C 2 = -7.094109E-04   X +0.31   33.16   0.010
    ebc= .5603604 + 9.845413E-02 * qef -7.094109E-04 * qef**2

    elseif(itube.eq.4 .and. ir(1).eq.11)then
C File = E114TBP.TXT
C Standard Deviation = .346298
C Error Sum of Squares = .3597669
C Coefficients   Significant Figures   F test (1/3)   Pr > F
C C 0 = -10.90721   X   43.00   0.007
C C 1 = 2.131048   X +0.89   274.83   0.000
C C 2 = -3.048937E-02   X +0.65   174.02   0.001
    ebc=-10.90721 + 2.131048 * qef -3.048937E-02 * qef**2

    elseif(itube.eq.4 .and. ir(1).eq.29)then
C File = E236TBR0.TXT
C Standard Deviation = .1865692
C Error Sum of Squares = .1044243
C Coefficients   Significant Figures   F test (1/3)   Pr > F
C C 0 = -.3412447   X   0.15   > 0.3
C C 1 = .838187   X +1.99   148.31   0.001
C C 2 = -1.197194E-02   X +1.74   92.40   0.002
    ebc=-.3412447 + .838187 * qef -1.197194E-02 * qef**2

    elseif(itube.eq.1 .and. ir(1).eq.29)then
C File = E236PLP0.TXT
C Standard Deviation = 1.864138E-02
C Error Sum of Squares = 1.042504E-03
C Coefficients   Significant Figures   F test (1/3)   Pr > F
C C 0 = 1.635299   X   339.18   0.000
C C 1 = 8.369637E-02   X -0.31   146.78   0.001
C C 2 = -7.727059E-04   X -0.12   38.43   0.008

```
            ebc- 1.635299 - 8.369637E-02 * qef -7.727059E-04 * qef**2


         elseif(itube.eq.2 .and. ir(1).eq.29)then
C File = E23626P0.TXT
C Standard Deviation = 1.816126E-02
C Error Sum of Squares = 9.89494E-04
C Coefficients          Significant Figures   F test (1/3)   Pr > F
C   C 0 = 2.22797              X              690.21      0.000
C   C 1 = .1742529             X +0.49        691.38      0.000
C   C 2 = -1.766886E-03        X +0.10        215.76      0.001
         ebc= 2.22797 + .1742529 * qef -1.766886E-03 * qef**2


         elseif(itube.eq.3 .and. ir(1).eq.29)then
C File = E23640P0.TXT
C Standard Deviation = 1.033823E-02
C Error Sum of Squares = 3.206369E-04
C Coefficients          Significant Figures   F test (1/3)   Pr > F
C   C 0 = 1.411047             X              837.85      0.000
C   C 1 = .1529635             X +0.64        1639.40     0.000
C   C 2  -1.333973E-03         X +0.18        383.88      0.000
         ebc= 1.411047 + .1529635 * qef -1.333973E-03 * qef**2


         endif


C convert evaporator boiling coefficient (ebc) to english units

         ebc=ebc*1000.    ! W/m^2/K
         ebc=ebc*0.17612  ! Btu/hr/ft^2/F

         UAe=(1./(hiev*atevsi)+1./(ebc*atevso))**(-1.)/60.  ! kW/F

         ff=Qe-UAe*eLMTD
         return

     2 cLMTD=((y(2)-tce)-(y(2)-Tcl))/log((y(2)-tce)/(y(2)-Tcl))


C convert Qc to SI units

         qcf=qc/atcdso*60.    ! Btu/hr/ft^2
         qcf=qcf/0.3171/1000. ! kW/m^2


C choose correlation to use

         if(itube.eq.2 .and. ir(1).eq.11)then
C File = C11426P.TXT
C Standard Deviation - 4.739834E-02
C Error Sum of Squares = 6.739808E-03
C Coefficients          Significant Figures   F test (1/3)   Pr > F
C   C 0 = 3.620498             X              251.58      0.000
C   C 1  .1494268              X +0.22        72.88       0.003
C   C 2 = -2.087891E-03        X -0.03        44.58       0.006
```

```
        cdc= 3.620498 + .1494268 * qcf -2.087891E-03 * qcf**2


      elseif((itube.eq.3 .or. itube.eq.4) .and. ir(1).eq.11)then
C File - C11440P.TXT
C Standard Deviation = .1500359
C Error Sum of Squares = 6.753228E-02
C Coefficients          Significant Figures  F test (1/3)   Pr > F
C   C 0 = 2.967423          X                 17.87    0.021
C   C 1 - .2155206          X +0.46           15.51       0.026
C   C 2 = -2.98224E-03      X ÷0.20            9.04        0.050
        cdc= 2.967423 + .2155206 * qcf -2.98224E-03 * qcf**2


      elseif(itube.eq.1 .and. ir(1).eq.11)then
C File = C114PLP.TXT
C Standard Deviation = 1.139951E-02
C Error Sum of Squares = 2.598976E-04
C Coefficients          Significant Figures  F test (1/2)   Pr > F
C   C 0 = 1.510632          X                 398.69    0.002
C   C 1 = -2.106263E-02     X -0.31           11.11       0.069
C   C 2 - 3.159286E-04      X -0.59           6.48        0.111
        cdc= 1.510632 -2.106263E-02 * qcf + 3.159286E-04 * qcf**2


      elseif(itube.eq.2 .and. ir(1).eq.29)then
C File = C23626P.TXT
C Standard Deviation = 4.463284E-02
C Error Sum of Squares = 5.97627E-03
C Coefficients          Significant Figures  F test (1/3)   Pr > F
C   C 0 = 4.093141          X                 388.58    0.000
C   C 1 = .1415326          X +0.14           77.74       0.003
C   C 2 = -1.620209E-03     X -0.20           31.53       0.010
        cdc= 4.093141 + .1415326 * qcf -1.620209E-03 * qcf**2


      elseif((itube.eq.3 .or. itube.eq.4) .and. ir(1).eq.29)then
C File = C23640P.TXT
C Standard Deviation = 3.473567E-02
C Error Sum of Squares = .0036197
C Coefficients          Significant Figures  F test (1/3)   Pr > F
C   C 0 = 2.953098          X                 339.66    0.000
C   C 1 = .187457           X +0.41           227.99      0.001
C   C 2 = -1.830992E-03     X -0.00           67.14       0.004
        cdc- 2.953098 + .187457 * qcf -1.830992E-03 * qcf**2


      elseif(itube.eq.1 .and. ir(1).eq.29)then
C File = C236PLP.TXT
C Standard Deviation = 2.255796E-02
C Error Sum of Squares = 1.526584E-03
C Coefficients          Significant Figures  F test (1/3)   Pr > F
C   C 0 = 2.438327          X                 557.62    0.000
C   C 1 = -5.335892E-02     X -0.05           44.93       0.006
C   C 2 = 7.070792E-04      X -0.33           24.58       0.014
        cdc- 2.438327 -5.335892E-02 * qcf + 7.070792E-04 * qcf**2
```

```fortran
      endif

C convert cdc to english units

      cdc=cdc*1000.    ! W/m^2/K
      cdc=cdc*0.17612 ! Btu/hr/ft^2/F

      UAc=(1./(hicd*atcdsi)+1./(cdc*atcdso))**(-1.)/60.  ! (kW/F)
      ff=Qc-UAc*cLMTD
      return

    3 T=(y(3)+459.67)/1.8                    ! (K)
      P=p2*6.8948                  ! (kPa)
      call vit(T,P,d,d,V,LLIQI,LVCON)
      ff=v2-v
      return
      end




C This function calculates numerical derivatives,  df(i)/dy(j)
      function df(i,j,y)
      implicit double precision(a-h,o-z)
      dimension y(50)
      dely=y(j)*0.001
      if(y(j).le.0.001)dely=0.001
      y(j)=y(j)+dely
      g1=ff(i,y)
      y(j)=y(j)-2*dely
      g2=ff(i,y)
      y(j)=y(j)+dely
      df=(g1-g2)/(2*dely)
      return
      end


      SUBROUTINE WATER(TEMP,kWATER,VISC,COND,CP,DENS,FOULF)
      implicit double precision (a-h,o-z)
C***********************************************************************
C  Mechanical and thermal properties of fresh water or seawater as a
C  function of temperature within the range (32 - 158 F)
C
C  Adapted From Oak Ridge Heat Pump Program
C***********************************************************************
C
C --- Inputs ---
C
C   TEMP    Water temperature (F)
C   kWATER  Kind of water:  1 - Fresh Water, 2 - Seawater
C
```

70

```
C --- Outputs ---
C
C    VISC    Viscosity of water (lbm/ft-hr)
C    COND    Thermal conductivity of water (Btu/hr-ft-F)
C    CP      Specific heat of water (Btu/lbm-F)
C    DENS    Density of water (lbm/cuft)
C    FOULF   Thermal fouling factor of water (hr-sqft-F/Btu)
C
      IF(kWATER.NE.2) THEN
C
C --- Fresh Water ---
C
      VISC=3600.*(.62111E-11*TEMP**4-.29839E-8*TEMP**3+
     &      .55359E-6*TEMP**2-.50665E-4*TEMP+.2345E-2)
      COND=-.18797E-5*TEMP**2+.85742E-3*TEMP+.2953
      CP=-.13254E-9*TEMP**4-.65618E-7*TEMP**3+.12373E-4*TEMP**2-
     &      .10208E-2*TEMP+1.029
C      DENS=62.366-.0163*(TEMP-59.)
C
C The following equation for density is from Robert P. Benedict's text,
C FUNDAMENTALS OF TEMPERATURE, PRESSURE, AND FLOW MEASUREMENTS, Equation 15.7
C
      DENS=62.2523+.978476E-2*TEMP-.145E-3*TEMP**2+.217E-6*TEMP**3
      FOULF=.00010
      ELSE
C
C --- Seawater ---
C
      VISC=3600.*(.62595E-11*TEMP**4-.29332E-8*TEMP**3+
     &      .53738E-6*TEMP**2-.49718E-4*TEMP+.2408E-2)
      COND=-.19056E-5*TEMP**2+.85917E-3*TEMP+.2884
      CP=.952-(TEMP-32.)*5.88E-5
      DENS=64.043-.00668*(TEMP-59.)
      FOULF=.00025
      END IF
      RETURN
      END


C
C -------------Definition of Variables ----------------
C
C    ** EVAPORATOR TUBE GEOMETRY **
C    DTEVI    - tube inside diameter  (root diameter - 2*wall thickness)  inches
C    DTEVO    - tube outside diameter (root diameter + 2*fin height)  inches
C    XLTEV    - effective tube length per pass (feet)
C    NTEV     - number of tubes
C    ATEVSO   - total evaporator tube outside area (based on diameter)
C
C    ** CONDENSER TUBE GEOMETRY **
C    DTCDI    - tube inside diameter (root diameter - 2*wall thickness)  inches
C    DTCDO    - tube outside diameter (root diameter + 2*fin height)  inches
```

```
C    XLTCD    - effective tube length per pass (feet)
C    NTCD     - number of tubes
C    ATCDSO   - total condenser tube outside area (based on diameter)
C
C    ** EVAPORATOR **
C    GPME     - chiller water flow rate (gpm)
C    EBC      - boiling coefficient (btu/hr-ft**2-F)
C
C    ** CONDENSER **
C    GPMC     - condenser water flow rate (gpm)
C    CDC      - condensing coefficient (btu/hr-ft**2-F)
C-------------------------------------------------------------------
```
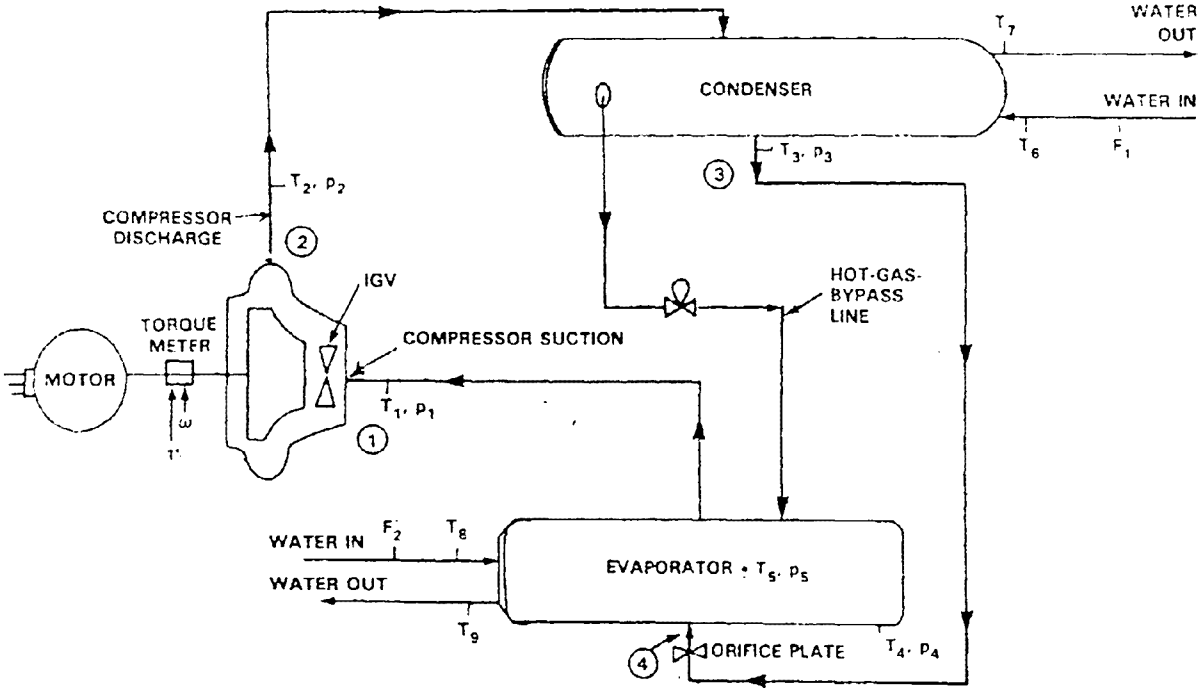
APPENDIX C. SAMPLE NSWC DATA

Binary File: C:/DATA/T1244D05.JUL
Run Title: HFC 236 EA 490 LBS
Test Date: 07/05/1994 1244 hours
Average of 25 data samples

Chn	Description	Avg Value	Max Value	Min Value	Unit
00	Open Channel				
01	Condenser Vapor	52.4724	52.5286	52.4155	psia
02	Compressor Discharge	53.2188	53.4079	53.1011	psia
03	Condenser Liquid	53.2145	53.2945	53.1486	psia
04	Evaporator Vapor Pressure	12.7113	12.7294	12.6963	psia
05	Compressor suction	12.5454	12.5725	12.5166	psia
06	Evaporator Liquid Pressure	12.6089	12.6452	12.5680	psia
07	Open Channel		13.2390	13.2380	
08	Compressor Suction Temp2	36.8633	36.9007	36.7931	deg F
09	Compressor Suction Temp1	37.5992	37.6317	37.5551	deg F
10	Oil Cooler Inlet Temp	67.4745	67.4880	67.4635	deg F
11	Compressor Oil Sump Temp	123.772	123.790	123.759	deg F
12	Chiller Water Inlet Temp	51.3134	51.3667	51.2593	deg F
13	Chiller Water Outlet Temp	44.0546	44.0852	44.0240	deg F
14	Oil Cooler Outlet Temp	69.2839	69.3016	69.2619	deg F
15	Evaporator Vapor Temp	37.1099	37.1322	37.0710	deg F
16	Condenser Water Inlet Temp	86.0839	86.1472	86.0216	deg F
17	Condenser Liquid Temp	101.821	101.840	101.807	deg F
18	Evaoporator Liquid Temp	37.0662	37.0991	37.0348	deg F
19	Condenser Vapor Temp	109.754	109.768	109.728	deg F
20	Compressor Discharge Temp	109.443	109.470	109.358	deg F
21	Condenser Water Outlet Temp	94.2320	94.2812	94.1923	deg F
22	Motor Torque	3062.56	3079.39	3051.52	in-lb
23	Motor Speed	3593.84	3598.70	3590.98	rpm
24	Inlet Guide Vane position	38.7936	38.8078	38.7844	degree
25	Hot Gas Valve Position	-.700720	.327406	-1.18651	degree
26	Power input to compressor	.231624	.451580	-.034150	kW
27	Evaporator Water Flow rate	450.493	454.933	446.935	gpm
28	Condenser Water Flow rate	501.856	504.121	499.604	gpm
29	Oil Cooler Water Flow rate	14.4711	14.7647	14.0511	gpm
30	Motor Temperature	184.602	184.940	184.360	deg F
31	Guideline Reference Temp	1.82038	1.90300	1.77330	deg F
32	Spare RTD	1.83802	1.89820	1.77460	deg F
33	Open Channel				

Note: A data point consists of taking the average of 155 samples over 10 minutes. The point is considered stable if the difference between the minimum and maximum temperatures of the inlet and outlet evaporator chilled water is within 0.1 °F.

APPENDIX D. CHILLER INFORMATION PROVIDED BY THE NSWC

The air conditioning plant consists of an open single-stage centrifugal compressor-motor driven unit, and a condenser-chiller shell package. The compressor is direct-driven through a torquemeter station. Compressor impeller speed is increased through an internal compressor gear arrangement. The refrigerant system is designed to use CFC-114.

Compressor capacity is controlled to maintain the desired water temperature and to prevent motor overloading. Control is achieved by varying the position of vanes located in the compressor suction inlet. The vanes are moved by a pneumatic operator which automatically responds to a chilled water thermostat.

TECHNICAL DATA

System capacity:	125 tons refrig. with following design conditions;
Chilled water circulation	450 gpm
Temperature entering	50.7 °F
Temperature leaving	44 °F
Condenser water flow	500 gpm
Temperature entering	88 °F
Refrigerant charge	500 lb. CFC-114 (approx.)

Driveline unit:
Centrifugal compressor

Type	Single-stage open
Capacity	125 tons
Impeller speed	11,918 rpm

Shell unit:
Condenser

Size	22 inches OD x 93.5 inches length
Class	B
Type	Shell-and-tube
Number of tubes	246
Tube type	0.75" nominal diameter, 26 fins per inch, copper, 0.049" wall
Cooling surface	1138 square feet
Water passes	2
Circulating water	500 gpm
Inlet temperature	88 °F
Outlet temperature	95.9 °F
Refrigerant pressure	50 psig
Condensing temperature	104.8 °F

Cooler

Size	32 inches OD x 93.5 inches length
Class	B
Type	Shell-and-tube (flooded)
Number of tubes	246
Tube type	0.75" nominal diameter, 26 fins per inch, copper, 0.049" wall
Cooling surface	1138 square feet
Water passes	2
Circulating water	450 gpm
Inlet temperature	50.7 °F
Outlet temperature	44 °F